Aus der Klinik für Strahlentherapie und Radioonkologie
Geschäftsführende Direktor: Prof. Dr. Sebastian Adeberg
des Fachbereichs Medizin der Philipps-Universität Marburg

Titel der Dissertation:

Dosimetry of high energy photon beams in the presence of magnetic fields

Inaugural-Dissertation zur Erlangung des Doktorgrades der Medizinwissenschaften
(Dr. rer. med.)
dem Fachbereich Medizin der Philipps-Universität Marburg
vorgelegt von

Mohamad Alissa
16.10.1985
aus Njran
Gießen , 2024

Angenommen vom Fachbereich Medizin der Philipps-Universität Marburg am:
15.05.2024

Gedruckt mit Genehmigung des Fachbereichs Medizin.

Dekan: Prof. Dr. Denise Hilfiker-Kleiner

Referenten: Prof. Dr. Rita Engenhart-Cabillic & Prof. Dr. Klemens Zink

1. Korreferent: Prof. Dr. Andreas H. Mahnken

Articles accepted in peer-reviewed journals

The present cumulative dissertation represents a summary of the research results, which have been published as follows in peer-reviewed journals:

[1] Mohamad Alissa, Klemens Zink, Frederic Tessier, Andreas A. Schoenfeld and Damian Czarnecki. Monte Carlo calculated beam quality correction factors for two cylindrical ionization chambers in photon beams.
Physica Medica 94 (2022) 17–23. doi:https://doi.org/10.1016/j .ejmp.2021.12.012

[2] Mohamad Alissa, Klemens Zink and Damian Czarnecki. Investigation of Monte Carlo simulations of the electron transport in external magnetic fields using Fano cavity test.
Zeitschrift fuer Medizinische Physik, (2022). https://doi.org/10.1016/j.zemedi.2022.07.002

[3] Mohamad Alissa, Klemens Zink, Andreas A. Schoenfeld, Ralf-Peter Kapsch, Stephan Frick and Damian Czarnecki. Experimental and Monte Carlo-based determination of magnetic field correction factorss $k_{B,Q}$ high-energy photon fields for two ionization chambers.
Medical Physics (2023) https://doi.org/10.1002/mp.16345

[4] Mohamad Alissa, Klemens Zink, Arnd Röser, Veronika Flatten, Andreas A. Schoenfeld and Damian Czarnecki. Monte Carlo calculated beam quality correction factors for high energy electron beams.
Physica Medica (2024) https://doi.org/10.1016/j.ejmp.2023.103179

Conference contributions

Throughout the doctoral period, the following contributions were presented at various conferences:

- Dreiländertagung der Medizinischen Physik 2017, Dresden, Deutschland, Postervorstellung.
- IUPESM 2018 World Congress on Medical Physics and Biomedical Engineering, Prague, Czech Republik, Vortrag.
- ECMP 2018 European Congress of Medical Physics, Copenhagen, Denmark,Vortrag.
- DGMP 2018 49. Jahrestagung der Deutschen Gesellschaft für Medizinische Physik 21. Jahrestagung der Deutschen Sektion der ISMRM, Nürnberg, Deutschland, zwei Vorträge.
- Dreiländertagung der Medizinischen Physik 2021, Wien, Österreich, zwei Vorträge.
- ESTRO 2022 European Society for Radiotherapy and Oncology Congress, Copenhagen, Denmark, zwei Postervorstellungen.
- AAPM 2022 64. Annual meeting of American Association of Physicists in Medicine, Washington D.C, USA, Vortrag.
- DGMP 2022 53. Jahrestagung der Deutschen Gesellschaft für Medizinische Physikm, 24. Jahrestagung der Deutschen Sektion der ISMRM, Aachen, Deutschland, Vortrag.
- DGMP 2023 54. Jahrestagung der Deutschen Gesellschaft für Medizinische Physikm, Magdeburg, Deutschland, two posters.

Zusammenfassung

Die moderne Strahlentherapie zielt darauf ab, gesundes Gewebe und Risikoorgane (OARs) optimal zu erhalten, während gleichzeitig eine hohe Dosis im Zielvolumen (PTV) appliziert wird. Um dieses Ziel zu erreichen, wurden mehrere Geräte entwickelt, darunter die Integration eines klinischen Elektronen-Linear-Beschleunigers mit einem Magnetresonanztomographie-Gerät (MRT). Diese Integration ermöglicht eine Echtzeitbildgebung der Anatomie des Patienten während der Strahlenbehandlung, was eine verbesserte Zielgenauigkeit und adaptive Behandlungsstrategien ermöglicht. Bilder können für die Lokalisierung des Tumors und die Positionierung des Patienten vor der Behandlung sowie für Techniken zur Bewegungsminderung, einschließlich Zielverfolgung und Gating, verwendet werden. Zusätzlich können Veränderungen in der Anatomie, wie Gewichtsverlust oder Organfüllung, durch Anpassung des Behandlungsplans an die aktuellsten MRT-Bilder berücksichtigt werden. Für eine präzise Dosisapplikation im MR-Linac ist es allerdings notwendig, die Wirkung der Lorentzkraft auf die Strahlung zu berücksichtigen. Aufgrund der Lorentzkraft kommt es zu einer Ablenkung der geladenen Sekundärteilchen und damit zu einem veränderten Ansprechen der eingesetzten Detektoren. Vor diesem Hintergrund bestand das Hauptziel der vorliegenden Arbeit darin, das Verhalten von Ionisationskammern in Magnetfeldern zu untersuchen. Daher wurden die Strahlqualitätskorrekturfaktoren für hochenergetische Photonenstrahlen in Ionisationskammern (SNC600c, SNC125c) und hochenergetische Elektronenstrahlen in (SNC600c, SNC125c, SNC350p) gemäß Dosimetrieprotokollen wie TG-51, TRS 398 und DIN 6800-2 berechnet. Zusätzlich wurde mittels des Fano-Hohlraumtests bestätigt, dass die Monte-Carlo-Codes eine hohe Genauigkeit (0,1%) in Anwesenheit eines Magnetfeldes aufweisen. Schließlich wurde die Änderung des Ansprechvermögens der beiden Ionisationskammerm SunNuclear SNC600c und SNC125c in äußeren magnetischen Feldern, d.h. der Korrektionsfaktor $k_{B,Q}$, experimentell und mittels Monte-Carlo Simulationen ermittelt. Die Ergebnisse haben gezeigt, dass der Korrektionsfaktor $k_{B,Q}$ sowohl von der Stärke des äußeren Magnetfeldes als auch von der Größe des Messvolumens und der Orientierung der Kammerachse, und die Änderung des Ansprechvermögens beider Kammern ist minimal, wenn die Magnetfeldrichtung und die Kammerachse ausgerichtet und senkrecht zur Strahlrichtung sind. Darüber hinaus war in Anwesenheit eines Magnetfeldes bei der größeren Kammer SNC600c größer war als bei der kleineren Kammer SNC125c.

Zusammenfassend deckte diese Studie einen wichtigen Teil der Dosimetrie bei Vorhandensein von Magnetfeldern ab und bestätigte die Möglichkeit, die beiden untersuchten Ionisationskammern zur genauen Dosisbestimmung in Anwesenheit von Magnetfeldern nach Anwendung der Magnetfeldkorrektionfaktoren zu verwenden.

Summary

Modern radiotherapy aims to optimally preserve healthy tissue and organs at risk (OARs) while accurately tailoring a high dose to the target. To achieve this objective, several devices have been developed, including the integration of an electron linear clinical accelerator with a magnetic resonance imaging (MRI) device. This integration enables real-time imaging of the patient's anatomy during radiation treatment, allowing for improved targeting precision and adaptive treatment strategies. Images can be utilized for target localization and patient positioning before treatment as well as motion mitigation techniques including target tracking and gating. Additionally, changes in the anatomy as weight loss or organ filling may be taken into account by adjusting the treatment plan in line with the most current MR imaging. However, this device faced a challenge due to the Lorentz force from the MRI, which affects the trajectories of charged particles, and may alter the dose distribution in patients or phantoms as well as the dose response in detectors. Considering this, the primary aim of this study was to investigate the behavior of ionization chambers in magnetic fields. Additionally, the study sought to conduct thorough research on the ionization chambers used and to verify the reliability of the Monte Carlo simulations in the presence of magnetic fields. Thus, the beam quality correction factors for the two chambers (SNC600c, SNC125c) in high energy photon beams and (SNC600c, SNC125c, SNC350p) in high energy electron beams were calculated according to dosimetry protocols such as TG-51, TRS 398 and DIN 6800-2. Additionally, it has been confirmed using the Fano cavity test that the Monte Carlo codes have a high degree of accuracy (0.1%) in the presence of a magnetic field. After that, the various responses of the two chambers (SNC600c, SNC125c) in the presence of external magnetic fields as well as the magnetic field correction factors $k_{B,Q}$ were investigated experimentally and using Monte Carlo simulations. It was found that the calculations and experimental findings were in good agreement. The correction factor $k_{B,Q}$ is highly dependent on the chambers sensitive volume and orientation of the chamber axis with respect to the external magnetic field and the beam direction. It was also found that the change of response in the presence of magnetic field of the large chamber

SNC600c was greater than that of the small chamber SNC125c, and the response change of both chambers is minimal when the magnetic field direction and chamber axis align and are perpendicular to the beam direction.

In conclusion, this study covered an important part of the dosimetry in external magnetic fields and confirmed the possibility of using the two studied ionization chambers to accurately measure doses in the presence of magnetic fields after applying the magnetic field correction factors.

Contents

List of Figures

Abbreviations

AAPM	American Association of Physicists in Medicine
CT	Computed Tomography
CTV	Clinical Target Volume
EGSnrc	Electron Gamma Shower, National Research Council of Canada
FFF	Flattening Filter-Free
GTV	Gross Target Volume
GEANT4	GEometry ANd Tracking
IAEA	International Atomic Energy Agency
ICRU	International Commission on Radiation Units and Measurements
IMRT	Intensity-Modulated Radiation Therapy
IPSS	Intermediate Phase Space Scoring
MC	Monte Carlo
MLC	Multi-Leaf Collimator
MRI	Magnetic Resonance Imaging
MR-Linac	Magnetic Resonance-guided Linear Accelerator
NRC	National Research Council Canada
OAR	Organs At Risk
PET	Positron Emission Tomography
PTB	Physikalisch-Technische Bundesanstalt
PTV	Planning Target Volume
SCD	Source to Chamber Distance
SSD	Source to Surface Distance
TG-51	Task Group 51,from the American Association of Physicists in Medicine

THM	Technische Hochschule Mittelhessen
TRS-398	Technical Report Series No. 398 (TRS-398) from the International Atomic Energy Agency
VRT	Variance Reduction Techniques

1 Introduction

Radiation therapy aims to target and destroy cancer cells with minimal harm to healthy tissue. The conventional approach to radiation therapy involves external irradiation using (MV) photon beams generated by a linear accelerator (linac). The linac precisely administers the required dose to the tumor, with the photon beams interacting with tissues through three fundamental processes: the photoelectric effect, Compton scattering and the generation of electron-positron pairs. These processes have the potential to cause harm to both malignant cells and surrounding healthy tissue. Consequently, treatment sessions are typically divided into fractions. This division permits healthy cells to undergo repair and recovery between fractions, whereas cancerous cells are hindered from accomplishing such repair within the given time frame [Liauw et al., 2013].
Fig. 1.1 represents the tumor control and normal tissue damage probability curves as a function of dose; the therapeutic window is located between these curves [Podgorsak et al., 2005].

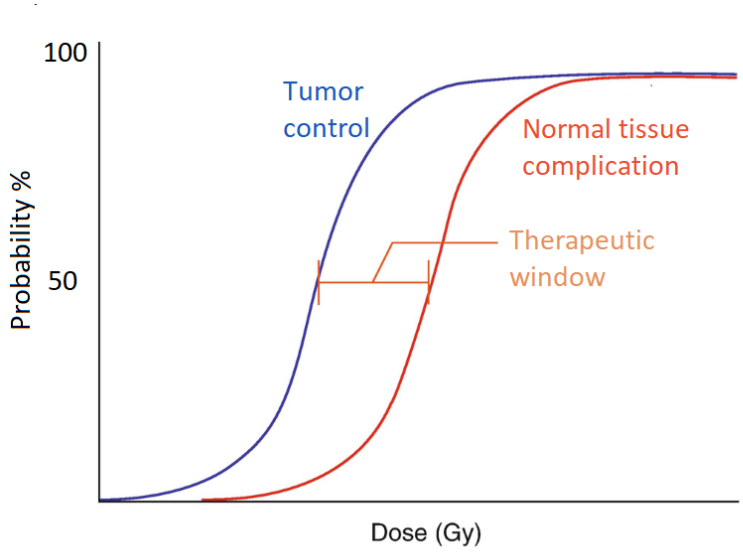

Figure 1.1: Relationship between the probability of tumor control and the likelihood of normal tissue complication.

Advanced imaging techniques such as Computed Tomography (CT), Magnetic Resonance

Imaging (MRI) and in specific cases, Positron Emission Tomography (PET) are essential to accurately determine the tumor's spatial position and dimensions. In radiation therapy, a challenge arises when imaging and treatment are done separately. However, these imaging techniques were not accompanied by treatment at the same time. This separation is problematic because internal organs can move due to physiological processes or changes in the patient's anatomy. For example, weight changes during treatment can affect the position of organs. This task complicates the accurate targeting of the tumor without affecting the surrounding healthy tissue. Key terms associated with tumor and target volumes are clearly defined: Gross Tumor Volume (GTV) is the visible or palpable extent of the tumor, and Clinical Target Volume (CTV) includes the GTV plus any areas likely to contain microscopic disease. Additionally, Organs at Risk (OARs) and Planning Target Volume (PTV) are identified. The PTV, designed to be larger than the CTV to account for potential tumor movement, ensures complete coverage despite tumor changes see Fig. 1.2. However, this intentional PTV enlargement presents a challenge: delivering necessary treatment accurately to the tumor while minimizing exposure of healthy tissue to excessive radiation [Burnet et al., 2004].

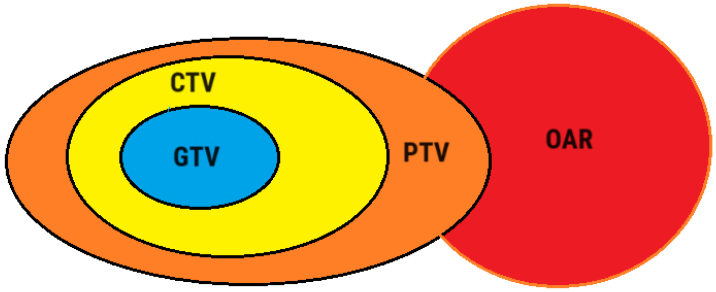

Figure 1.2: Schematic of a treated volume and organ at risk (OAR) located in the irradiated/patient volume. (PTV) a primary target volume, (CTV) a clinical target volume and (GTV) a gross tumour volume.

In the field of radiation therapy, many new methods have been developed to ensure that the tumors are targeted without damaging the healthy tissues. One notable method that has been introduced is called Intensity-Modulated Radiation Therapy (IMRT), a sophisticated approach that capitalizes on modern technologies such as multi-leaf collimators (MLCs) and complex treatment planning algorithms. IMRT facilitates the delivery of multiple photon beams from various angles, allowing for the modulation of beam intensities to conform to the contours of complex tumor shapes. This dynamic modulation ensures that high radiation doses are concentrated precisely within the tumor, while neighboring healthy tissues receive significantly reduced exposure. This approach not only enhances treatment efficacy but

also minimizes the risk of adverse effects on surrounding organs [Bortfeld, 2006]. In the context of smaller tumors, the evolution of treatment strategies has led to the prominence of stereotactic radiotherapy. This technique capitalizes on advancements in imaging and treatment delivery precision, enabling the administration of highly focused, non-uniform radiation fields. By concentrating a higher percentage of the total radiation dose onto a confined area within the patient, stereotactic radiotherapy maximizes its impact on the tumor while minimizing exposure to healthy tissues. The strategic implementation of this approach is especially valuable for cases where conventional surgery may be impractical or risky [Bortfeld, 2006]. In tandem with these therapeutic advancements, the realm of radiation devices has witnessed a transformative development: the emergence of Flattening Filter-Free (FFF) linear accelerators linacs. Unlike their predecessors, "FFF-linacs" omit the traditional flattening filter, resulting in a higher dose rate and reduced production of scattered radiation. This innovative design enhances treatment efficiency by accelerating the delivery of radiation, thus minimizing the time patients spend under the beam. Additionally, the reduction in scattered radiation contributes to diminishing the risk of unnecessary radiation exposure to healthy tissues, aligning with the overarching objective of personalized and precise treatment [Georg et al., 2011]. A significant advancement in radiation therapy devices is the introduction of Magnetic Resonance-guided Linear Accelerators (MR-linac). This combined technology merges a linear accelerator with the imaging capabilities of magnetic resonance imaging (MRI). The MRI's ability to visualize in real-time, especially with its high soft tissue contrast, is beneficial in guiding radiation treatment. By monitoring anatomical changes as they happen, MR-linac allows for adaptive treatment planning, ensuring radiation is accurately targeted. A notable feature of MR-linac is the on-line imaging functionality, which doesn't add any extra imaging-induced dose to the patient [Lagendijk et al., 2008, 2014].

In the presence of magnetic fields, the trajectories of secondary electrons are influenced by the Lorentz force, causing them to follow a spiral motion. This motion results from the Lorentz force acting perpendicular to both the electron's velocity and the magnetic field lines. Such helical motion influences the dose distribution in water and alters the behavior of radiation detectors. Specifically, detectors like ionization chambers might respond differently in this magnetic environment. Considering these effects, dosimetry protocols, such as TG-51 from the American Association of Physicists in Medicine (AAPM), TRS 398 from the International Atomic Energy Agency (IAEA) and the German DIN 6800-2 dosimetry protocol, need to be reviewed and adjusted because of the magnetic fields. [Almond et al., 1999a, int, 2001, DIN 6800-2, 2020].

1.1 Aims and motivations

The primary objective of this doctoral research is to comprehensively investigate the effects of external magnetic fields on the dosimetry of high-energy photon beams.
The study was initiated by assessing the behavior of specific ionization chambers without the influence of magnetic fields. This assessment provided foundational knowledge on the chamber's typical behavior. Additionally, the beam quality correction factors k_Q for the investigated ionization chambers were determined. These factors are crucial in dosimetry to correct for the difference in chamber response between the user's beam quality Q and the reference beam quality, typically Co-60. They were calculated in accordance with dosimetry protocols TG-51, TRS 398, and DIN 6800-2 [Almond et al., 1999a, int, 2001, DIN 6800-2, 2020]. In the next phase of this work, the effects of external magnetic fields on the investigated ionization chambers for high-energy photon beams were examined. This was achieved through both experimental investigations and Monte Carlo simulations. The measurements were performed at the Physikalisch-Technische Bundesanstalt (PTB) in Braunschweig, Germany, while the simulations utilized the Monte Carlo code EGSnrc [Kawrakow et al., 2000] to explore the responses of ion chambers in various magnetic field strengths and orientations.
Given the significant reliance on Monte Carlo simulations in this research, ensuring the accuracy of these methods in simulating radiation transport within diverse materials, even in the presence of magnetic fields, is of paramount importance. In response to these challenges, this research employed the Fano cavity test to investigate radiation transport in the presence of magnetic fields. The test was conducted on the ionization chambers SNC125c and SNC600c that were the subject of this study. In addition, the Fano cavity test was extended to include a detailed study on the PTW31021 ionization chamber and the Si diode T60016. The purpose was to study charged particle transport in the materials of these detectors and to determine optimal step size restrictions for charged particle transport. After confirming the accuracy and reliability of the Monte Carlo simulation, the magnetic field correction factors $k_{B,Q}$ were determined across a variety of magnetic field strengths and directions. This comprehensive analysis also included differences in the dimensions of the sensitive volume of the ionization chamber. It is worth noting that the study resulted in valuable insights that led to the formulation of recommendations related to the optimal orientation of the ionization chamber in relation to the direction of the magnetic field and the path of the incident beam. These results contribute to a thorough understanding of the complex interaction between external magnetic fields and the behavior of the ionization chamber. Furthermore, there was an additional study conducted outside the purview of the thesis, involving the determination of beam quality correction factors for high-energy electron beams experimentally and through Monte Carlo calculations. It's important to clarify that the ionization chambers used in this supplementary study were

identical to those examined for photon radiation. Worth noting is that the determination of correction factors for electron radiation doses significantly enhances the overarching comprehension of dosimetry in diverse clinical scenarios. The outcomes of this work carry significant implications for the field of medical radiation therapy. This research sheds light on the intricate interplay between ionization chambers and external magnetic fields and to contribute to the refinement of dosimetry protocols.

1.2 Fundamentals of dosimetry

Typically, ionizing radiation can be classified as either directly or indirectly ionizing. Directly ionizing particles, such as electrons, protons, positrons or heavy charged particles, are charged particles that interact directly with the medium along their path within the material via Coulomb interactions. Additionally, uncharged particles like photons are considered indirectly ionizing radiation; they transfer energy to a charged particle, which then deposits energy in the medium [Rogers, 1995]. Consequently, the absorbed dose can be calculated or measured based on the imparted energy ϵ, which represents the energy deposited within a defined volume of the medium [Seltzer et al., 2014] :

$$\epsilon[J] = R_{\text{in}} - R_{\text{out}} + \sum Q \tag{1.1}$$

In which R_{in} is the radiant energy entering the specified volume, R_{out} is the radiant energy leaving the specified volume and $\sum Q$ is the rest mass to energy conversion within the specified volume.

Moreover, the energy imparted ϵ within a medium is a stochastic quantity for a real particle field [Attix, 2008]. The absorbed dose by a medium is defined as the mean energy conferred per unit mass in a volume:

$$D = \frac{d\bar{\epsilon}}{dm} \tag{1.2}$$

where $d\bar{\epsilon}$ represents the average energy imparted to the infinitesimally small mass dm.

To determine the dose absorbed in a medium, an instrument with a physical or chemical response to ionizing radiation is required and these responses must be proportional to the dose absorbed in the material. In teletherapy with photon beams generated by a linear accelerator, the reference dose is measured in water and ionizing radiation raises the water's temperature, which can be precisely measured using a water calorimeter with a thermistor and a Wheatstone bridge circuit. This temperature change is proportional to the amount of energy absorbed in the water. Consequently, the calorimeter is utilized to measure the absorbed dose in water and is the primary standard in radiation therapy, whereas it is not practical to use in clinical routine [Kubo, 1983]. Still, many materials, such as air, semiconductors and photographic films, could be utilized as radiation detectors [Andreo et al., 2017]. The principle of an ionization chamber is to generate ion pairs in

the air cavity and then capture the resulting charge with the electrodes [Krieger, 2011]. To calculate the cavity dose D_{cav}, the following equation has to be applied:

$$D_{\text{cav}} = \frac{Q_{ion}}{\rho \cdot V \cdot (1-g)} \cdot \frac{W_{air}}{e} \tag{1.3}$$

Where Q_{ion} is the measured charge, ρ is the cavity gas density, V is the cavity volume, g representing the fraction of energy lost to bremsstrahlung within the medium, W_{air} is the mean energy needed to create an ion pair in dry air and e is the elementary charge. In practice, it is difficult to determine the exact dimensions of the cavity volume of ionization chambers due to variations in manufacturing and the fact that the chamber itself perturbs the ionizing radiation field. Consequently, the ionization chambers must be calibrated before use. In accordance with dosimetry protocols as TG-51, TRS 398 and DIN 6800-2 [Andreo et al., 2006, Almond et al., 1999b, DIN 6800-2, 2020], the dose to water D_w in the absence of the detector must be determined from the dose in the sensitive volume of detectors or cavity D_{cav}, this conversion method is achieved by cavity theory.

1.3 Cavity theory

A cavity theory represents a relationship between the absorbed dose in a cavity medium D_{cav} and the absorbed dose D_w at the point of measurement within the water phantom for a given beam quality Q [Podgorsak et al., 2005]. This can be expressed by the following relation:

$$f(Q) = \frac{D_w}{D_{cav}} \tag{1.4}$$

The Bragg-Gray cavity theory was the first cavity theory to establish a relationship between an absorbed dose in a dosimeter and an absorbed dose in the medium containing the cavity. The Bragg-Gray condition states that the electron fluence does not change in its spectral and spatial distribution when the electrons enter the cavity from the surrounding medium. Consequently, it must be fulfilled:

- The size of the cavity is small in relation to the range of charged particles. This means that the cavity medium does not impact the electron fluence inside the surrounding medium, resulting in the electron fluence remaining constant and equivalent to the equilibrium fluence within surrounding medium.
- In the cavity, there are no occurrences of photon interactions. Consequently, the absorbed dose within the cavity is solely attributed to the deposition of charged particles as they traverse the cavity .i.e. no electrons are created or absorbed within the cavity.

Hence, the equation 1.3 can be used to calculate the dose ratio between the cavity and the medium surrounding the cavity:

$$\frac{D_{med}}{D_{cav}} = \frac{\int_0^{E_{max}} \Phi_{med}(S/\rho)_{med} dE}{\int_0^{E_{max}} \Phi_{cav}(S/\rho)_{cav} dE} = \frac{\int_0^{E_{max}} \Phi_{med}(S/\rho)_{med} dE}{\int_0^{E_{max}} \Phi_{med}(S/\rho)_{cav} dE} = (\frac{S}{\rho})_{med,cav} \tag{1.5}$$

(S/ρ) is the average unrestricted mass collision stopping power and D_{med} can be determined using the subsequent equation when charge Q is generated in a gas cavity by ionizing radiation :

$$D_{med} = \frac{Q}{m}(\frac{\bar{W}}{e})_{cav}(\frac{\bar{S}}{\rho})_{med,cav} \tag{1.6}$$

$(\frac{\bar{W}}{e})_{cav}$ is the average energy expended per unit charge generated within the cavity material [Attix, 2008]. In the Bragg-Gray theory, delta electrons produced from hard collisions within the sensitive cavity volume are not accounted for. A more comprehensive theoretical formulation that considers delta electrons with sufficient energy to induce further ionization was developed by Spencer and Attix [Spencer and Attix, 1955]. This theory also leans on the Bragg-Gray conditions. In Spencer and Attix's theory, the secondary electron fluence is divided into two categories based on an energy threshold Δ

- Secondary electrons having kinetic energies below the threshold Δ are characterized as slow electrons, they deposit their energy locally.
- Secondary electrons with energies equal to or greater than Δ are classified as fast electrons and are considered to be part of the electron spectrum.

The Spencer-Attix relation can be formulated as:

$$\frac{D_{med}}{D_{cav}} = s^{\Delta}_{med,cav} \tag{1.7}$$

$s^{\Delta}_{med,cav}$ is the ratio of the mean restricted mass collision stopping powers of the medium and the cavity.

$$s^{\Delta}_{med,cav} = \frac{\int_{\Delta}^{E_{kin,0}} \Phi^{e-}_{med}(E)(\frac{L}{\rho})_{\Delta,med} dE + TE_{med}}{\int_{\Delta}^{E_{kin,0}} \Phi^{e-}_{med}(E)(\frac{L}{\rho})_{\Delta,cav} dE + TE_{cav}} \tag{1.8}$$

where $(\frac{L}{\rho})_{\Delta}$ represents the restricted stopping power ratio with a threshold Δ, and Φ^{e-}_{med} represents the fluence of fast electrons. TE_{med} and TE_{cav} account for the energy deposition of electrons that fall below Δ while passing through the cavity, and they are known as track end terms [Nahum, 1978]. In the context of high-energy photons, the ratio of collision stopping powers between two media changes very gradually with energy, making the choice

of the cut-off energy minimally influential on the stopping power ratio from water to air. Typically, for Farmer-type ionization chambers used in radiation therapy, a threshold of 10 keV is sufficient [Podgorsak et al., 2005].
In practice, real ionization chambers result in fluence perturbations as the chambers consist of other materials than water. Therefore, to confirm the absorbed dose in specific depth z in water, the measured dose in the chamber must be corrected by the perturbations p_Q according to this equation:

$$D_w(z) = D_{chamber}\ s^{\Delta}_{w,air}\ p_Q = \frac{Q}{m}\ (\frac{\bar{W}}{e})\ s^{\Delta}_{w,air}\ p_{repl}\ p_{cel}\ p_{wall}\ p_{stem} \tag{1.9}$$

with

- p_{repl} : perturbation factor arises from the multiplication of two factors, p_{cav} and p_{dis}. The p_{cav} factor corrects the ionization chamber's response for air cavity-related effects, mainly electron in-scattering, which causes a different electron fluence inside the cavity compared to the surrounding medium without the cavity. The p_{dis} factor addresses the impact of replacing a volume of water with the detector cavity concerning the chamber's reference point.
- p_{cell} : perturbation factor that adjusts the ionization chamber response for the impact of the central electrode during measurements in high-energy photon beams within a phantom.
- p_{wall} : perturbation factor for compensating the response of an ionization chamber due to the material non-equivalence between the chamber wall and any waterproofing material.
- p_{stem} : The chamber stem perturbation factor is a factor that accounts for the perturbation caused by the presence of the chamber's stem.

1.4 Reference dosimetry

The aim of dosimetric procedures is to guarantee that the patient obtains the prescribed dose. To achieve this objective, it is necessary to specify calibration coefficients and correction factors to convert the measured signal in the detector to dose. As measurement conditions vary, they must be well defined, standardized reference conditions in order to ensure that the measurement results of various institutions are comparable. For the fulfillment of these conditions, national and international protocols have been established [Andreo et al., 2002]. Current protocols outline how to determine the absorbed dose to water in clinical dosimetry using calibrated ionization chambers for external radiation

therapy. In both German protocol DIN6800-2 and the international dosimetry protocol TRS 398 [DIN 6800-2, 2020, Andreo et al., 2006], the beam quality Q is determined by the tissue phantom ratio TPR_{10}^{20}. This ratio represents dosimeter readings at 10 cm and 20 cm depths, maintaining a constant source to chamber distance (SCD) within a water phantom. Meanwhile, in TG-51, beam quality Q is described as the percentage value of the relative dose at a depth of 10 cm, normalized to the maximum depth dose $\%dd(10)_x$ under absence of contaminant electrons [Almond et al., 1999a].
Because of production variations, the exact air cavity volume in the chambers may not be precisely known. Therefore, instead of directly using the cavity theory, these calibrated chambers are employed. It is also worth noting that the chamber's structure can disturb the radiation field, as previously mentioned. Hence, a calibration coefficient is considered necessary. The absorbed dose to water for a reference beam quality Q_0 (typically ^{60}Co) at a reference depth z_{ref} in the absence of the chamber is given by:

$$D_{w,Q_0} = M_{Q_0} \cdot N_{D,w,Q_0} \tag{1.10}$$

The calibration coefficient N_{D,w,Q_0} is required to have traceability to a primary standard laboratory, this coefficient correlates the dosimeter reading M_{Q_0} from the ionization chamber and electrometer, to the dose to water D_w under standardized conditions within a reference field. These conditions take into account factors such as air pressure, temperature, field dimensions, measurement depth, phantom size and the beam quality Q_0 of the incident beam. The geometrical reference conditions to photon beams are given in table 1.1.

Table 1.1: Reference conditions for the determintion of absorbed dose [Andreo et al., 2002].

Influencing Quantity	**beam quality Q_0 (^{60}Co)**	**beam quality Q**
Measurement Depth	5 cm	10 cm
Phantom Size	$30 \times 30 \times 30\,\text{cm}^3$	$30 \times 30 \times 30\,\text{cm}^3$
Source to Surface Distance (SSD)	95 cm	100 cm
Field Size	$10 \times 10\,\text{cm}^2$ (at ref)	$10 \times 10\,\text{cm}^2$ (at SSD)
Temperature (T_0)	293.15 K	
Pressure (P_0)	101.325 kPa	

Typically, it is feasible to maintain only a limited number of the prescribed reference conditions within a user's beam.Thus, corrections are made for deviations caused by influence quantities by multiplying correction factors of two classes. The initial category accounts for variations in beam quality relative to the reference beam quality Q_0, which is usually ^{60}Co. Therefore, the dose to water within a user's beam, as determined by an ionization chamber dosimeter, is represented as

$$D_{w,Q} = M_Q^\star \cdot k_{T,p} \cdot k_{pol} \cdot k_s \cdot k_Q \cdot N_{D_w,Q_0} \tag{1.11}$$

Where:

- $M_Q^\star$ is the uncorrected reading of the dosimeter.
- $k_{T,p} = \frac{TP_0}{T_0P}$ is the temperature and pressure correction, where T and P represent the measured temperature and pressure, respectively, while The reference temperature T_0 is set at 293.15 K and the reference pressure P_0 at 101.325 kPa. This correction accounts for the effect of air mass variations in the chamber on the measured charge under different temperature and pressure conditions.
- $k_{pol} = \frac{|M_+|+|M_-|}{2M}$ is the polarity correction with chamber reading M for positive and negative polarity.
- k_s is the incomplete charge collection correction, caused by ion recombination in the cavity volume.
- k_Q is the beam quality correction factor, to correct for the different chamber response between the user's beam quality Q and the reference beam quality Q_0.

.

According to the Spencer-Attix theory, the correction factor can be calculated as the ratio of the calibration factors:

$$k_Q = \frac{N_{D,w,Q}}{N_{D,w,Co60}} = \frac{(s^\Delta_{w,a} \cdot p_{cel} \cdot p_{wall} \cdot p_{repl} \cdot p_{stem})_Q}{(s^\Delta_{w,a} \cdot p_{cel} \cdot p_{wall} \cdot p_{repl} \cdot p_{stem})_{Co60}} \tag{1.12}$$

Or, in its simplified form:

$$k_Q = \frac{N_{D,w,Q}}{N_{D,w,Co60}} = \frac{D_{w,Q}}{D_{w,Q_0}} \cdot \frac{M_{Q_0}}{M_Q} \tag{1.13}$$

Dosimetry protocols provide the correction factor k_Q for different ionization chambers and beam qualities.

1.5 Dosimetry in the presence of magnetic fields

The intense magnetic field of the MR-linac influences secondary electrons via Lorentz force. So electrons are deflected perpendicular to the magnetic field and the direction of electron motion according to equation 1.14. As a result, electron trajectories become spirals with varying radi (see Fig. 1.3).

$$\overrightarrow{F_L} = e\overrightarrow{v} \times \overrightarrow{B} \tag{1.14}$$

e is the elementary charge, v is the velocity of the electron and $\overrightarrow{B}$ is the magnetic field strength. The radius of curvature of electron trajectories can be calculated using the

centrifugal force equation 1.15.

$$F_z = \frac{mv^2}{r} \tag{1.15}$$

In relativistic case $m = \gamma m_0$, $\gamma = \frac{1}{\sqrt{1-\left(\frac{v}{c}\right)^2}}$ and the relativistic kinetic energy $E_{kin,rel} = m_0c^2 \cdot (\gamma - 1)$. Thus, the radius can be expressed as:

$$r = \frac{mv}{eB} = \frac{m_0\gamma\beta c}{eB}\sqrt{1 - \frac{1}{\gamma^2}} \tag{1.16}$$

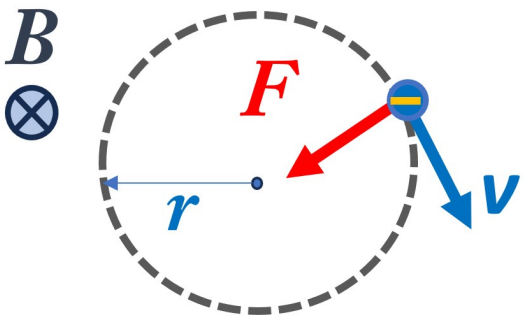

Figure 1.3: Electron deflection onto a circular track due to a perpendicular magnetic field and electron velocity.

In the field of high-energy photon radiation dosimetry, the Lorentz force affects both the number of electrons reaching the sensitive volume of the ionization chamber and the average lengths of the trajectories of the secondary electrons. This alteration depends on factors such as the beam's energy, the magnetic field strength, the orientation of the chamber in relation to the magnetic field, beam directions and the chamber's material composition [Delfs et al., 2021].

In light of the preceding, it is necessary to develop protocols for dosimetry in magnetic fields. As was mentioned in the previous section, dose to water determined in equation 1.11:

$$D_{w,Q} = M_Q N_{D,w,Q_0} k_Q \tag{1.17}$$

In which M_Q is the reading of the dosimeter corrected for influence quantities such as polarity, air density and ion combination, N_{D,w,Q_0} is the calibration coefficient under standard reference conditions for the beam quality Q_0, k_Q is the beam quality correction factor considering the energy dependence of the detector dose response between the beam quality Q_0 and Q. To take the magnetic field into account, the correction factor $k_{B,Q}$ can be added to the last equation [Smit et al., 2013]:

$$D_w^B = M_Q^B N_{D,w,Q_0} k_Q k_{B,Q} \tag{1.18}$$

Where D_w^B is the absorbed dose to water in a presence of magnetic field, M_w^B is the dosimeter reading at beam quality Q in the presence of magnetic field B. From the two previous equations, 1.18 and 1.17, and the replacement of the measured charges M_Q and M_B^Q with the scored dose per incident fluence on the phantom $\bar{D}_{det,Q}$ and $\bar{D}_{det,Q}^B$ in the air filled cavity of the ion chamber model without and with an external magnetic field, the magnetic field correction factor $k_{B,Q}$ is given as [O'Brien et al., 2016b]:

$$k_{B,Q} = \frac{D_{w,Q}^B}{D_{w,Q}} \cdot \frac{\bar{D}_{det,Q}}{\bar{D}_{det,Q}^B} \tag{1.19}$$

1.6 Monte Carlo simulations

The Monte Carlo method is a statistical technique for numerical integration based on the use of random numbers. The first descriptions and implementations of this technique were introduced in 1777 by Comte de Buffon [Buffon, 1777, Kalos and Whitlock], but the term "Monte Carlo" wasn't introduced until 1947 [Seco and Verhaegen, 2013]. In the Monte Carlo simulation of radiation transport, each microscopic particle interaction with matter is simulated with its corresponding probability distribution in order to derive a macroscopic distribution of quantities such as dose. The random trajectories of particles can be characterized by sampling from the underlying probability distributions based on the differential cross sections of the interaction mechanisms. In accordance with the central limit theorem, the Monte Carlo result follows a Gaussian distribution and the uncertainty of the mean σ decreases as the sample size or number of fundamental particles N increases [Bielajew, 2001].

$$\sigma \propto \frac{1}{\sqrt{N}} \tag{1.20}$$

Monte Carlo simulations are able to accurately calculate dose distributions in heterogeneous density geometries. Consequently, they are extensively used in medical physics to calculate doses in treatment planning, to simulate clinical linear accelerators and ionization chambers [Wang and Rogers, 2009, Muir and Rogers, 2010a, Czarnecki and Zink, 2013, Benmakhlouf et al., 2014, Gomà et al., 2016], as well as for image correction and patient dose calculation in diagnostic X-ray examinations [Chan and Doi, 1985, DeMarco et al., 2005]. Considering that Monte Carlo methods are stochastic techniques, a statistical uncertainty must be incorporated into the results. By increasing the number of statistically unrelated particles, the uncertainty can be reduced; as a consequence, the computation time also increases [Bielajew, 2001], therefore, the Monte Carlo efficiency is computed using the following equation :

$$\epsilon \propto \frac{1}{\sigma^2 \cdot T} \tag{1.21}$$

Where σ^2 is the variance of the simulation result, T represents the computation time needed

to obtain this variance σ^2, T is directly proportional to the number of simulated particles N. This thesis employed the EGS (Electron Gamma Shower) Monte Carlo simulation [Kawrakow et al., 2000]. EGS is a specialized Monte Carlo code developed for simulating the transportation of electrons and photons within various geometries, accommodating particle energies ranging from 1 keV to several hundred GeV [Kawrakow et al., 2017].

Simulation efficiency is one of the primary challenges of Monte Carlo simulation; therefore, variance reduction techniques (VRT) have been devised to improve simulation efficiency [Wulff et al., 2008].

Photon splitting

When an electron strikes the target in a typical MC simulation, it generates one bremsstrahlung photon, which is rendered as one photon in the simulation and has a statistical weight of $w = 1$. In contrast, when particle splitting is considered, this photon is sampled as multiple independent bremsstrahlung photons and each photon will have a statistical weight of $w = 1/N_{split}$. In other words, as the number of particles increased, so did the probability of dose deposition. As a result, the dividing technique shortens the time required for the production of multiple photons and the simulation of the transport of additional electrons [Kawrakow and Fippel, 2000].

Russian roulette

Russian roulette is the opposite of uniform particle splitting, despite the fact that both techniques are used in tandem. In this technique, a decision is made whether each particle survives or is annihilated. If a particle survives, the statistical weight of the surviving particle must be increased by the inverse of the probability of survival to account for those eliminated. This process effectively decreases the number of particles in the simulation, thereby reducing simulation time. It's crucial to note that particles not surviving the Russian roulette game are completely removed from the simulation, which is a key aspect of reducing the computational load [Kawrakow et al., 2017].

Range rejection

In this technique, the maximum range of the charged particle within the region material is compared to the shortest distance between its location and the region boundary. If this range is smaller than the distance (i.e., the charged particle's kinetic energy is too low), then the charged particle can never exit this region and it makes sense to finish the simulation. However, this method is an approximation of the physics of charged particle transport, as bremsstrahlung is disregarded [Kawrakow et al., 2017].

Cross section enhancement

This method involves enhancing the photon cross-section of an air cavity inside water. This decreases the mean free path length of the photons, resulting in an increase in the electron fluence generated along the photon path.

Correlated sampling and intermediate phase space scoring (IPSS)

To calculate the depth dose curves and profiles in a water phantom, the ionization chamber

must be simulated at various depths multiple times, which is time-consuming, despite the fact that a simple change in the chamber's position does not substantially affect the results. This technique permits the definition of a virtual geometry containing all chamber positions and the storage of the phase space of all particles entering this volume and the simulations of the various chamber positions are conducted consecutively, utilizing the stored phase space as the source.

1.7 Fano cavity test

Fano's theorem, as stated in 1954 proposes that "in a medium of a given composition exposed to a uniform flux of primary radiation, the flux of secondary radiation will also be uniform and independent of the density of the medium" [Fano, 1954]. To understand the essence of this principle, envision an infinite medium characterized by a consistent chemical composition and atomic interaction properties. In such a medium, ionizing radiation, namely electrons, transmits uniformly. This uniformity continues even if the medium's mass density changes at different points. Consequently, the emitted particle fluence is proportional to the local mass density. Under these conditions, the theorem holds that the angular- and energy-dependent electron fluence is identical everywhere. Additionally, given that the properties of atomic interactions are also constant, the absorbed dose D is the same everywhere [Sempau and Andreo, 2006].

This principle is applicable to an ion chamber subjected to an external photon field, as long as photon attenuation in the cavity walls and variations in chemical composition and atomic interaction properties are negligible. In an optimal scenario, the generation of secondary electrons would occur with a probability per unit volume that is directly proportional to the mass density. While this case does not reflect the real situation, it is possible to exactly reproduce Fano conditions by bypassing the primary photons and directly simulating the secondary electrons as source in Monte Carlo simulations.Thus the Fano conditions can be used as a reference way to test the consistency of charged particle transport in Monte Carlo methods [Smyth, 1986].

To effectively implement Fano conditions within the EGSnrc Monte Carlo code, detectors must be placed within a water phantom. This setup ensures that every point within the water phantom acts as an electron source. Therefore, it is crucial that the phantom's dimensions are sufficient to establish charged particle equilibrium for the detectors. At the same time, the radiation source should be configured to emit particles and their emission should be directly proportional to the local mass density. It's noteworthy that these particles are emitted in orientations that are uniformly distributed across the entire solid angle 4π.

In order to fulfill the aforementioned Fano requirements, it is necessary to replace every material included in the detector geometry with an identical atomic composition, while also taking into account the density of the original material. This ensures that all regions inside

the detectors have the same density correction factors and average ionization potential (I-value).

By applying the conditions, the simulated outcomes can be contrasted with the expected results derived from Fano's theorem. Through this, the condensed history of the Monte Carlo code can be assessed using the equation:

$$D_{MC,i} = n_i \frac{E_0}{m_i} \tag{1.22}$$

Here $D_{MC,i}$ represents the absorbed dose calculated via Monte Carlo calculations, m_i is the mass of region i, E_0 is the initial particle energy, n_i is the number of particles emitted from the Fano source.

In the context of magnetic fields, charged particle trajectories become intricate due to the influence of the Lorentz force. This complexity implies that the conventional Fano cavity theorem isn't directly applicable for the transport of these charged particles. However, it can be effectively applied using the conditions previously described [Bouchard et al., 2015]. Current Monte Carlo algorithms, which are intended to simulate charged particle transport in these external magnetic fields, contain inherent approximations that can potentially affect electron trajectories. When the scattering of charged particles and their deflection due to a magnetic field are considered discrete entities, it becomes crucial to observe that the step size of the charged particle must be limited. Failure to adhere to this restriction may result in particle transport biases. This is notably true when multiple interactions within a single transport step are combined, a phenomenon known as the condensed history step. So the accuracy of the adaptive Fano cavity test is highly affected by the electron step size.

The EGSnrc uses two distinct macros to transport charged particles in external magnetic field.

The first, *emf_macros.mortran* ('EMF'), has been a part of EGSnrc since its evolution from EGS4 and is based on the theory of Bielajew [Bielajew, 1993a]. The second macro, *eemf_macros.mortran* ('EEMF'), which is more refined, was introduced by Malkov and Rogers in 2017 [Malkov and Rogers, 2016]. These algorithms provide improved management of particle scattering near interfaces in the presence of a Lorentz force, as well as a superior mechanism for boundary crossing. Both of these enhancements are intended to address the difficulties encountered when particles traverse boundaries [De Pooter et al., 2015]. However, when employing the 'EMF' macros in EGSnrc and utilizing the appropriate electron step size, an accuracy of up to 0.1% can be achieved. Additionally, this level of accuracy was also observed with the Geant4 Monte Carlo code,[O'Brien et al., 2016a] and PENELOPE code demonstrated an accuracy of 0.3% [De Pooter et al., 2015].

2 Summary of the published results

2.1 Publication 1
Monte Carlo calculated beam quality correction factors for two cylindrical ionization chambers in photon beams

2.1.1 Summary of publication 1

The goal of this study was to investigate the SNC600c and SNC125c ionization chambers and provide data for various dosimetry protocols, including TG-51, TRS 398 and DIN 6800-2 [Almond et al., 1999a, int, 2001, DIN 6800-2, 2020]. Despite their widespread global clinical use, there were no existing quality correction factors k_Q for these chambers before this work. To address this, two independent research institutions, THM (University of Applied Sciences in Giessen, Germany) and NRC (National Research Council Canada, Ottawa, Canada), conducted the beam quality correction factors k_Q for the chambers both experimentally and through the Monte Carlo code EGSnrc. In the context of TG-51, the k_Q values are presented as a function of the beam quality parameter $\%dd(10)_x$, while for the TRS 398 and DIN 6800-2 protocols, they are presented in relation to the beam quality parameter TPR_{10}^{20} [Almond et al., 1999a, int, 2001, DIN 6800-2, 2020].

In this study, the Monte Carlo model for the SNC600c chamber differs from the model presented by the NRC Report [McEwen and Muir, 2021]. The wall thickness at the chamber's top is a bit thicker in the THM model, and the chamber stem also varies minimally. However, the dimensions of the sensitive volume and electrode are similar (see Fig. 1 in publication 1). Despite these differences, there was high agreement between the simulation results, which agreed with the experimental values of the NRC results (see Fig. 2 in publication 1).

Additionally, the k_Q values of the SNC600c chamber in the current study exhibited agreement with those obtained in other studies involving the PTW 30012 chamber [Aalbers et al., 2003, McEwen, 2010, Muir and Rogers, 2010b]. Both chambers share a sensitive volume with a radius of 3.05 mm and a length of 23.1 mm, featuring an aluminum electrode with

a radius of 1.1 mm and a graphite wall measuring 0.42 mm in thickness. It is worth noting that the PTW 30012 chamber is not waterproof and includes a PMMA sleeve, setting it apart from the chamber under investigation. Nevertheless, the effect of the 1 mm thick waterproof PMMA sleeve is particularly noticeable in photon beams with energies greater than 10 MV. It was found that the greatest impact of the PMMA sleeve does not exceed 0.3%, as noted by [Ross and Shortt, 1992, McEwen, 2010].

In addition, the correction factors k_Q for the SNC125c chamber were calculated and compared with both the NRC Monte Carlo simulations and the calorimetric measurements from the NRC Report [Muir and McEwen, 2021]. The results of k_Q were compared with two similar ionization chambers. The first is the Exradin A1SL (Standard Imaging, Middleton, Wisconsin) with a sensitive volume of 0.053 cm^3 [Muir and Rogers, 2010b], and the second chamber is the IBA CC13 (Schwarzenbruck,Germany) with a sensitive volume of 0.13 cm^3 [Andreo et al., 2020]. Furthermore, the studied chamber has sensitive volume of 0.125 cm^3. As expected and in line with the TG-51 dosimetry protocol recommendations, the result confirms that similar ionization chambers have comparable beam quality correction factors k_Q and it is possible to use a similar chamber when data for the utilized chamber is unavailable.

According to the DIN 6800-2 dosimetry protocol, the effective point of measurement needs to be shifted by half the inner radius of the chamber. This is because the chamber displaces a certain volume of water, leading to two primary effects. Firstly, the chamber's air cavity reduced attenuation compared to water, which increased the chamber reading. In contrast, there's less scatter in the chamber's cavity than in the surrounding water, which reduces the chamber reading [Podgorsak et al., 2005]. While TRS 398 does not implement this shift, the values of k_Q according to DIN 6800-2 are found to be greater than those in TRS 398, and this difference decreases with increasing photon energy. (see Fig. 2b and 3b in publication 1). Furthermore, a Fano test was performed on all regions in the two ionization chambers described in section 1.7. The results showed that all regions successfully passed the Fano test.

2.1.2 Contribution

M.Alissa simulated ion chambers in this study

M.Alissa and D.Czarnecki wrote the manuscript.

Experimental measurements and part of the simulations were done at National Research Council, Ottawa, Canada by F.Tessier.

A.A.Schoenfeld provided us with all the required data about the ionization chambers and established the contact to the National Research Council, Ottawa, Canada.

D.Czarnecki and K. Zink supervised this work and supported designing the study.

All authors revised this manuscript, substantively.

2.2 Publication 2
Investigation of Monte Carlo simulations of the electron transport in external magnetic fields using Fano cavity test

2.2.1 Summary of publication 2

In this study, a Fano cavity test was conducted using EGSnrc to evaluate the accuracy of electron transport algorithms within magnetic fields. To provide a more comprehensive coverage of the subject, different detectors were selected than those used in other studies in this work, including SNC600c and SNC125c, and it should be noted that a Fano test was also conducted on these detectors (see Fig. 4 in publication 1 and Fig. A.1 in publication 3). The detectors chosen for this study were the SemiFlex 3D ionization chamber (PTW 31021) and the diode detector (PTW T60016), both of which were sourced from PTW, Freiburg, Germany. Detailed data provided by the manufacturer was used to model these detectors. Furthermore, the ionization chamber has a sensitive air volume of 0.07 cm^3, an aluminum electrode with a radius of 0.04 cm, and a wall made of graphite and PMMA. The diode detector has a sensitive volume made of silicon, measuring 3.4x$10^{-4}$$cm^3$. In the Monte Carlo modeling, the ionization chamber was divided into 47 regions, while 30 regions were identified for the diode detector (see Fig 2 in publication 2). To meet the Fano test requirements, all materials in the examined detector geometries were replaced with water, holding onto the original material's density.

In addition, the particle source `egs_fano_source` from the EGSnrc C++ class library was employed, and the default magnetic field setting provided by *emf_macros.mortran* ('EMF') were used [Bielajew, 1993a].

Initially, the Fano test was applied in absence of magnetic field and the relative difference in absorbed dose from the theoretical value under Fano conditions was examined as a function of EM ESTEPE for both detectors. Using monoenergetic electrons of 1 MeV as the radiation source, it was found that the difference between the calculated dose and the theoretical value for all geometrical regions of the studied ionization chamber is less than 0.1%. Furthermore, for each region of the diode, the difference was less than 0.02%. These results were obtained for a maximum fractional energy loss per step value EM ESTEPE of 0.25 (see Fig. 3 in publication 2).

These simulations were also conducted in the presence of an external magnetic field, with a strength of B = 1.5 T, oriented perpendicular to the detector's symmetry axis. For the diode T60016, when using an EM ESTEPE value of 0.25, the deviation from the expected theoretical dose to the calculated dose was 0.11% within the silicon-sensitive volume. In

certain regions, the deviation peaked at 0.17%. However, the average difference across all regions hovered around 0.1%. When EM ESTEPE was reduced to 0.025, there was a significant shift in the results. Specifically, the deviation between the theoretical and calculated doses in the sensitive region shrank to 0.05%, and the highest deviation in any diode region did not exceed 0.06% (see Fig. 4 in publication 2). This observation implies that an EM ESTEPE value of 0.025 or lower is apt for analyzing diode responses in magnetic fields. Further reductions in EM ESTEPE to 0.005 showed that the gap between the projected theoretical and computational outcomes remained below 0.02%.

In the studied ion chamber PTW 31021, the sensitive volume is represented by two distinct regions. When setting the EM ESTEPE at 0.25, one of these regions displayed the most substantial relative difference between the Monte Carlo and theoretical values, peaking at 8%. However, by adjusting the EM ESTEPE downward to 0.1, this discrepancy was reduced to 2.4%. A further reduction of the EM ESTEPE to 0.05 diminished the difference to a mere 1.1%. Additionally, when the EM ESTEPE was set at 0.01, the mean value of the relative difference in absorbed dose from the theoretical value for the two air-filled regions of the chamber stabilized at 0.03%. This data suggests that an EM ESTEPE value of 0.01 is optimal, consistently keeping the difference below 0.1% (see Fig. 6 in publication 2).

The effect of different electron energies on the success of the Fano cavity test was thoroughly explored within the geometric regions of the PTW 31021 ionization chamber. The study specifically focused on three distinct initial electron energies: 0.1 MeV, 1 MeV, and 6 MeV. It became evident that the 6 MeV initial electron energy produced the smallest discrepancies between the Monte Carlo-based results and the theoretical expectations. However, electrons with lower initial energies demonstrated more significant differences. In particular, with an EM ESTEPE set at 0.01, the discrepancies for the 0.1 MeV electron energy exceeded 0.1%. This finding indicates that conventional Fano test parameters may not be universally optimal across all energies. To obtain acceptable results, especially for the 0.1 MeV electron energy, it was imperative to adjust the EM ESTEPE value. Setting it to 0.005 effectively minimized the differences, ensuring they remained below 0.1% throughout all regions of the ionization chamber (see Fig. 8 in publication 2). The study's results distinctly showed that for both the PTW 31021 and PTW T60016 detectors, decreasing the EM ESTEPE value led to a corresponding increase in simulation time. Specifically, for the PTW 31021 chamber, reducing the EM ESTEPE value from 0.25 to 0.005 caused the simulation time to jump from 2565 hours to 5350 hours. At the same time, the efficiency declined from 3.22 to 1.54. Nevertheless, the standard deviation remained stable, hovering around 0.011% (see table 3 in publication 2). For the PTW T60016, the efficiency experienced a sharper decrease, shifting from 18.83 at an EM ESTEPE of 0.25 down to 11.06 at 0.005. Concurrently, the simulation time grew from 3320 hours to 5649 hours. Remarkably, its standard deviation was consistently around 0.004%. In the absence of a magnetic field, the PTW 31021 chamber, using an EM ESTEPE value of 0.25, registered a simulation time of 2656 hours

and achieved an efficiency of 4.65. Conversely, the PTW T60016 chamber showed the same simulation duration of 2656 hours but had a notably higher efficiency, reaching 23.53. Based on the findings, choosing the right EM ESTEPE value is vital. It's essential to maintain a balance between the computation time and the efficiency of the simulation.

2.2.2 Contribution

M.Alissa simulated the detectors in this study.
M.Alissa and D.Czarnecki wrote the manuscript.
D.Czarnecki and K. Zink supervised this work and supported designing the study.
All authors revised this manuscript, substantively.

2.3 Publication 3
Experimental and Monte Carlo-based determination of magnetic field correction factors $k_{B,Q}$ in high-energy photon fields for two ionization chambers

2.3.1 Summary of publication 3

In this study, the response of two ionization chambers, SNC125c and SNC600c under different magnetic field strengths and directions was investigated both through experiments and Monte Carlo simulations. Measurements were conducted at the German National Metrology Institute (PTB, Braunschweig, Germany). As seen in the section 2.1, the model of the two studied chambers was verified through independent Monte Carlo simulations and experimental data.

In the orientation labeled as (d), as depicted in (Fig. 2 in publication 3), the Lorentz force acts in a direction parallel to the chamber's axis. This force causes the secondary electrons to drift either towards the top or the stem of the chamber. For this specific orientation, the change of SNC125c response in a positive magnetic field strength of 0.8 T peaked at 1.9%. Conversely, in a negative magnetic field strength of -1.5 T, the change of response decreased to 0.5%. Moreover, the chamber's response changes by 0.7% and 0.8% at magnetic field strengths of 1.5 T and 0.35 T, respectively, as used in MR-linac devices. Additionally, a negative field strength of -0.35 T results in a response variation of 0.1% (see Fig. 4a in publication 3). Compared to the SNC125c, the SNC600c chamber shows a symmetrical response alteration in both positive and negative magnetic fields, peaking at 6.6% for 1 T and reducing to 4.1% at -1.5 T. The pronounced sensitivity of the SNC600c to magnetic field changes is a notable difference from the SNC125c (see Fig. 4b in publication 3). In configuration (c) as shown in (Fig. 2 in publication 3), the Lorentz force steers electrons towards the chamber's lateral wall, with the SNC125c displaying a largely symmetrical response change around zero magnetic field. As the field increases negatively, its response change decreases to 3.2% at -1.2 T, whereas a positive field direction first reduces the response variation to 2.6% at 0.8 T, then shows a slight increase. In contrast, the SNC600c's response diminishes to 6.2% at 1 T.

Consequently, for the previously mentioned orientations, there was a notable agreement between the experimental measurement results and the Monte Carlo simulation outcomes for the two studied ionization chambers (see Fig. 4c and 4d in publication 3).

In the orientation (a), the ion chamber's axis aligns with the magnetic field and is perpendicular to the beam direction. For this setup, the SNC600c chamber response varies by

less than 0.5%, and the SNC125c by less than 0.1% across all magnetic field strengths, as shown in (Fig. 4e and 4f in publication 3).

Building on the previous discussions about the orientations, this study also delved into determining magnetic field correction factors k_Q^B for two energy spectra, 6 MV and 7 MV. These determinations utilized two Set-Ups, the first was realized at the PTB facility with water phantom dimensions of 20 $\times$ 20 $\times$ 5.9 cm^3, a source surface distance (SSD) of 110 cm, and a surface chamber distance (SCD) of 120 cm. The second setup adhered to the TRS 398 protocol, as depicted in (Fig. 1 in publication 3). Interestingly, the discrepancy in k_Q^B between these two setups was slight, not exceeding 0.1%. The correction factors were assessed for the three orientations mentioned earlier, and the results indicated that the variations in these correction factors closely matched the chamber responses in the presence of a magnetic field. The first chamber orientation (d), is especially important in this study, because it effectively reverses the compartment stem effect in the sensitivity of the ionization compartment to magnetic fields. Still, as the magnetic field strength increased, both spectra exhibited a declining trend, reaching their lowest values around 1.2 T for SNC600c with $k_Q^B = 0.94$ and for SNC125c $k_Q^B = 0.98$ of 1 T (see Fig. 6a and 6b in publication 3) (Correction: In the figure within the paper, 'orientation c' should be referred to as 'orientation d'). In another orientation (a), which showed the least magnetic field influence on the ion chamber response, the magnetic field correction factor values ranged between 0.997 and 1 for SNC125c and between 0.993 and 1 for SNC600c (see Fig. 6e and 6f in publication 3).

This study also investigates the 'dead volume' inside the ionization chamber. This 'dead volume' denotes specific regions in the chamber that are electrically shielded, with a particular focus on areas near the chamber stem within its cavity. Electrons generated in these areas cannot move towards the central electrode due to the shielding, which means they don't contribute to the dosimeter's reading [De Pooter et al., 2015, Lee et al., 2018, Delfs et al., 2021]. To represent this 'dead volume' in computational models, the 'dead volume' was modeled as a slice with a certain thickness d, positioned directly above the guard ring. For the cylindrical chamber SNC125c, thicknesses of d values of 0.1 mm, 0.2 mm, and 0.3 mm were considered. For the SNC600c chamber, thicknesses were set at d values of 0.3 mm, 0.5 mm, and 0.7 mm. It's worth noting that the chosen slice thicknesses for the SNC600c were larger than those for the SNC125c, reflecting the SNC600c's larger chamber cavity. The dose was then scored in the active volume after excluding the slice of the designated thickness d. The greatest agreement was found between measurement and Monte Carlo simulation results for chambers with zero dead volume (see Fig. 5 in publication 3). This implies that the two studied ionization chambers, SNC125c and SNC600c, do not contain any dead volume. Consequently, the entire air cavity within these chambers is considered as a sensitive volume.

2.3.2 Contribution

M.Alissa simulated must of the ion chambers in this study.
M.Alissa and D.Czarnecki wrote the manuscript.
Experimental measurements done in German National Metrology Institute (PTB), Braunschweig, Germany by R. Kapsch, S. Frick, A.A.Schoenfeld, M.Alissa, D.Czarnecki,and K. Zink.
A.A.Schoenfeld provided us with all the required data about the ionization chambers
D.Czarnecki and K. Zink supervised this work and supported designing the study.
All authors revised this manuscript, substantively.

2.4 Publication 4
Monte Carlo calculated beam quality correction factors for high energy electron beams

2.4.1 Summary of publication 4

In this work, beam quality correction factors for electron beam reference dosimetry were calculated using different detectors: the farmer type SNC600c, the cylindrical ionization chamber SNC125c, and the planar parallel chamber SNC350p. All simulations were conducted in accordance with TRS 398 and AAPM TG-51 recommendations [Almond et al., 1999a, int, 2001] using the Monte Carlo code EGSnrc. The ICRU Report [Seltzer et al., 2014] was also referenced for density corrections related to water and graphite. The study evaluated the chambers' performance across electron spectra from 5 MeV to 22 MeV by comparing experimental results with Monte Carlo simulations.For high-energy electron beam dosimetry, the reference depth z_{ref} is a fundamental parameter, defined according to the dosimetry protocols of TRS 398 and the TG-51 from AAPM by the following equation:

$$z_{\text{ref}} = 0.6\, R_{50} - 0.1\,\text{g cm}^{-2} \tag{2.1}$$

Here, R_{50} is the beam quality specifier in high-energy electron beams, defined as the depth at which the electron dose drops to 50% of its maximum value. There are two approaches to calculate the beam quality correction factor. The first approach is based on the reference beam quality ^{60}Co and can be calculated as given in equation 2.2:

$$k_Q = \left(\frac{D_w}{D_{det}}\right)_Q \Big/ \left(\frac{D_w}{D_{det}}\right)_{\text{Co-60}} \tag{2.2}$$

Where D_{det} represents the absorbed dose in the detector's sensitive volume, and D_w is the absorbed dose to water. The terms "^{60}Co" and "Q" indicate the beam qualities ^{60}Co and the specific beam quality, respectively.
The second approach utilizes an intermediate beam quality Q_{int}, which is recommended to have a depth dose R_{50} of 7.5 g/cm^2, as proposed by the dosimetry protocols TG-51 and TRS 398. Regarding the intermediate beam quality method, the correction factor $k_{Q,Q_{\text{int}}}$ is determined as:

$$k_{Q,Q_{int}} = \left(\frac{D_w}{D_{det}}\right)_Q \Big/ \left(\frac{D_w}{D_{det}}\right)_{Q_{int}} \tag{2.3}$$

Both the TRS 398 and TG-51 protocols provide distinct positioning guidelines for thimble ionization chambers. TG-51 places the chamber's reference point at z_{ref}, located at the cavity volume's center. On the other hand, TRS 398 recommends a position shifted downstream by half the chamber's air cavity radius. For the SNC350p parallel plate

chamber, the reference is set at the inner surface of its entrance window, factoring in the window material's density [Almond et al., 1999a, int, 2001].

The simulation results for the SNC125c chamber show that, across all R_{50} values, the results with the shift of the chamber according to TRS 398 are consistently higher compared to those for TG-51. Notably, at $R_{50} = 2.091$ g/cm^2, the highest difference is seen, approximately 0.69%. However, as R_{50} increases, these differences gradually decrease. At $R_{50} = 7.711$ g/cm^2, the lowest difference is achieved, at just 0.32%. With the increase in R_{50} values, the effect of the shift of the chamber becomes more pronounced, ultimately resulting in the smallest difference observed in the simulations. In comparison with the simulation results for the SNC600c chamber, the shift has a more pronounced effect on the SNC125c chamber.

For the ionization chamber SNC350p, there were notable agreements between the simulation and measurement results. The most significant deviation was observed at $R_{50} = 8.075$ g/cm^2 with a difference of 1.85%. However, the closest match was at $R_{50} = 6.014$ g/cm^2, showing only a 0.18% difference. Generally, as R_{50} values rise, deviations between Monte Carlo simulation and measurements become more pronounced.

Furthermore, upon comparing the Monte Carlo calculated values with experimental measurements and published data from NRC Reports for all investigated chambers, a significant degree of agreement was observed.

2.4.2 Contribution

M.Alissa simulated the ion chambers in this study.

M.Alissa and D.Czarnecki wrote the manuscript.

Experimental measurements done in Helios University Hospital Wuppertal by A.Reoserc, V.Flatten.

A.A.Schoenfeld provided us with all the required data about the ionization chambers.

D.Czarnecki and K. Zink supervised this work and supported designing the study.

All authors revised this manuscript, substantively.

3 Discussion

The MR-linac represents a significant advancement in radiation therapy, combining precise MRI imaging with the targeted delivery of radiation doses through a linear accelerator. This integration allows real-time tumor monitoring during treatment. However, the presence of magnetic fields introduces specific challenges in dose measurement. The Lorentz force, induced by the magnetic field, can alter the trajectory of secondary electrons, complicating dose assessment. Ionization chambers, as standard tools for dose measurement, are directly affected by this phenomenon. The behavior of chambers in the magnetic field needs to be understood in detail and a protocol for dosimetry has to be developed.

Building upon this context, our study set out to examine the response of two thimble ionization chambers, SNC125c and SNC600c, to high-energy photon beams and the various factors influencing them. An essential first step was to investigate the behavior of these chambers in the absence of magnetic fields. Such a step is of paramount importance as it sets the base for understanding the behavior of the studied chambers when exposed to magnetic fields. It aids in identifying influential factors and determining whether the observed changes are inherently tied to the magnetic field or not. To delve further into this, we employed both Monte Carlo simulations and experimental approaches.

In addition, it's noteworthy that the beam quality correction factors for these chambers were not available into the dosimetry protocols. Thus, k_Q values calculated independently by two separate research teams, THM and NRC. This led to subtle design differences in the chambers. For instance, the wall of the SNC600 chamber was slightly thicker at the tip for one research group compared to the other. Additionally, variations were observed in the chamber's stem design (see Fig. 1 in publication 1). However, despite these differences in modeling, consistent results were achieved across both teams. This consistency indicates that the finer details of the ionization chamber's design do not significantly affect the correction factors. This aligns with what was found by Tantot et al. [Tantot and Seuntjens, 2008], in their study of the Farmer chamber Exradin A12 with a collecting volume of 0.64 cm^3. They found that both the detailed and simplified chamber models yielded results in agreement within 0.1%, with a relative uncertainty of 0.2%. For his simulations, they utilized the CAVRZnrc/EGSnrc Monte Carlo code for the simplified model and the CAVITY code for the more complex model. Muir and Rogers [Muir and Rogers, 2010a] also employed the Exradin A12 chamber and agreed with these findings. Hence, a Monte Carlo model for

an ionization chamber doesn't need to be overly complex in all parts, especially those located in the stem and away from the chamber's air cavity. This simplification, which involves simulating radiation transport across multiple small geometric regions, is particularly valid in the absence of a magnetic field. While using a simplified chamber model can significantly reduce computation time compared to a full chamber model, it still maintains accuracy. However, for photons in the keV range [Ubrich et al., 2008] or when a magnetic field is present, a more detailed modeling approach may be necessary. In addition to variations in chamber models, the new recommendations from the ICRU Report 90 play a significant role in influencing the beam quality correction factors. This report updates the mean excitation energy values for materials frequently utilized in radiation dosimetry, particularly graphite and liquid water. The results of this study were compared with various other studies that utilized correction factors from ICRU Report 37. This comparison underscores the impact of the ICRU Report 90 recommendations on the correction factors for reference dosimetry. [Czarnecki et al., 2018, Mainegra-Hing and Muir, 2018, Pimpinella et al., 2019].

Mainegra-Hing [Mainegra-Hing and Muir, 2018] observed differences in the dose to the chamber when comparing the recommendations of the ICRU Report 90 and the ICRU Report 37. The difference in dose for the NE2571 and Exradin A19 chambers were 0.39% and 0.37%, respectively. While it was around 0.15% for the PTW 30013 chamber, these observations were based on a $\%dd(10)_x = 58.4$. However, when evaluating the impact of the ICRU Report 90 recommendations on ion chamber response, it was observed that these recommendations have a relatively minor influence on the k_Q values. This minimal influence is attributed to the fact that k_Q is a ratio of two dose values, meaning that the effects of changes introduced by ICRU 90 nearly cancel each other out. Specifically, the maximum deviation in k_Q was 0.14% for the NE2571 chamber, which has a graphite wall thickness of 0.36 mm, and 0.13% for the PTW 30013 with a wall thickness of 0.09 mm. Given the graphite wall thicknesses of the two chambers examined in this study, the SNC600c and SNC125c (0.43 mm and 0.25 mm, respectively), similar effects are expected. Moreover, in dosimetry setups where the source-to-surface distance (SSD) is either 100 cm or 90 cm, no statistically significant difference in measured doses was found between the two protocols, suggesting that they can be used interchangeably without compromising result accuracy.

In light of this study's heavy reliance on Monte Carlo simulations using Egsnrc, especially in the presence of a magnetic field, the accuracy of the Montre Carlo results became paramount. The Fano test was extensively utilized, not only as a means to validate the accuracy of the results and the models of the ionization chambers but also to verify the deposition of charged particle energy in heterogeneous media. This thorough examination also encompassed the charged particle step algorithm within the specified geometry and the boundary crossing algorithm in the intricate details of the detectors. Indeed, the Fano test stands out as an exemplary method for such comprehensive verification.

By applying the Fano test in the absence of a magnetic field, it was demonstrated that

the deviation from the theoretical values of the Monte Carlo simulation was below 0.1% for all regions of the ionization chamber and below 0.02% for each diode region, with an EM ESTEPE value of 0.25 (see Fig. 6 and 7 in publication 2). This result is consistent with the findings of Ito et al. [Ito et al., 2022], who conducted a Fano test on geometries involving a gas disk sandwiched between two solid wall disks. Additionally, de Pooter et al. [De Pooter et al., 2015] carried out a Fano test on a Farmer-type ionization chamber with a 3.15 mm cavity diameter, a 24.1 mm cavity length and a wall thickness of 0.35 mm and their results aligned with the study's findings.

In the presence of a magnetic field, using the older EMF macros from [Bielajew, 1993b] with an appropriately chosen step size yields good results. The deviation from the theoretical values of the Monte Carlo simulation dose can be up to 0.1%, which is within the acceptable threshold for the Fano test. For the air cavity, achieving this level of correspondence between Monte Carlo results and the theoretical expected value requires an EM ESTEPE value below 0.01. On the other hand, for regions forming the electrode and the chamber wall, the Fano test is passed starting at an EM ESTEPE of 0.05. It's noteworthy that the diode passed the Fano test at a higher EM ESTEPE values than the ionization chamber. This can be attributed to the diode's effective material being silicon, which is denser than the ionization chamber's air cavity. Thus, the selected EM ESTEPE value, combined with the region's density and size, plays a significant role. The challenge of the Fano test increases as the material becomes less dense and its size becomes larger. Ito et al. [Ito et al., 2022] used the same macro but for the larger gas cavity and found 1% deviation from the theoretical values at an EM ESTEPE of 0.01 and a 2% difference at 0.2.

This study emphasized the significance of selecting the initial electron energy in a Fano test in order to maintain its validity in a realistic radiation field. Due to the deviation from theoretical values of the calculated dose in Egsnrc for electrons with a low energy (0.1 MeV), the parameter EM ESTEPE had to be set to 0.005 in order to pass the Fano test. As for high energy, EM ESTEPE $= 0.1$ is acceptable.

Furthermore, this research highlighted the balance that must be struck between accuracy and computational efficiency. The choice of EM ESTEPE, in particular, is pivotal. A decrease in the EMSTEPE value, while increasing accuracy, adversely impacts the calculation's efficiency. For instance, with the PTW 31021 chamber, the computation time increases by a factor of 2.5 when comparing an EM ESTEPE of 0.01 to an EM ESTEPE of 0.25 in order to achieve an accuracy of 0.1% in every region (see Table 3 in publication 1). This is further corroborated by the newer EEMF macros in EGSnrc from Malkov and Rogers [Malkov and Rogers, 2016], where the calculation time for a simplified NE2571 chamber model sees an approximate 50% increase. Consequently, based on these findings, an EM ESTEP of 0.01 was adopted for all simulations in the presence of magnetic fields in this study.

After a detailed examination of the ionization chambers in the absence of a magnetic field

and an assessment of the accuracy of Monte Carlo simulations in the presence of magnetic fields using the Fano test, this work focused on studying the effects of magnetic fields on these chambers. This investigation utilized a combination of experimental methods and Monte Carlo simulations to understand how chamber responses vary depending on the chamber model, magnetic field intensity, and field orientation. For the orientation in which the Lorentz force deflects electrons within the air or stem region of the SNC600c chamber, there is an increase in response to the magnetic field, peaking at 1 T with a 6.5% increase. However, this change in response decreases to 4.3% at 1.5 T (see Fig. 4.b in publication 3). A similar behavior was observed by Meijsing et al. [Meijsing et al., 2009] for the NE2571 chamber, with a maximum response increase of 8% around 1.0 T, followed by a decrease. Smit et al. [Smit et al., 2013] also documented comparable behavior, noting a decrease to 4.9% at 1.5 T for the same chamber. While the chambers exhibit similar behavior, variations in response magnitude can be attributed to differences in their construction.

On the other hand, Spindeldreier [Spindeldreier et al., 2017] investigated the impact of the chamber radii on their response in a photon beam in presence of a magnetic field. She simulated ion chambers with six different radii, ranging from 1 mm to 6 mm. The results showed that for a magnetic field of 1.5 T, the increase in response was 4.3% for the chamber with a radius of 3 mm. This result aligns with our study's findings, given the 3.05 mm radius of the SNC600c chamber. This response results from changes in the number of electrons reaching the sensitive volume and their path length within it. As the field strength increases, the path length of electrons in the chamber's sensitive volume gets longer. However, in a 1 T magnetic field for a chamber with a 3 mm radius, the electron radii become so small that the average path length starts to decrease within the chamber's effective cavity.

Additionally, in contrast to the SNC600c chamber, which exhibits symmetric responses to both positive and negative magnetic field directions, the SNC125c chamber displays asymmetry. This phenomenon can be attributed to the difference in the effective volume of the two chambers relative to the adjacent region near the chamber stem. While the radius of the two chambers is relatively similar, there is a noticeable difference in their lengths. As a result, the impact of the stem is more pronounced in the smaller chamber compared to the larger one. In this context, the smaller chamber shows an increase in response, peaking at 0.6% at 0.8 T, before gradually decreasing to 0.5% at 1.5 T (see Fig. 4.a in publication 3)

For other orientations of the magnetic field relative to the chamber axis and the incoming beam, labeled as orientation (c), a similar behavior was observed for both ion chambers (see Fig. 4.c and d in publication 3). This was attributed to the absence of the effect of the chamber stem on the response. The Lorentz force is responsible for directing electrons to the chamber's lateral wall, resulting in a geometry that's symmetrical with respect to the magnetic field's direction. In this particular orientation, the change in response is most

significant, peaking at 9% for the SNC600c and 4% for the SNC125c (see Fig. 4.c and d in publication 3).

Regarding the orientations examined in the study, orientation (a) (see Fig. 4.c and d in publication 3) was particularly significant. It showed that the magnetic field's effect on the chamber readings in this orientation is minimal. This characteristic makes orientation (a) suitable for clinical measurements. When considering the detector's readings, those taken in the presence of the magnetic field were almost identical to those taken in its absence. For the chamber in this orientation, the deviation observed was less than 0.6% for the SNC600c and less than 0.2% for the SNC125c (see Fig. 4.e and f in publication 3).

A significant aspect further explored in the study was the consideration of the geometric volume of the ion chamber cavity as the sensitive volume, instead of the actual collection volume. This difference between the cavity volume and the sensitive volume is due to the complex electric field distribution near the stem inside the chamber. Monte Carlo calculations might not capture these detailed electric field behaviors within the ion chamber [Miller et al., 2016]. It's worth noting that in the presence of a magnetic field, even a minor variation in volume can lead to significant changes in the ion chamber's response [Malkov and Rogers, 2017]. In this work the hypothetical dead volume was modeled in Monte Carlo simulation as a slice of varying thickness d above the guard ring for both cylindrical chambers, SNC125c and SNC600c. Different thicknesses were applied for each chamber, and the dose was recorded in the active volume minus the thickness d. The best agreement between the measurement results and the Monte Carlo simulations was observed in the absence of a dead volume for both chambers. As a result, the entire air volume of the chamber can be considered as the sensitive volume. This feature of the chamber arises because the guard electrode doesn't extend into the air cavity (see Fig. 5 in publication 3). In a study by Malkov and Rogers [Malkov and Rogers, 2017] examining the effective volume of various ion chambers, it was discovered that three of the smallest chambers, PTW 31010, PTW 31006, and Exradin A1SL, exhibited the most significant variations in response. These chambers, which have sizes comparable to that of the SNC125c chamber, showed a maximum deviation of 3.39% for Co-60 and 2% for 7 MeV photon sources when a volume of 1 mm from the stem was removed. The PTW30013 chamber, with a similar 0.607 cm^3 sensitive volume as the SNC600c, showed smaller response variations, with deviations of 0.6% and 0.46% for the mentioned photon sources. This difference in response was attributed to the ratio of dead volume to the total air cavity volume of the chamber and the radius of its sensitive volume. This explanation also helps to clarify why the stem has a more pronounced effect in the smaller chamber when a magnetic field is present, as discussed earlier.

In a comparison of the k_Q^B values between two different set-ups the PTB set-up, which involves an electromagnet coupled with an Elekta Precise linear accelerator (linac) at 6 MV, and the MR-linac a notable finding emerged. The difference in k_Q^B values for both chambers

was less than 0.2% across all magnetic field (B) values for orientation (d), as illustrated in Figure 6 in publication 3. This outcome is significant as it indicates that the PTB device can serve as a reliable alternative to the MR-linac for experimental measurements.

3.1 Monte Carlo calculated beam quality correction factors for high energy electron beams

Based on the TRS 398 and TG 51 dosimetry protocols, this study determines k_Q and $k_{Q,Q_{int}}$-values for reference dosimetry in high-energy electron beams. TRS 398 promotes the intercomparison of independent data sets from various research institutions in order to obtain high-quality k_Q data. This research can be used to enhance the precision and consistency of electron beam dosimetry. The data obtained for the studied chambers SNC350p and SNC600c are in good accord with the data publication in NRC reports IRS-1860r [McEwen, 2014] and IRS-2065 [Tessier, 2015], respectively. This investigation provides k_Q data for SNC600c, SNC125c, and SNC350p for the AAPM TG 51 and TRS 398 Dosimetry protocols. In addition, the values of $k_{Q,Q_{int}}$ are determined for a reference radiation quality of $R_{50} = 7.5$ g/cm^2. Regarding the density correction and the mean ionization energies of water and graphite, this study followed the updated recommendations of ICRU Report 90, whereas the NRC reports utilized the recommendations of ICRU Report 37. As demonstrated by previous studies, the excellent agreement between the data sets confirms that the updated recommendations have only minor effects in k_Q in electron reference dosimetry.

4 Conclusion

This study presents a comprehensive exploration of radiation dosimetry, emphasizing the behavior of two widely used ionization chambers in high-energy photon fields. Moreover, it delves into the specifics of ionization chamber in a presence of magnetic fields. In this regard, the response of the ionization chambers SNC600c and SNC125c in various magnetic field strengths and orientations was examined experimentally and numerically using the Monte Carlo EGSnrc code. In addition, magnetic field correction factors for use in national and international dosimetry protocols have been calculated.

Due to the lack of data for the studied ionization chambers, it was necessary to calculate the beam quality correction factor k_Q for high-energy photon beams. It used a wide range of clinical photon beams ranging from 4 MV to 25 MV, obtained according to various protocols such as TRS 398, DIN 6800-2, and TG-51. In addition, Monte Carlo simulations were used to calculate the electron beam quality correction factors k_Q and the intermediate beam quality $k_{Q,Qint}$ for the reference radiation quality of $R_{50} = 7.5$ g/cm^2 for three ionization chambers used in electron dosemetry, SNC600c and SNC350p. In addition, the recommendations of ICRU 90, which differ from those of ICRU 37, were adopted, regarding changes in the density correction parameter of graphite and water. The AAPM TG-268 report recommend the Fano test for Monte Carlo calculations of gaseous cavity detectors. In this work, the EMF-macro for the transport of charged particles in electro-magnetic fields of the EGSnrc code system was investigated, and various step size parameters EM ESTEPE are selected to adequately characterize this transport in external magnetic fields. This study demonstrates that the Fano cavity test is primarily used to verify the appropriateness of the chamber geometry and the accuracy of the particle transport algorithms in ionization chambers and diode detectors. The step size parameters EM ESTEPE $= 0.1$ for the diode and EM ESTEPE $= 0.01$ for the ion chamber produced satisfactory Fano test results for an external magnetic field. The differences between Monte Carlo-based dose values and analytical dose values are less than 0.1%. Consequently, these step sizes were adopted for all simulations in the present study. The findings of this study have significant implications for improving the accuracy of dose calculations in radiation therapy. The impact of external B-fields on the response of ion chambers SNC600c and SNC125c ionization chambers to magnetic fields with varied orientations were analyzed, and the magnetic field correction factors were computed experimentally and using the EGSnrc Monte Carlo code.

The significant alignment between the experimental and Monte Carlo data highlights the robustness of applying correction factors to measurements conducted using these ionization chambers in the presence of magnetic fields. This finding carries substantial importance within the scope of our study. It fosters confidence in the utility of Monte Carlo simulations and suggests the potential for substituting resource-intensive experiments with simulation-based approaches in future research endeavors. This transition promises increased efficiency and precision in the field of radiation dosimetry and related studies. With this key point in mind, the subsequent research focuses on a detailed analysis of how ionization chambers respond, a crucial element that highlights the importance of magnetic field orientation relative to the chamber and the radiation beam, chamber's sensitive volume, magnetic field intensities, and their relative orientation to the radiation beam. Notably, when the magnetic field is aligned parallel to the chamber axis and perpendicular to the beam axis, it minimizes response deviation. This discovery holds significant practical importance, strongly recommending this specific chamber orientation for clinical measurements. It plays a critical role in enhancing measurement accuracy and simplifying the setup process, potentially improving overall efficiency in clinical radiation dosimetry. In the orientation in which the Lorentz force directs electrons toward or away from the inactive volume near the chamber stem, it is necessary to determine the dead volume of the chambers. Therefore, the dead volumes were investigated by contrasting the results of experimental measurements and simulations of chambers with various dead volumes. It was discovered that neither chamber has an inactive volume, and the Monte Carlo-calculated correction factors are accurate and do not require adjustment.

References

Absorbed Dose Determination in External Beam Radiotherapy. Number TRS-398 in Technical Reports Series. International Atomic Energy Agency - IAEA, Vienna, 2001. ISBN 92-0-102200-X.

A. Aalbers, L. de Prez, and M. Pieksma. Dosimetry of high-energy photon beams with the NMi water calorimeter. In *Proc. Workshop on Recent Advances in Absorbed Dose Standards (ARPANSA, Melbourne, 19-21 August 2003)*, 2003.

P. R. Almond, P. J. Biggs, B. M. Coursey, W. F. Hanson, M. S. Huq, R. Nath, and D. W. Rogers. Aapm's tg-51 protocol for clinical reference dosimetry of high-energy photon and electron beams. *Medical physics*, 26(9):1847–1870, 1999a.

P. R. Almond, P. J. Biggs, B. M. Coursey, W. F. Hanson, M. S. Huq, R. Nath, and D. W. O. Rogers. AAPM's TG-51 protocol for clinical reference dosimetry of high-energy photon and electron beams. *Medical Physics*, 26(9):1847–1870, 1999b. doi: https://doi.org/10.1118/1.598691.

P. Andreo, M. S. Huq, M. Westermark, H. Song, A. Tilikidis, L. DeWerd, and K. Shortt. Protocols for the dosimetry of high-energy photon and electron beams: a comparison of the iaea trs-398 and previous international codes of practice. *Physics in Medicine & Biology*, 47(17):3033, 2002.

P. Andreo, D. T. Burns, K. Hohlfeld, M. S. Huq, T. Kanai, F. Laitano, V. Smyth, and V. Stefaan. *Absorbed Dose Determination in External Beam Radiotherapy: An International Code of Practice for Dosimetry Based on Standards of Absorbed Dose to Water; Technical Reports Series No. 398*. International Atomic Energy Agency, 2006.

P. Andreo, D. T. Burns, A. E. Nahum, J. Seuntjens, and F. H. Attix. *Fundamentals of ionizing radiation dosimetry*. John Wiley & Sons, 2017.

P. Andreo, D. T. Burns, R. P. Kapsch, M. McEwen, S. Vatnitsky, C. E. Andersen, F. Ballester, J. Borbinha, F. Delaunay, P. Francescon, M. D. Hanlon, L. Mirzakhanian, B. Muir, J. Ojala, C. P. Oliver, M. Pimpinella, M. Pinto, L. A. de Prez, J. Seuntjens, L. Sommier, P. Teles, J. Tikkanen, J. Vijande, and K. Zink. Determination of consensus

k_q values for megavoltage photon beams for the update of IAEA TRS-398. *Physics in Medicine & Biology*, 65(9):095011, may 2020. doi: $10.1088/1361\text{-}6560/\mathrm{ab807b}$.

F. H. Attix. *Introduction to radiological physics and radiation dosimetry*. John Wiley & Sons, 2008.

H. Benmakhlouf, J. Sempau, and P. Andreo. Output correction factors for nine small field detectors in 6 mv radiation therapy photon beams: a penelope monte carlo study. *Medical physics*, 41(4):041711, 2014.

A. F. Bielajew. The effect of strong longitudinal magnetic fields on dose deposition from electron and photon beams. *Medical Physics*, 20(4):1171–1179, 1993a. doi: https://doi.org/10.1118/1.597149. URL https://aapm.onlinelibrary.wiley.com/doi/abs/10.1118/1.597149.

A. F. Bielajew. The effect of strong longitudinal magnetic fields on dose deposition from electron and photon beams. *Medical physics*, 20(4):1171–1179, 1993b.

A. F. Bielajew. Fundamentals of the monte carlo method for neutral and charged particle transport. *The University of Michigan*, 1, 2001.

T. Bortfeld. Imrt: a review and preview. *Physics in Medicine & Biology*, 51(13):R363, 2006.

H. Bouchard, J. de Pooter, A. Bielajew, and S. Duane. Reference dosimetry in the presence of magnetic fields: conditions to validate monte carlo simulations. *Physics in Medicine & Biology*, 60(17):6639, 2015.

G. Buffon. Essai d'arithmétique morale, supplément à l'histoire naturell. *vol*, 4:1777, 1777.

N. G. Burnet, S. J. Thomas, K. E. Burton, and S. J. Jefferies. Defining the tumour and target volumes for radiotherapy. *Cancer Imaging*, 4(2):153, 2004.

H.-P. Chan and K. Doi. Physical characteristics of scattered radiation in diagnostic radiology: Monte carlo simulation studies. *Medical physics*, 12(2):152–165, 1985.

D. Czarnecki and K. Zink. Monte carlo calculated correction factors for diodes and ion chambers in small photon fields. *Physics in Medicine & Biology*, 58(8):2431, 2013.

D. Czarnecki, B. Poppe, and K. Zink. Impact of new icru report 90 recommendations on calculated correction factors for reference dosimetry. *Physics in Medicine & Biology*, 63 (15):155015, 2018.

J. De Pooter, L. De Prez, and H. Bouchard. Application of an adapted fano cavity test for Monte Carlo simulations in the presence of B-fields. *Physics in Medicine & Biology*, 60 (24):9313, 2015.

B. Delfs, I. Blum, T. Tekin, A.-B. Schönfeld, R. Kranzer, D. Poppinga, U. Giesen, F. Langner, R.-P. Kapsch, B. Poppe, et al. The role of the construction and sensitive volume of compact ionization chambers on the magnetic field-dependent dose response. *Medical Physics*, 48(8):4572–4585, 2021.

J. DeMarco, C. Cagnon, D. Cody, D. Stevens, C. H. McCollough, J. O'Daniel, and M. McNitt-Gray. A monte carlo based method to estimate radiation dose from multidetector ct (mdct): cylindrical and anthropomorphic phantoms. *Physics in medicine & biology*, 50(17):3989, 2005.

DIN 6800-2. *Procedures of dosimetry with probe-type detectors for photon and electron radiation - Part 2: Ionization chamber dosimetry of high energy photon and electron radiation*. DIN - Normenausschuss Radiologie (NAR), 2020.

U. Fano. Note on the bragg-gray cavity principle for measuring energy dissipation. *Radiation Research*, 1(3):237–240, 1954.

D. Georg, T. Knöös, and B. McClean. Current status and future perspective of flattening filter free photon beams. *Medical physics*, 38(3):1280–1293, 2011.

C. Gomà, P. Andreo, and J. Sempau. Monte carlo calculation of beam quality correction factors in proton beams using detailed simulation of ionization chambers. *Physics in Medicine & Biology*, 61(6):2389, 2016.

K. Ito, N. Kadoya, Y. Katsuta, S. Tanaka, S. Dobashi, K. Takeda, and K. Jingu. Evaluation of the electron transport algorithm in magnetic field in egs5 monte carlo code. *Physica Medica*, 93:46–51, 2022.

M. Kalos and P. Whitlock. Monte carlo methods. 2008.

I. Kawrakow and M. Fippel. Investigation of variance reduction techniques for monte carlo photon dose calculation using xvmc. *Physics in Medicine & Biology*, 45(8):2163, 2000.

I. Kawrakow, D. Rogers, E. Mainegra-Hing, F. Tessier, R. Townson, and B. Walters. Egsnrc toolkit for monte carlo simulation of ionizing radiation transport. *EGSnrc toolkit for Monte Carlo simulation of ionizing radiation transport*, 2000.

I. Kawrakow, E. Mainegra-Hing, D. Rogers, F. Tessier, and B. Walters. The egsnrc code system: Monte carlo simulation of electron and photon transport technical report pirs-701 (ottawa: National research council canada). 2017.

H. Krieger. *Strahlungsmessung und Dosimetrie*. Springer, 2011.

H. Kubo. Absorbed dose determination with a water calorimeter in comparison with an ionisation chamber. *Physics in Medicine & Biology*, 28(12):1391, 1983.

J. J. Lagendijk, B. W. Raaymakers, A. J. Raaijmakers, J. Overweg, K. J. Brown, E. M. Kerkhof, R. W. van der Put, B. Hårdemark, M. van Vulpen, and U. A. van der Heide. Mri/linac integration. *Radiotherapy and Oncology*, 86(1):25–29, 2008.

J. J. Lagendijk, B. W. Raaymakers, and M. Van Vulpen. The magnetic resonance imaging–linac system. In *Seminars in radiation oncology*, volume 24, pages 207–209. Elsevier, 2014.

J. Lee, J. Lee, D. Ryu, H. Lee, and S.-J. Ye. Fano cavity test for electron monte carlo transport algorithms in magnetic fields: comparison between egsnrc, penelope, mcnp6 and geant4. *Physics in Medicine & Biology*, 63(19):195013, 2018.

S. L. Liauw, P. P. Connell, and R. R. Weichselbaum. New paradigms and future challenges in radiation oncology: an update of biological targets and technology. *Science translational medicine*, 5(173):173sr2–173sr2, 2013.

E. Mainegra-Hing and B. R. Muir. On the impact of icru report 90 recommendations on kq factors for high-energy photon beams. *Medical Physics*, 45(8):3904–3908, 2018.

V. Malkov and D. Rogers. Charged particle transport in magnetic fields in EGSnrc. *Medical Physics*, 43(7):4447–4458, 2016.

V. N. Malkov and D. Rogers. Sensitive volume effects on monte carlo calculated ion chamber response in magnetic fields. *Medical Physics*, 44(9):4854–4858, 2017.

M. McEwen and B. Muir. Characterization of SNC 600c ionization chambers for measurements in linear accelerator photon beams. In *Report number – PIRS-3327 (National Research Council Canada, April 2021)*, 2021.

M. R. McEwen. Measurement of ionization chamber absorbed dose factors in megavoltage photon beams. *Medical Physics*, 37(5):2179–2193, 2010. doi: https://doi.org/10.1118/1.3375895.

T. McEwen. Characterization of a SNC350p parallel-plate ionization chamber for electron beam reference dosimetry. *National Research Council of Canada, Report IRS-1860r, Ottawa, Canada*, 2014.

I. Meijsing, B. Raaymakers, A. Raaijmakers, J. Kok, L. Hogeweg, B. Liu, and J. Lagendijk. Dosimetry for the mri accelerator: the impact of a magnetic field on the response of a farmer ne2571 ionization chamber. *Physics in Medicine & Biology*, 54(10):2993, 2009.

J. R. Miller, B. D. Hooten, J. A. Micka, and L. A. DeWerd. Polarity effects and apparent ion recombination in microionization chambers. *Medical physics*, 43(5):2141–2152, 2016.

B. Muir and M. McEwen. Characterization of SNC 125c ionization chambers for measurements in linear accelerator photon beams. In *Report number – PIRS-3224 (National Research Council Canada, January 2021)*, 2021.

B. Muir and D. Rogers. Monte carlo calculations of, the beam quality conversion factor. *Medical physics*, 37(11):5939–5950, 2010a.

B. R. Muir and D. W. O. Rogers. Monte Carlo calculations of k_q, the beam quality conversion factor. *Medical Physics*, 37(11):5939–5950, 2010b. doi: $\mathrm{https://doi.org/10.1118/1.3495537}$.

A. Nahum. Water/air mass stopping power ratios for megavoltage photon and electron beams. *Physics in Medicine & Biology*, 23(1):24, 1978.

D. O'Brien, D. Roberts, G. Ibbott, and G. O. Sawakuchi. Reference dosimetry in magnetic fields: formalism and ionization chamber correction factors. *Medical physics*, 43(8Part1): 4915–4927, 2016a.

D. J. O'Brien, D. A. Roberts, G. S. Ibbott, and G. O. Sawakuchi. Reference dosimetry in magnetic fields: formalism and ionization chamber correction factors. *Medical Physics*, 43(8Part1):4915–4927, 2016b.

M. Pimpinella, L. Silvi, and M. Pinto. Calculation of kq factors for farmer-type ionization chambers following the recent recommendations on new key dosimetry data. *Physica Medica*, 57:221–230, 2019.

E. B. Podgorsak et al. *Radiation oncology physics.* IAEA Vienna, 2005.

D. Rogers. Ionizing radiation dosimetry and medical physics. *Physics in Canada*, 51(4): 178–181, 1995.

C. Ross and K. Shortt. The effect of waterproofing sleeves on ionization chamber response. *Physics in Medicine & Biology*, 37(6):1403, 1992.

J. Seco and F. Verhaegen. *Monte Carlo techniques in radiation therapy*. CRC press Boca Raton, FL:, 2013.

S. M. Seltzer, J. M. Fernandez-Varea, P. Andreo, P. M. Bergstrom, Jr., D. T. Burns, I. Krajcar Bronic, C. K. Ross, and F. Salvat. Report 90: Key Data for Ionizing-Radiation Dosimetry: Measurement Standards and Applications. *Journal of the ICRU*, 14(1), 2014. ISSN 1742-3422.

J. Sempau and P. Andreo. Configuration of the electron transport algorithm of penelope to simulate ion chambers. *Physics in Medicine & Biology*, 51(14):3533, 2006.

K. Smit, B. Van Asselen, J. Kok, A. Aalbers, J. Lagendijk, and B. Raaymakers. Towards reference dosimetry for the MR-linac: magnetic field correction of the ionization chamber reading. *Physics in Medicine & Biology*, 58(17):5945, 2013.

V. G. Smyth. Interface effects in the monte carlo simulation of electron tracks. *Medical physics*, 13(2):196–200, 1986.

L. Spencer and F. H. Attix. A theory of cavity ionization. *Radiation research*, 3(3):239–254, 1955.

C. Spindeldreier, O. Schrenk, A. Bakenecker, I. Kawrakow, L. Burigo, C. Karger, S. Greilich, and A. Pfaffenberger. Radiation dosimetry in magnetic fields with farmer-type ionization chambers: determination of magnetic field correction factors for different magnetic field strengths and field orientations. *Physics in Medicine & Biology*, 62(16):6708, 2017.

L. Tantot and J. Seuntjens. Modelling ionization chamber response to nonstandard beam configurations. In *Journal of Physics: Conference Series*, volume 102, page 012023. IOP Publishing, 2008.

F. Tessier. Monte carlo calculation of the kq quality conversion factor for the snc600c ionization chamber for photon beam reference dosimetry. *NRCC Report Number: IRS-2066. Canada: National Research Council*, 2015.

F. Ubrich, J. Wulff, R. Kranzer, and K. Zink. Thimble ionization chambers in medium-energy x-ray beams and the role of constructive details of the central electrode: Monte carlo simulations and measurements. *Physics in Medicine & Biology*, 53(18):4893, 2008.

L. Wang and D. Rogers. The replacement correction factors for cylindrical chambers in high-energy photon beams. *Physics in Medicine & Biology*, 54(6):1609, 2009.

J. Wulff, K. Zink, and I. Kawrakow. Efficiency improvements for ion chamber calculations in high energy photon beams. *Medical physics*, 35(4):1328–1336, 2008.

Published Articles

In the following, the original articles are presented.

[1] Monte Carlo calculated beam quality correction factors for two cylindrical ionization chambers in photon beams.

page 44

[2] Investigation of Monte Carlo simulations of the electron transport in external magnetic fields using Fano cavity test.

page 51

[3] Experimental determination of modulation power of lung tissue for particle therapy

page 63

[4] Monte Carlo calculated beam quality correction factors for high energy electron beams

page 76

Physica Medica 94 (2022) 17–23

Contents lists available at ScienceDirect

Physica Medica

journal homepage: www.elsevier.com/locate/ejmp

Original paper

Monte Carlo calculated beam quality correction factors for two cylindrical ionization chambers in photon beams

Mohamad Alissa [a,*], Klemens Zink [a,b,c], Frédéric Tessier [d], Andreas A. Schoenfeld [e], Damian Czarnecki [a]

[a] Institute of Medical Physics and Radiation Protection, University of Applied Sciences Giessen (THM), Giessen, Germany
[b] Department of Radiotherapy and Radiation Oncology, University Medical Center Giessen and Marburg, Marburg, Germany
[c] Marburg Ionbeam Therapycenter (MIT), Marburg, Germany
[d] Ionization Radiation Standards, National Research Council, Ottawa, Canada
[e] Sun Nuclear Corporation, 3275 Suntree Blvd, Melbourne, Florida 32940 USA

ARTICLE INFO

Keywords:
Dosimetry
Beam quality correction factor
Ionization chamber
Monte Carlo simulation
MV photon beams

ABSTRACT

Purpose: Although several studies provide data for reference dosimetry, the SNC600c and SNC125c ionization chambers (Sun Nuclear Corporation, Melbourne, FL) are in clinical use worldwide for which no beam quality correction factors k_Q are available. The goal of this study was to calculate beam quality correction factors k_Q for these ionization chambers according to dosimetry protocols TG-51, TRS 398 and DIN 6800-2.
Methods: Monte Carlo simulations using EGSnrc have been performed to calculate the absorbed dose to water and the dose to air within the active volume of ionization chamber models. Both spectra and simulations of beam transport through linear accelerator head models were used as radiation sources for the Monte Carlo calculations.
Results: k_Q values as a function of the respective beam quality specifier Q were fitted against recommended equations for photon beam dosimetry in the range of 4 MV to 25 MV. The fitting curves through the calculated values showed a root mean square deviation between 0.0010 and 0.0017.
Conclusions: The investigated ionization chamber models (SNC600c, SNC125c) are not included in above mentioned dosimetry protocols, but are in clinical use worldwide. This study covered this knowledge gap and compared the calculated results with published k_Q values for similar ionization chambers. Agreements with published data were observed in the 95% confidence interval, confirming the use of data for similar ionization chambers, when there are no k_Q values available for a given ionization chamber.

1. Introduction

Ionization chamber measurements of the absorbed dose to water in high energy photon beams are described in national and international dosimetry protocols. Therein, the water calibration factor $N_{D,w,Co-60}$ and the beam quality correction factor k_Q, also called conversion factor k_Q, are used to determine the dose to water in photon fields of the radiation quality Q. The determination of k_Q values with high accuracy and the investigation of its influencing quantities are essential to reduce the uncertainties of dose measurements. However, k_Q values depend on the design and size of an ionization chamber, as well as on the materials of the chamber components.

Numerous research groups have published experimental and Monte Carlo based correction factors k_Q which may be used for an update of national and international dosimetry protocols [1–3]. Data sets obtained by Monte Carlo simulations and measurements at primary standards laboratories have been used to derive consensus data for beam quality correction factors k_Q according to the international dosimetry protocol TRS 398 of the IAEA (International Atomic Energy Agency) [4]. The underling study by Andreo et al. [4] summarized k_Q data of 23 widely used cylindrical ionization chamber types, but more chamber types are in clinical use worldwide. Moreover, k_Q values are only valid in the respective reference conditions, which vary between different dosimetry protocols.

In this Monte Carlo based study, the beam quality correction factor k_Q was calculated for a Farmer-type ionization chamber, the SNC600c, and a small volume ionization chamber, the SNC125c, both Sun Nuclear Corporation (Melbourne, FL). These ionization chambers are widely

* Corresponding author.
E-mail address: mohamad.alissa@lse.thm.de (M. Alissa).

https://doi.org/10.1016/j.ejmp.2021.12.012
Received 19 May 2021; Received in revised form 4 October 2021; Accepted 19 December 2021
Available online 28 December 2021

Table 1
Reference conditions used according to the dosimetry protocols TG-51, TRS 398 and DIN 6800-2 for high energy photon and ^{60}Co γ-beams. r_{cyl} denotes the radius of the cylindrical sensitive volume of the ionization chamber.

	High energy photon beams			^{60}Co γ-beam
Influencing quantity	TG-51	TRS 398	DIN 6800-2	
Beam quality specifier	$\%dd(10)_x$	TPR_{10}^{20}	TPR_{10}^{20}	–
Measurement depths		10 g/cm^2		5 g/cm^2
Field size at a 100 cm distance from source		10 × 10 cm^2		10 × 10 cm^2
Position of reference point of chamber	10 g/cm^2		10 g/cm^2+0.5r_{cyl}	5 g/cm^2
Source to phantom surface distance (SSD)		100 cm		95 cm
Source to chamber distance (SCD)		110 cm		100 cm

used in radiation therapy facilities. As far as we know, there are no k_Q values published for these ionization chambers in high energy photon beams. In such case, the TG-51 dosimetry protocol [2] of the American Association of Physicists in Medicine (AAPM) recommends to use available data of similar ionization chambers, where the wall material is the most critical property. The closest match to the chamber SNC600c is the Farmer-type ionization chamber PTW30012 (PTW, Freiburg, Germany). Both ionization chambers feature a Farmer type chamber design with a 0.43 mm graphite wall and 0.6 cm^3 active volume. However, the wall material of SNC600c is not pure graphite but rather resin impregnated graphite. There has been no clarity on how this may affect the correction factor k_Q and the uncertainty of dose measurements with the given ionization chamber. To address this knowledge gap, values for k_Q were calculated according to the dosimetry protocol TG-51 [2], TRS 398 [3] and DIN 6800-2 [1] of the German Institute for Standardization.

2. Materials and methods

2.1. The beam quality correction factor in dosimetry protocols

According to the ICRU Report 90 [5] it can be assumed that the average amount of energy W_{air} required to create an ion pair in dry air is constant for the investigated beam qualities Q. Therefore, the beam quality correction factor k_Q can be calculated using:

$$k_Q = \left(\frac{D_w}{D_{det}}\right)_Q \Big/ \left(\frac{D_w}{D_{det}}\right)_{^{60}Co} \tag{1}$$

where D_w is the absorbed dose to water at the reference depth and D_{det} is the absorbed dose in the sensitive volume of the ionization chamber. The input quantities of Equation (1) are calculated using Monte Carlo simulations. The indices Q and ^{60}Co represent the beam qualities of a high-energy photon beam and the ^{60}Co γ-ray beam, respectively. It should be noted that the calculated values D_w and D_{det} are determined under reference conditions defined respectively in the above mentioned dosimetry protocols. Table 1 summarizes the different reference conditions of the applied dosimetry protocols. The reference point given in Table 1 is on the long axis of the ionization chamber. All dosimetry protocols allow two different setups for reference dose measurements: a setup with a source to surface distance (SSD) of 100 cm and a setup with a source to chamber distance (SCD) of 100 cm. In this study we calculated the beam quality correction factor for the SSD = 100 cm setup. The impact of both setups on the k_Q values was investigated.

In the dosimetry protocols the beam quality correction factor k_Q is presented as a function of the beam quality specifier Q. In the international dosimetry protocol TRS 398 and the German dosimetry protocol DIN 6800-2 the beam quality specifier for high energy photon fields is the tissue phantom ratio TPR_{10}^{20}:

$$TPR_{10}^{20} = \frac{D_w^{SSD=80}(z = 20\text{ cm})}{D_w^{SSD=90}(z = 10\text{ cm})} \tag{2}$$

where $D_w^{SSD=80}(z = 20\text{ cm})$ is the dose to water in 20 cm water depth in a water phantom placed at a SSD of 80 cm and $D_w^{SSD=90}(z = 10\text{ cm})$ is the dose to water in 10 cm water depth and an SSD of 90 cm. The AAPM dosimetry protocol TG-51 uses $\%dd(10)_x$ as the beam quality specifier for high energy photon beams. According to the dosimetry protocol $\%dd(10)_x$ is the percentage depth dose at 10 cm depth in a water phantom placed at an SSD of 100 cm. Note that the depth dose curve is caused only by photon (e.g. all electrons reaching the water phantom from the linac are excluded from the radiation field). Both beam quality specifiers are measured in a 10 x 10 cm^2 radiation field. The Monte Carlo calculated beam quality specifiers were determined according to these definitions from Monte Carlo calculated absorbed dose to water.

2.2. Beam quality correction factor k_Q as a function of beam quality specifier Q

As proposed by Muir and Rogers [6], the beam quality correction factor k_Q can be fitted by a polynomial function of $\%dd(10)_x$:

$$k_Q = a + b\cdot10^{-3}\left(\%dd(10)_x\right) + c\cdot10^{-5}\left(\%dd(10)_x\right)^2 \tag{3}$$

This function has been included in the Addendum of the TG-51 dosimetry protocol [7].

The beam quality correction factor k_Q as a function of TPR_{10}^{20} was fitted according to Andreo et al. [4] using

$$k_Q\left(TPR_{10}^{20}\right) = \frac{1 + \exp\left(\frac{a-0.572}{b}\right)}{1 + \exp\left(\frac{a-TPR_{10}^{20}}{b}\right)} \tag{4}$$

According to Giménez-Alventosa et al. [8], the equation is very likely to be adopted in the upcoming TRS 398 update. The equation is designed to be unity at $TPR_{10}^{20} = 0.572$, i.e. the TPR_{10}^{20} value of ^{60}Co beam quality. The TPR_{10}^{20} value of ^{60}Co calculated by Monte Carlo simulation in this work is 0.571. However, the equation has not been adjusted for better comparability with literature.

To fit the k_Q values according to DIN 6800-2, the equation has to be extended by the additional fitting parameter k_{Co-60}. This parameter takes into account the influence of two different positioning of the ionization chamber during calibration and measurement. According to the dosimetry protocol DIN 6800-2, the gradient effect is corrected by a shift of the effective point of measurement when measuring in the clinical reference field with beam quality Q. However, an effective point of measurement shift is not applied under reference conditions for calibration at the beam quality of ^{60}Co. This results in a beam quality correction factor that is not unity at a beam quality Q which equals the beam quality of a ^{60}Co beam [1]. Thus, k_{Co-60} is the beam quality

Table 2
Summary of simulation properties and parameters with EGSnrc used by THM and NRC.

Item	Description	References
Code	EGSnrc code system,	Kawrakow et al. [9]
	egs++ library,	Kawrakow et al. [14]
	egs_chamber	Wulff et al. [15]
Validation	Fano cavity test	Results in Appendix
Timing	Absorbed dose to water D_w in the sensitive volume of chamber for photon spectra and full linac head simulations took 2800 and 11000 single CPU hours (2.1 GHz), respectively, for each energy and ionization chamber.	
Source description	Collimated isotropic MV photon energy spectra and full linac head simulations.	See Tables 3 and 4
Cross-sections	XCOM photon cross section with multiconfiguration DiracFock renormalization factor for the photoelectric effect (mcdf-xcom).	
Transport parameters	Boundary crossing algorithm: Exact; transport and particle production threshold energy of 512 keV (THM), 521 keV (NRC) for electrons and 1 keV (THM), 10 keV (NRC) for photons.	
Variance reduction techniques	Intermediate phase space storage (IPSS); Photon cross-section enhancement (XCSE) volume with an XCSE factor of 128 (THM), 32 (NRC) and Russian Roulette range rejection technique with a survival probability of 1/128 (THM), 1/64 (NRC).	Wulff et al. [15]
Scored quantities	Absorbed dose to water and dose to air	
Statistical uncertainties	⩽0.1% for all calculated quantities	
Statistical method	History-by-history	
Postprocessing	None	

Table 3
Photon beam radiation sources applied at THM.

Source		TPR_{10}^{20}	$\%dd(10)_x$
Linac head models			
Elekta Precise	6 MV	0.659	66.1
Siemens KD	15 MV	0.777	80.3
Varian Clinac	6 MV	0.659	66.1
	10 MV	0.735	73.7
	15 MV	0.758	78.0
	18 MV	0.780	82.4
Photon spectrum			
Varian Clinac [20]	4 MV	0.629	63.4
	6 MV	0.672	67.5
	10 MV	0.732	73.2
	15 MV	0.764	78.2
Varian Clinac [21]	4 MV	0.621	62.8
	6 MV	0.662	66.1
	10 MV	0.729	74.2
	15 MV	0.755	77.9
	18 MV	0.766	81.9

correction factor k_Q at $TPR_{10}^{20} = 0.572$, i.e. the beam quality of a ^{60}Co radiation source. This results in the following fit function for k_Q as a function of TPR_{10}^{20} for the dosimetry protocol DIN 6800-2:

$$k_Q\left(TPR_{10}^{20}\right) = k_{Co-60}\frac{1+\exp(\frac{a-0.572}{b})}{1+\exp(\frac{a-TPR_{10}^{20}}{b})} \quad (5)$$

It should be noted that the parameter a and b in Eq. (4) and (5) have different numerical values.

Table 4
Tabulated photon spectra applied at NRC.

Source		TPR_{10}^{20}	$\%dd(10)_x$
Varian Clinac [20]	4 MV	0.623	62.7
	6 MV	0.666	66.5
	10 MV	0.734	73.8
	15 MV	0.763	77.8
	18 MV	0.785	81.5
	24 MV	0.805	86.1
Siemens KD [21]	6 MV	0.671	67.0
	18 MV	0.762	77.7
Elekta SL25 [21]	6 MV	0.672	67.3
	25 MV	0.791	82.8

2.3. Monte Carlo simulation

The Monte Carlo calculations presented in this publication were performed with EGSnrc 2020 [9]. The EGSnrc code system was used, since it has been shown that EGSnrc is able to calculate the dose to the cavity of an ionization chamber with a systematic accuracy of 0.1% or better relative to the cross sections [10,11]. Moreover, EGSnrc is available with a wide range of applications designed for the simulation of the radiation transport through ionization chambers, such as variance reduction technics for an efficient dose calculation in ionization chambers in a high energy photon field [12]. The Monte Carlo calculations and the processing of the simulation results were performed independently by two research groups, THM (Technische Hochschule Mittelhessen University of Applied Sciences, Giessen, Germany) and NRC (National Research Council Canada, Ottawa, Canada). All details of the Monte Carlo simulations are summarized in Table 2 according to the recommendations of AAPM TG-268 [13].

2.3.1. Radiation sources

The research groups THM and NRC used different radiation sources, except for an overlap of benchmark sources available in literature.

At THM, particle transport simulations through linear accelerator head models, as well as MV photon spectra were used as radiation sources (see Table 3) for the Monte Carlo simulations. The Monte Carlo based linac head models have been investigated in previous studies [16–19]. Moreover, five standard photon spectra of a Varian Clinac, which were published by Mohan et al. [20] and are included in the standard EGSnrc installation, and five Varian Clinac photon spectra published by Sheikh-Bagheri and Rogers [21] were used as radiation sources.

The calculations at NRC were performed using an incident beam with spectral point sources of photons collimated to a field size of 10×10 cm^2 at isocenter. The tabulated spectral photon distributions were taken from Mohan et al. [20] as well as Sheikh-Bagheri and Rogers [21]. Table 4 summarizes all applied radiation sources and their respective beam quality specifiers TPR_{10}^{20} and $\%dd(10)_x$.

Comparing the radiation sources used by both research groups, a difference can be observed between the calculated beam quality specifiers in Table 3 and 4. The difference between the values of the beam quality specifier for the same radiation source may be explained by the statistical uncertainty of the Monte Carlo simulation (0.4%) and systematic uncertainties in the determination of the beam quality, e.g., the determination of the maximum of the depth dose curve. It should be emphasized that this difference does not have an impact on the determined functional relationship between k_Q and the beam quality specifiers TPR_{10}^{20} as well as $\%dd(10)_x$.

2.3.2. Ionization chamber models

Two different ionization chambers have been investigated - a "Farmer type" ionization chamber (SNC600c, Sun Nuclear Corporation, Melbourne, FL) and a "scanning" ionization chamber (SNC125c, Sun Nuclear Corporation, Melbourne, FL) with sensitive volumes of 0.6 cm^3

Table 5
A summary of the materials and geometric data of the ionization chambers.

Ionization chamber	Wall Material	Thickness	Central electrode Material	Radius	Sensitive volume Radius	Length
SNC125c	Graphite	0.25 mm	Al	0.4 mm	2.375 mm	7.05 mm
	PMMA	0.30 mm				
	Paint	0.05 mm				
SNC600c	Graphite	0.43 mm	Al	0.55 mm	3.05 mm	22.7 mm
	Paint	0.05 mm				

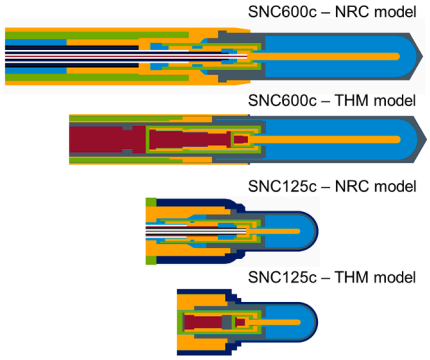

Fig. 1. Cross sections of the Monte Carlo based models of the investigated ionization chambers. The images of the chambers are not to scale. Different colors represent different materials.

and 0.1 cm^3, respectively. Table 5 lists further specifications of the investigated ionization chambers. Detailed ionization chamber models were built independently by THM and NRC according to manufacturer data using the egs++ class library [14].

The cross sections of the models are displayed in Fig. 1. The ionization chamber models of the two research groups differ in some details. In particular, the stem sections of the chambers were modeled in greater detail at NRC. Furthermore, it is noticeable that the chamber tip of the THM model of the SNC600c has a slightly thicker wall.

It should be noted that the SNC600c wall consists of resin impregnated graphite, while the chamber wall of the SNC125c is made of high purity graphite. Consequently, two different graphite materials were generated. The density effect correction for the two wall materials was used according to the recommendations of ICRU Report 90 [5]. The material properties of water were as specified in the ICRU Report 90 [5].

3. Results

Fig. 2 presents the beam quality correction factor k_Q for the SNC600c ionization chamber according to all considered dosimetry protocols TG-51, TRS 398 and DIN 6800-2. The data sets were calculated by THM and NRC independently. Fig. 2 (a) shows k_Q values as a function of the beam quality specifier $\%dd(10)_x$. The polynomial function proposed by Muir and Rogers [6] (see Eq. (3)) was fitted to the joint data sets calculated by THM as well as NRC. Fig. 2 (b) presents beam quality correction factors k_Q according to TRS 398 and DIN 6800-2 dosimetry protocols as a function of the beam quality specifier TPR_{10}^{20}. The values of k_Q according to DIN 6800-2 are greater than TRS 398 k_Q values due to the shift of the effective point of measurement. The k_Q values according to TRS 398 are fitted by the function given in Eq. (4) of the forthcoming update of TRS 398. The k_Q values for the DIN 6800-2 dosimetry protocol are fitted by the function given in Eq. (5). The presentation of all fit functions includes the 95% confidence interval indicated by a shaded area. The Monte Carlo calculated data are presented in comparison with calorimetric measurements of two SNC600c ionization chambers that have been taken from NRC Report PIRS 3327 [22].

Moreover, the calculated k_Q values in this work were compared to published data of the PTW 30012. Both ionization chambers have an aluminum electrode with an approximate diameter of 1.1 mm and a chamber wall made of graphite. It is worth noting that PTW 30012 is not waterproof. For a more realistic simulation Muir and Rogers [6] included a waterproof PMMA sleeve around the PTW 30012 model of 1 mm thickness. However, McEwen 2010 et al. [23] and Ross and Shortt et al. [24] have confirmed, that a 1 mm PMMA sleeve has a significant effect only for photon beam energies higher than 10 MV and is within 0.3% independent of the chamber within the sleeve.

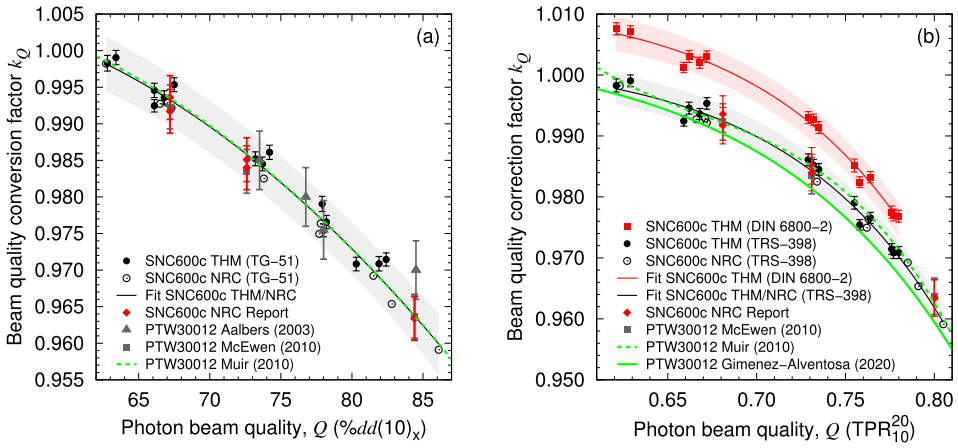

Fig. 2. Monte Carlo calculated beam quality correction factor k_Q for the Farmer-type ionization chamber SNC600c as a function of $\%dd(10)_x$ (a) and TPR_{10}^{20} (b). k_Q values were calculated independently by THM (black filled circles) and NRC (open black circles) using different radiation sources and chamber models. Figure (b) shows k_Q values according to the TRS 398 (black) and DIN 6800-2 dosimetry protocols (red). The error bars indicate the statistical uncertainties (1 σ). The statistical uncertainty of the NRC calculated values are within the symbol size. The fits describing the THM and NRC data sets are shown with 95% confidence intervals, as represented by the shaded areas. The results are compered to experimentally determined k_Q values (red diamonds) from the NRC Report [22]. Figure (a) and (b) additionally shows experimentally determined k_Q values of the similarly built PTW 30012 ionization chamber published by McEwen et al. [26]. Figure (a) also presents experimentally determined k_Q values for the PTW 30012 published by Aalbers et al. [25]. The error bars of the experimental data represent type A and B uncertainties. Fit functions of k_Q values of the PTW 30012 published by Muir and Rogers [6] and Giménez-Alventosa et al. [8] are represented by dashed green lines and solid green line, respectively.

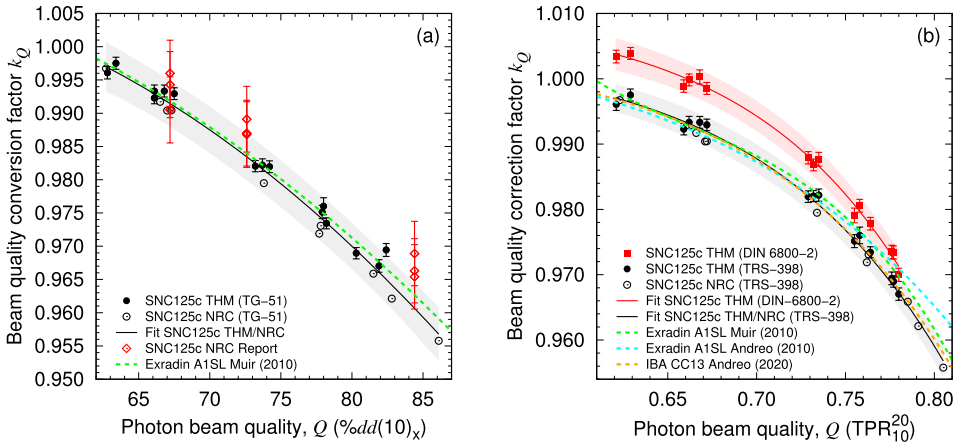

Fig. 3. Monte Carlo calculated beam quality correction factor k_Q of the SNC125c ionization chamber as a function of %dd(10)$_x$ (a) and TPR$^{20}_{10}$ (b). k_Q values were calculated independently by THM (black filled circles) and NRC (open black circles) using different radiation sources and chamber models. Figure (b) shows k_Q values according to the TRS 398 (black) and DIN 6800-2 dosimetry protocols (red). The error bars indicate the statistical uncertainties (1 σ). The statistical uncertainty of the NRC calculated values are within the symbol size. The fits describing the THM and NRC data sets are shown with 95% confidence intervals represented by the shaded areas. Figure (a) additionally shows experimentally determined k_Q values of the SNC125c chamber taken from the NRC Report PIRS-3224 [27]. The error bars of the experimental data represent type A and B uncertainties. The data sets are compared to fit functions published by Muir and Rogers [6] (dashed green line) and Andreo et al. [4] (dashed blue line) for the similar ionization chamber Exradin A1SL. The orange dashed line represents the fit function for the IBA CC13 ionization chamber taken from Andreo et al. [4].

Table 6
Fitting parameters of functions (3), (4) and (5) for the SNC600c and SNC125c ionization chambers.

Function	Parameter	SNC600c	SNC125c
k_Q(%dd(10)$_x$)	a	0.9468	0.9649
Eq. (3)	b	2.607	2.134
	c	−2.852	−2.589
k_Q(TPR$^{20}_{10}$)	a	1.068	1.097
Eq. (4)	b	−0.08485	−0.09749
k_Q(TPR$^{20}_{10}$)	k_{Co-60}	1.009	1.007
Eq. (5)	a	1.056	1.061
	b	−0.08386	−0.08721

In Fig. 2 (a) and (b), the polynomial fit of the PTW 30012's k_Q values published by Muir and Rogers [6] is represented by a dashed green line. The Monte Carlo calculated k_Q values in Fig. 2 are supported by calorimetric measurements published by Aalbers et al. [25] and McEwen [26]. In addition, the fitted k_Q data of the PTW 30012 published by Giménez-Alventosa et al. [8] is shown in Fig. 2 (b).

In analogy to Fig. 2, the correction factors k_Q for the SNC125c ionization chamber are presented in Fig. 3. The k_Q values calculated according to TG-51, TRS 398 and DIN 6800-2 were fitted by the corresponding functions, see Eqs. (3)–(5). The calculated k_Q values are compared to calorimetric measurements of three SNC125c ionization chambers reported in NRC Report PIRS 3224 [27]. As reference, Fig. 3 shows k_Q values of the similar Exradin A1SL ionization chamber (Standard Imaging, Middleton, Wisconsin) and IBA CC13 (Schwarzenbruck, Germany) displayed as fit function according to Muir and Rogers [6] and Andreo et al. [4]. All fit parameters calculated in this work are summarized in Table 6.

4. Discussion

4.1. Ionization chamber models

This study provides calculated k_Q data for reference dosimetry according to three different dosimetry protocols (TG-51, TRS 398 and DIN 6800-2). Beam quality correction factors k_Q according to the TG-51 and TRS 398 dosimetry protocols were calculated independently by two research groups (THM and NRC). The resulting data sets are in good agreement, although the underlying ionization chamber models of the research groups differed slightly (see Fig. 1). The provided technical drawings of manufacturers are often very detailed at some points and some aspects of the ionization chamber underlie fabrication tolerances or are even unknown. However mostly small details of an ionization chamber have no impact on the simulation results. On the other hand, a Monte Carlo model of an ionization chamber cannot be arbitrary complex, since this would result in a lot of small geometrical regions in which the radiation transport must be simulated. This would be computing time and RAM consuming with no significant gain in accuracy of the calculated result. For this reason, Monte Carlo based models may vary even when modeled with the same information provided by the manufacturer. During the creation of the Monte Carlo model of an ionization chamber the level of detail can be reduced in selected parts of the chamber without affecting the simulation results. These generalizations must often be made to improve computation time and reduce the number of potential errors. Consequently, the visual representation of a chamber model depends on the creator and can differ from other implementations. The extent to which an ionization chamber can be simplified without having a significant effect on the calculated k_Q values must be clarified in further investigations.

In this study we observed that the modeled cable in the chamber stem did not affect the dose within the cavity. In addition, we observed that the different wall thickness of the chamber tip as well as the small air gap around the guard ring had no significant effect on the beam quality correction factor k_Q.

It should be noted that the data from Muir and Rogers [6] referred in this work were published before the ICRU Report 90 [5]. Thus, the calculations were not performed according to the recommendations of the ICRU Report 90. However, Mainegra-Hing and Muir [28] have shown that the impact of changes in recommendations between ICRU Report 37 [29] and 90 [5] is less than 0.15% for k_Q values of a similar Farmer-type ionization chamber NE2571. Czarnecki et al. [30] achieved similar results, observing a maximum change of up to 0.35% for the highest investigated energy (24 MV, TPR$^{20}_{10}$ = 0.806). Additional calculations (not presented in this work) indicate that the change recommendations between ICRU Report 37 and 90 for the density correction parameter of graphite as well as the updated ionization constants of graphite and water result in a difference of the k_Q values of up to 0.5% for the SNC600c ionization chamber. The increased impact of the ICRU Report 90 recommendation on k_Q values of the SNC600c may be due to the thicker graphite chamber wall compered to the NE2571.

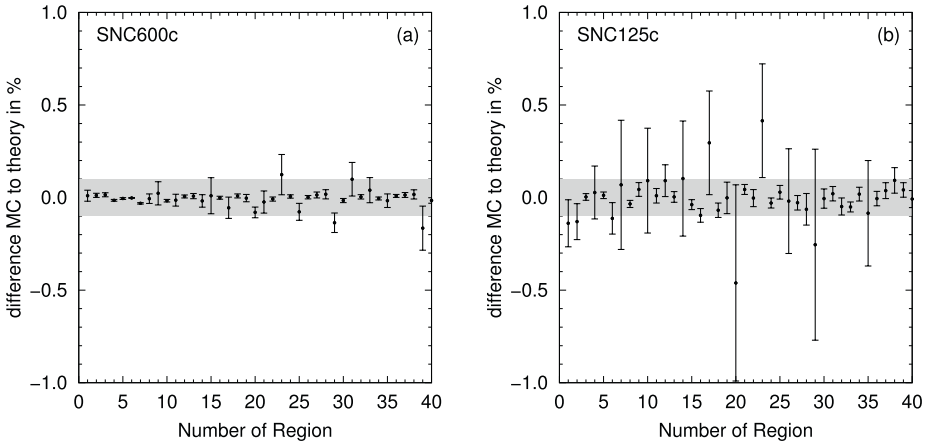

Fig. 4. Results of the Fano cavity test for the SNC600c and SNC125c. The left and right panels show the relative deviation from the expected value for each geometrical region in the ionisation chamber modell SNC600c and SNC125c, respectively.

4.2. Beam quality correction factors for different dosimetry protocols

A source to surface distance (SSD) of 100 cm was chosen for all simulations presented in this study. Further investigations were made showing no significant difference between calculated k_Q values at SSD = 100 cm and SCD = 100 cm (SSD = 90 cm).

The k_Q values of the large-volume SNC600c ionization chamber calculated with a full treatment head as a particle source are systematically smaller than those with collimated isotropic spectra as particle sources. This effect has been investigated in previous studies [30,31] and can be traced back to the volume averaging effect. Therefore, this systematic deviation of the k_Q values of the smaller SNC125c ionization chamber is less pronounced. The fitting curves through the Monte Carlo calculated k_Q values showed a root mean square deviation between 0.0010 and 0.0017.

In accordance with the recommendations of the TG-51 dosimetry protocol, the results have provided further evidence that identical or similar ionization chambers have comparable beam quality correction factors k_Q. The published fits for the ionization chamber PTW 30012 and Exradin A1SL or IBA CC13 were within the 95% confidence intervals determined in this work for the ionization chamber SNC600c and SNC125c, respectively.

5. Conclusion

The goal of this study was to provide data for reference dosimetry using the ionization chambers SNC600c as well as SNC125c with regard to the recommendations of the ICRU Report 90 [5]. The beam quality correction factor k_Q was calculated for clinical photon beams from 4 MV up to 25 MV. The data was fitted by the recommended fitting functions of the respective dosimetry protocols. Following the fit function that will be adopted by the TRS 398 protocol, a fit function was also introduced for the DIN 6800-2 dosimetry protocol.

Declaration of Competing Interest

The authors declare that they have no known competing financial interests or personal relationships that could have appeared to influence the work reported in this paper.

Appendix A. Appendix

Fano tests were performed on the investigated ionization chamber models using the egs_fano_source of EGSnrc C++ class library [14]. To perform the Fano test, all materials in the ionization chamber models were replaced with water having the corresponding density of the replaced material. Fig. 4 shows the ratio between calculated and expected values for all created geometric regions of the ionization chambers SNC600c and SNC125c. In Fig. 4 (a) the regions 2 and 6 correspond to the sensitve volume and regions > 8 belong to the chamber stem of the ionization chamber SNC600c. In Fig. 4 (b) the Regions 2 und 4 are the sensitive volume and regions > 10 belong to the chamber stem of the ionization chamber SNC125c.

References

[1] DIN 6800-2, Procedures of dosimetry with probe-type detectors for photon and electron radiation - Part 2: Ionization chamber dosimetry of high energy photon and electron radiation, DIN – Normenausschuss Radiologie (NAR), 2020. doi: https://dx.doi.org/10.31030/3152276.

[2] P.R. Almond, P.J. Biggs, B.M. Coursey, W.F. Hanson, M.S. Huq, R. Nath, D.W.O. Rogers, AAPM's TG-51 protocol for clinical reference dosimetry of high-energy photon and electron beams, Med Phys 26(9) (1999) 1847–1870. arXiv:https://aapm.onlinelibrary.wiley.com/doi/pdf/10.1118/1.598691, doi:10.1118/1.598691.

[3] P. Andreo, D.T. Burns, K. Hohlfeld, M.S. Huq, T. Kanai, F. Laitano, V. Smyth, V. Stefaan, Absorbed Dose Determination in External Beam Radiotherapy: An International Code of Practice for Dosimetry Based on Standards of Absorbed Dose to Water; Technical Reports Series No. 398, International Atomic Energy Agency, 2006.

[4] Andreo P, Burns DT, Kapsch RP, McEwen M, Vatnitsky S, Andersen CE, Ballester F, Borbinha J, Delaunay F, Francescon P, Hanlon MD, Mirzakhanian L, Muir B, Ojala J, Oliver CP, Pimpinella M, Pinto M, de Prez LA, Seuntjens J, Sommier L, Teles P, Tikkanen J, Vijande J, Zink K. Determination of consensus k_Q values for megavoltage photon beams for the update of IAEA TRS-398. Phys Med Biol 2020; 65(9):095011. https://doi.org/10.1088/1361-6560/ab807b.

[5] S.M. Seltzer, J.M. Fernandez-Varea, P. Andreo, P.M. Bergstrom, Jr., D.T. Burns, I. Krajcar Bronic, C.K. Ross, F. Salvat, Report 90: Key Data for Ionizing-Radiation Dosimetry: Measurement Standards and Applications, J ICRU 14 (1).

[6] Muir BR, Rogers DWO. Monte Carlo calculations of k_Q, the beam quality conversion factor. Med Phys 2010;37(11):5939–50. https://doi.org/10.1118/1.3495537. arXiv:https://aapm.onlinelibrary.wiley.com/doi/pdf/10.1118/1.3495537.

[7] M. McEwen, L. DeWerd, G. Ibbott, D. Followill, D.W.O. Rogers, S. Seltzer, J. Seuntjens, Addendum to the AAPM's TG-51 protocol for clinical reference dosimetry of high-energy photon beams, Med Phys 41(4) (2014) 041501. arXiv:https://aapm.onlinelibrary.wiley.com/doi/pdf/10.1118/1.4866223, doi:10.1118/1.4866223.

[8] Giménez-Alventosa V, Giménez V, Ballester F, Vijande J, Andreo P. Monte Carlo calculation of beam quality correction factors for PTW cylindrical ionization chambers in photon beams. Phys Med Biol 2020;65(20):205005.

[9] I. Kawrakow, D. Rogers, E. Mainegra-Hing, F. Tessier, R. Townson, B. Walters, EGSnrc toolkit for Monte Carlo simulation of ionizing radiation transport, doi: 10.4224/40001303 [release v2020] (2000).
[10] Kawrakow I. Accurate condensed history Monte Carlo simulation of electron transport. I. EGSnrc, the new EGS4 version. Med Phys 2000;27(3):485–98.
[11] Kawrakow I. Accurate condensed history Monte Carlo simulation of electron transport. II. Application to ion chamber response simulations. Med Phys 2000;27 (3):499–513.
[12] Wulff J, Zink K, Kawrakow I. Efficiency improvements for ion chamber calculations in high energy photon beams. Med Phys 2008;35(4):1328–36.
[13] Sechopoulos I, Rogers DW, Bazalova-Carter M, Bolch WE, Heath EC, McNitt-Gray MF, Sempau J, Williamson JF. RECORDS: improved reporting of Monte Carlo Radiation transport studies: Report of the AAPM Research Committee Task Group 268. Med Phys 2018;45(1):e1–5.
[14] I. Kawrakow, E. Mainegra-Hing, F. Tessier, B.R.B. Walter, The EGSnrc C++ class library, NRC Report PIRS-898 (rev A), Ottawa, Canada.
[15] J. Wulff, K. Zink, I. Kawrakow, Efficiency improvements for ion chamber calculations in high energy photon beams, Med Phys 35(4) (2008) 1328–1336. arXiv:https://aapm.onlinelibrary.wiley.com/doi/pdf/10.1118/1.2874554, doi: 10.1118/1.2874554.
[16] Wulff J, Heverhagen JT, Karle H, Zink K. Investigation of correction factors for non-reference conditions in ion chamber photon dosimetry with Monte-Carlo simulations. Zeitschrift für Medizinische Physik 2010;20(1):25–33. https://doi.org/10.1016/j.zemedi.2009.09.003.
[17] Czarnecki D, Zink K. Monte Carlo calculated correction factors for diodes and ion chambers in small photon fields. Phys Med Biol 2013;58(8):2431–44. https://doi.org/10.1088/0031-9155/58/8/2431.
[18] F. Horst, D. Czarnecki, K. Zink, The influence of neutron contamination on dosimetry in external photon beam radiotherapy, Med Phys 42(11) (2015) 6529–6536. arXiv:https://aapm.onlinelibrary.wiley.com/doi/pdf/10.1118/1.4933246, doi:10.1118/1.4933246.
[19] D. Czarnecki, B. Poppe, K. Zink, Monte Carlo-based investigations on the impact of removing the flattening filter on beam quality specifiers for photon beam dosimetry, Med Phys 44(6) (2017) 2569–2580. arXiv:https://aapm.onlinelibrary.wiley.com/doi/pdf/10.1002/mp.12252, doi:10.1002/mp.12252.
[20] Mohan R, Chui C, Lidofsky L. Energy and angular distributions of photons from medical linear accelerators. Med Phys 1985;12(5):592–7. https://doi.org/10.1118/1.595680.
[21] Sheikh-Bagheri D, Rogers DWO. Monte Carlo calculation of nine megavoltage photon beam spectra using the BEAM code. Med Phys 2002;29(3):391–402. https://doi.org/10.1118/1.1445413.
[22] M. McEwen, B. Muir, Characterization of SNC 600c ionization chambers for measurements in linear accelerator photon beams, in: Report number PIRS-3327 (National Research Council Canada, April 2021), 2021.
[23] McEwen MR. Measurement of ionization chamber absorbed dose k_Q factors in megavoltage photon beams. Med Phys 2010;37(5):2179–93.
[24] Ross C, Shortt K. The effect of waterproofing sleeves on ionization chamber response. Phys Med Biol 1992;37(6):1403.
[25] A. Aalbers, L. de Prez, M. Pieksma, Dosimetry of high-energy photon beams with the NMi water calorimeter, in: Proc. Workshop on Recent Advances in Absorbed Dose Standards (ARPANSA, Melbourne, 19–21 August 2003), 2003.
[26] M.R. McEwen, Measurement of ionization chamber absorbed dose k_Q factors in megavoltage photon beams, Med Phys 37(5) (2010) 2179–2193. arXiv:https://aapm.onlinelibrary.wiley.com/doi/pdf/10.1118/1.3375895, doi:10.1118/1.3375895.
[27] B. Muir, M. McEwen, Characterization of SNC 125c ionization chambers for measurements in linear accelerator photon beams, in: Report number PIRS-3224 (National Research Council Canada, January 2021), 2021.
[28] E. Mainegra-Hing, B.R. Muir, On the impact of ICRU report 90 recommendations on k_Q factors for high-energy photon beams, Med Phys 45(8) (2018) 3904–3908. arXiv:https://aapm.onlinelibrary.wiley.com/doi/pdf/10.1002/mp.13027, doi: 10.1002/mp.13027.
[29] M.J. Berger, M. Inokuti, H.H. Anderson, H. Bichsel, J.A. Dennis, D. Powers, S.M. Seltzer, J.E. Turner, Report 37: Stopping powers for electrons and positrons, J ICRU.
[30] Czarnecki D, Poppe B, Zink K. Impact of new ICRU Report 90 recommendations on calculated correction factors for reference dosimetry. Phys Med Biol 2018;63(15): 155015. https://doi.org/10.1088/1361-6560/aad148.
[31] Pimpinella M, Silvi L, Pinto M. Calculation of k_Q factors for Farmer-type ionization chambers following the recent recommendations on new key dosimetry data. Phys Med 2019;57:221–30.

ORIGINAL PAPER

Investigation of Monte Carlo simulations of the electron transport in external magnetic fields using Fano cavity test

Mohamad Alissa [a,b,*], **Klemens Zink** [a,b,c], **Damian Czarnecki** [a]

[a] Institute of Medical Physics and Radiation Protection, University of Applied Sciences Giessen (THM), Giessen, Germany
[b] Department of Radiotherapy and Radiation Oncology, University Medical Center Giessen and Marburg, Marburg, Germany
[c] Marburg Ionbeam Therapycenter (MIT) Marburg, Germany

Received 21 January 2022; accepted 4 July 2022

Abstract

Purpose: Monte Carlo simulations are crucial for calculating magnetic field correction factors k_B for the dosimetry in external magnetic fields. As in Monte Carlo codes the charged particle transport is performed in straight condensed history (CH) steps, the curved trajectories of these particles in the presence of external magnetic fields can only be approximated. In this study, the charged particle transport in presence of a strong magnetic field $\overrightarrow{B}$ was investigated using the Fano cavity test. The test was performed in an ionization chamber and a diode detector, showing how the step size restrictions must be adjusted to perform a consistent charged particle transport within all geometrical regions.
Methods: Monte Carlo simulations of the charged particle transport in a magnetic field of 1.5 T were performed using the EGSnrc code system including an additional EMF-macro for the transport of charged particle in electro-magnetic fields. Detailed models of an ionization chamber and a diode detector were placed in a water phantom and irradiated with a so called Fano source, which is a monoenergetic, isotropic electron source, where the number of emitted particles is proportional to the local density.
Results: The results of the Fano cavity test strongly depend on the energy of charged particles and the density within the given geometry. By adjusting the maximal length of the charged particle steps, it was possible to calculate the deposited dose in the investigated regions with high accuracy ($< 0.1\%$). The Fano cavity test was performed in all regions of the detailed detector models. Using the default value for the step size in the external magnetic field, the maximal deviation between Monte Carlo based and analytical dose value in the sensitive volume of the ion chamber and diode detector was 8% and 0.1%, respectively.
Conclusions: The Fano cavity test is a crucial validation method for the modeled detectors and the transport algorithms when performing Monte Carlo simulations in a strong external magnetic field. Special care should be given, when calculating dose in volumes of low density. This study has shown that the Fano cavity test is a useful method to adapt particle transport parameters for a given simulation geometry.

Keywords: Monte Carlo simulation; Fano cavity test; Detector; Dosimetry in external magnetic fields

* Corresponding author: Mohamad Alissa, Institute of Medical Physics and Radiation Protection, University of Applied Sciences Giessen (THM), Giessen, Germany.
E-mail: mohamad.alissa@lse.thm.de (M. Alissa).

Z Med Phys **xxx** (2022) xxx–xxx
https://doi.org/10.1016/j.zemedi.2022.07.002
www.elsevier.com/locate/zemedi

1 Introduction

Integrating magnetic resonance tomography (MRI) with medical linear accelerators allows monitoring the tumour during radiotherapy treatment [1–5]. Due to the Lorentz force, the magnetic field impacts the trajectories of the secondary charged particles, affecting both the dose distribution and the dose response of a detector. Current Monte Carlo methods accurately describe the radiation transport in different materials, even in the presence of a magnetic field. Therefore, they are the ideal approach for evaluating the impact of magnetic fields on clinical dosimetry [6–8]. However, Monte Carlo codes use condensed history steps to calculate the trajectory of charged particles [9]. Therefore, trajectories of charged particles determined by Monte Carlo simulations are an approximation of the real particle trajectory. Considering the way currently available Monte Carlo algorithms account for charged particle transport in external magnetic fields, approximations are made that may affect the electron path. When treating the charge particle scattering and magnetic field deflection as independent processes, the step size of the charge particle must be restricted. Otherwise, there is a possibility that a bias may occur in the particle transport [10], especially if several interactions are combined in a single particle transport step (condensed history step).

Today, many general purpose Monte Carlo codes like GEANT4, PENELOPE, MCNP6 or EGSnrc are able to describe the charged particle transport in external electric or magnetic fields [11]. For the EGSnrc code system two different macros for this purpose exist: a version called *emf_macros.mortran* ('EMF'), available in EGSnrc already since the transition from EGS4 to EGSnrc. This macro is based on the theory proposed by Bielajew [12]. A more sophisticated macro called *eemf_macros.mortran* ('EEMF') was introduced in 2017 by Malkov and Rogers [13]. Within these macros the single scattering mode used in the vicinity of interfaces was improved for the charged particle transport in presence of a Lorentz force. Moreover, an improved boundary crossing algorithm (BCA) was implemented. Both improvements were implemented to avoid artifacts when particles cross boundaries [14]. When particles approach an interface, Monte Carlo transport algorithms typically switch from multi scatter to single scatter mode. The B-field does not change the nearest distance to the next boundary of a region, but the trajectory can be bent to such an extent that a region may be skipped. This can occur especially with very complex geometries and regions of very low density and can result in incorrect dose calculations in individual regions of the geometry. The Fano theorem [15] plays an important role in Monte Carlo simulations of the response of gas-filled ion chambers by providing a consistency test of the particle transport. This test is the only known method allowing the validation of charged particle energy deposition in heterogeneous media against an analytic expression, this way testing the charged particle step algorithm in the given geometry and also the bounding crossing algorithm [16]. According to the recommendations of the AAPM TG-268 report [17] a Fano test is strongly recommended when reporting Monte Carlo calculated results of detectors with gaseous cavities. In the presence of external magnetic fields where the trajectories of the charged particles are more complex due to the Lorentz force, Fano's theorem may also be applied, but its validity prerequisites special conditions for the primary particle source, the isotropy and spatial uniformity of the source [14,16].

There are several studies investigating the consistency of Monte Carlo transport algorithms in the presence of a magnetic field using the Fano cavity test. Pooter *et al.* [14] used a simplified geometry of a Farmer-type ionization chamber consisting only of an air-filled cavity and a surrounding wall. The results suggest that a comparable accuracy to Monte Carlo simulations without a B-field may not be achieved in presence of a B-field with the investigated Monte Carlo algorithms. The authors recommend that each simulation geometry and set-up should be carefully validated before use. Lee *et al.* [11] compared the charged particle transport of different Monte Carlo algorithms (EGSnrc, Geant4, PENELOPE and MCNP6). They studied the electron transport in the energy range from 0.01 MeV to 3 MeV in different magnetic field strengths from 0 T to 3 T, showing that care should be taken when the step size of the electron transport is in the range of the Larmor radius r_G of the electrons. They also investigated the dose deposition in a cylindrical gas-filled disk between two solid walls. Ito *et al.* [18] compared the EGS5 and the EGSnrc codes with the above mentioned EEMF macros. They evaluated the accuracy of the charged particle transport in external B-fields of 0.35 and 1.5 T within a simple cylinder geometry. Electrons with energies between 0.01 and 10 MeV were used for the Fano source.

While Lee *et al.* [11] used the egs_chamber code in his study, Malkov *et al.* used the DOSRZnrc user code for simple geometries like a gas slab of 0.2 and 2 cm thicknesses. In both studies an accuracy of 0.1% in the Fano test was achieved. Ito *et al.* used the Fano cavity test with EEMF macros to evaluate the accuracy of electron transport in 0.35 and 1.5 T for EGS5 code. They simulated a simple cylinder made of three layers, the energy of the Fano source was varied between 0.01 to 10 MeV [18]. In further Monte Carlo based studies calculating the detector response in the presence of external magnetic fields [4,19–21] the authors performed the Fano test only with one electron energy and investigated only the sensitive volume of the detector.

So, most of the existing studies using the Fano theorem to investigate Monte Carlo radiation transport in external magnetic fields were limited to highly simplified ionization

Please cite this article as: Alissa, M., Zink, K., & Czarnecki, D., Investigation of Monte Carlo simulations of the electron transport in external magnetic fields using Fano cavity test, Z Med Phys, https://doi.org/10.1016/j.zemedi.2022.07.002

chamber geometries. It remains an open question whether Monte Carlo algorithms can achieve comparable accuracy's for a Fano test for complex detector geometries. A Fano test of all regions of a detector model and not only for the sensitive volume of the detector, might be necessary under the following hypothetical circumstances: Suppose there exists a region A outside the sensitive volume in which there is a statistically significant deviation from the expected value under Fano conditions, but this has no effect on the sensitive volume. This leads to the conclusion that on the one hand the radiation transport in and out of this region is calculated incorrect, but on the other hand this has hardly any influence on the dose contribution in the sensitive volume when using a radiation source which fulfills the Fano conditions. But if the detector model is positioned in a clinical radiation field in such a way that region A is the largest source of secondary electrons scattering into the sensitive volume, this may lead to an incorrectly calculated dose in the sensitive volume, even though in the Fano cavity test the dose in the sensitive volume was in agreement with the expected values.

The objective of this work was to investigate the particle transport in presence of a strong magnetic field using the Fano test. The consistency of charged particle transport in dependence of the maximum step size of the charged particles was investigated in all geometrical regions of two detailed detector models, an ionization chamber and a Si diode, with the question, which geometrical regions of a detector model are most critical with regard to particle transport in external magnetic fields. Since the radius of the curved trajectory of the charged particles depends on their energy, the Fano test was performed for different primary electron energies.

2 Materials and methods

2.1 Theoretical background

2.1.1 Basic description of electron trajectories in external magnetic fields

Considering an electron moving in the direction $\vec{u}$ in an external magnetic field $\vec{B}$ in vacuum, the change of particle direction $\mathrm{d}\vec{u}$ with the path length $\mathrm{d}s$ of the particle can be described as follows,

$$\frac{\mathrm{d}\vec{u}}{\mathrm{d}s} = \frac{e}{m_0 c \beta \gamma} \vec{u} \times \vec{B} \tag{1}$$

where e is the elementary charge, m_0 the electron rest mass, β the relative electron velocity with respect to the speed of light c and γ is the Lorentz factor [22]. From Eq. (1) it can be seen that the influence of the magnetic field on the particle trajectory is energy dependent. To estimate the order of magnitude of the particle deflection, the Larmor radius or gyroradius r_G of the electron can be calculated from Eq. (1) as follows:

$$r_G = \frac{m_0 c \beta \gamma}{e\left|\vec{u} \times \vec{B}\right|} \tag{2}$$

The radius r_G is shown in Fig. 1 as a function of the kinetic energy of an electron in a magnetic field perpendicular to the direction of movement with a magnetic field strength of 1.5 T. As can be seen, the gyroradius r_G for low energy electrons (< 1 MeV) is within the order of magnitude of the components of an ionization chamber (sensitive volume, central electrode etc.). This means that special care should be taken when the low-energy electron transport is simulated through an ionization chamber. The circular path of kV-electrons is in the range of a few millimeters. For high-energy electrons, on the other hand, the influence of the magnetic field is smaller.

Class II Monte Carlo algorithms simulate charged particle transport in condensed history (CH) steps, summarizing multiple elastic scattering events in one single transport step. A CH step-length depends on the density ρ of the medium in which particles are transported, since the probability of hard collisions increases with ρ. A more detailed description of the particle transport algorithm can be found in the work of Berger [23].

With respect to particle transport in CH steps in external magnetic fields, it is useful to look at the directional change $\mathrm{d}u$ with the mass-path length $\rho \mathrm{d}s$ to account for the density dependence of the interaction probability along the path length. This transforms Eq. (1) as follows

$$\frac{\mathrm{d}\vec{u}}{\rho\,\mathrm{d}s} = \frac{e}{\rho m_0 c \beta \gamma} \vec{u} \times \vec{B} \tag{3}$$

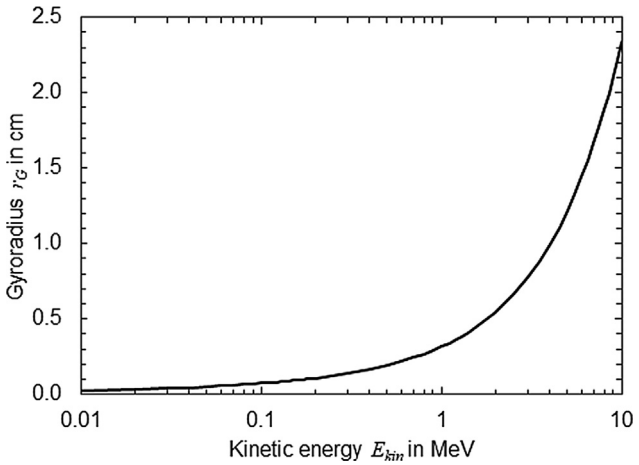

Figure 1. The gyroradius r_G of an electron moving perpendicular to an external magnetic field (B = 1.5 T) as a function of E_{kin}.

Please cite this article as: Alissa, M., Zink, K., & Czarnecki, D., Investigation of Monte Carlo simulations of the electron transport in external magnetic fields using Fano cavity test, Z Med Phys, https://doi.org/10.1016/j.zemedi.2022.07.002

According to this equation, it can directly be seen that the curvature of an electron trajectory depends on the density of the medium, when the trajectory is observed in mass-thickness spatial coordinates $\rho\vec{x}$. This was very well elaborated in the work of Bouchard *et al.* [16]. Thus, there is a reciprocal dependence of the change of direction $\mathrm{d}\vec{u}$ on the density of the medium ρ. From Eq. 3 it is clear that the influence of the external magnetic field on the particle trajectory increases in media with decreasing density and with decreasing particle energy. Thus, special care should be given when the radiation transport of low-energy charged particles is calculated by class II Monte Carlo simulation algorithms in regions of low density ρ in an external magnetic field $\vec{B}$.

2.1.2 Condensed history steps in external magnetic fields

Regarding the charged particle transport using CH steps in external magnetic fields, the following approximations have to be respected. In the work of Bielajew *et al.* [10], a general expression for a CH step is formulated, from which the velocity $\vec{v}$ of a charged particle can be calculated after a transport step s in a homogeneous medium:

$$\vec{v} = \vec{v}_0 + \frac{1}{m_0\gamma}\int_0^t \vec{F}_{ret}(E(t)) + \vec{F}_{ms}(E(t)) + \vec{F}_L\left(\vec{x}(t'), E(t), \vec{u}(t')\right)\mathrm{d}t' \quad (4)$$

where $\vec{v}_0$ is the velocity of the particle before the step s and t is the time interval of the step. $\vec{F}_{ret}$ and $\vec{F}_{ms}$ are the forces from inelastic and multiple scattering, respectively. Here, the Lorenz force of the external magnetic field $\vec{B}$ is referred to as $\vec{F}_L$. All forces $\vec{F}_{ret}$, $\vec{F}_{ms}$ and $\vec{F}_L$ acting on the electron, have an particle energy E dependency. For uniform magnetic fields, the dependence of the Lorenz force $\vec{F}_L$ on the location $\vec{x}$ of the particle does not exist. An important aspect of Monte Carlo simulations in CH steps is to keep the steps s small enough so that the energy dependence E of the forces acting on the particle is negligible. For particle transport in a homogeneous magnetic field, the change in particle direction $\vec{u}$ must also be as small as possible, so that the equation can be simplified as follows:

$$\vec{v} = \vec{v}_0 + \frac{1}{m_0\gamma}\left(\vec{F}_{ret}(E_0) + \vec{F}_{ms}(E_0) + \vec{F}_L\left(E_0, \vec{u}_0\right)\right) \quad (5)$$

with E_0 the initial energy and $\vec{u}_0$ the propagation direction of the particle. To ensure that the assumptions leading to Eq. (5) do not lead to transport artefacts, the length of the path s must be adjusted or checked with respect to the magnitude of $\mathrm{d}\vec{u}$. An inaccurate trajectory of a particle would not necessarily lead to a miscalculated dose deposition if the particle would never leave its geometric region due to energetic reasons. Problems occur when particles cross borders of different regions. Critical parameters with respect to the length of a CH step are the energy (or velocity) of the charged particle and the density of the medium in which the particle transport is calculated [22].

2.1.3 Fano cavity test

If the particle trajectory is only approximated, it is not clear whether in between a single CH step the particle might have interacted in another region of a different medium. For this reason, a self-consistency test of the charged particle transport algorithm based on the Fano theorem was developed for Monte Carlo calculations [24]. The Fano test states that under charged particle equilibrium and for uniform cross-sections, the fluence of the charged particles is independent of the mass density [15]. If we consider charged particles in an external magnetic field, the Fano conditions are violated because, unlike the other forces in Eq. (5), the Lorenz force does not scale with mass density [25].

For this reason, Bouchard *et al.* [16] have proposed further special conditions under which the Fano theorem remains valid in the presence of an external magnetic field. Either the radiation source must be spatially uniform and isotropic so that the Fano conditions are satisfied for any external magnetic field, or the intensity of the magnetic field must be scaled with density. In this work we used a spacial uniform and isotropic radiation source to perform the Fano cavity test in an external uniform magnetic field, The Fano radiation source used in this work generated electrons propagating uniformly in all directions within a given rectangular volume. The size of the volume was chosen according to the energy of the electrons: $(7 \times 5 \times 5)$ cm^3 for 0.1 and 1 MeV and $(10 \times 9 \times 9)$ cm^3 for 6 MeV electrons. The detector was placed at the center of this volume.

2.2 Monte Carlo simulation set-up

This study is based on Monte Carlo simulations performed using the EGSnrc code system [26] including the standard EGSnrc macro *emf_macros.mortran* [12] ('EMF') for transporting charged particles in external magnetic and electric fields. The electron transport was investigated for different `EM ESTEPE` values from 0.25 to as low as 0.005. The `EM ESTEPE` value within the EMF macros is used to control the maximum step length s according to the equation:

$$s = (\texttt{EM ESTEPE}) \times r_G \quad (6)$$

i.e. the step length in presence of an external magnetic field is limited to a fraction of the Larmor radius r_G. This ensures, that the step size s is always adapted to the B-field and the particle energy. For Monte Carlo simulations without an

Please cite this article as: Alissa, M., Zink, K., & Czarnecki, D., Investigation of Monte Carlo simulations of the electron transport in external magnetic fields using Fano cavity test, Z Med Phys, https://doi.org/10.1016/j.zemedi.2022.07.002

external $\vec{B}$-field, the parameter EM ESTEPE has no relevance, the normal step-size parameter ESTEPE was set to the default value ESTEPE = 0.25, meaning that the maximum energy loss within one CH step is 25%. Further details of the investigated Monte Carlo simulation set-up are summarized in Table 1.

The EM ESTEPE value also impacts the efficiency ϵ of a Monte Carlo simulation, where ϵ is given as:

$$\epsilon = \frac{1}{T\,\sigma^2} \tag{7}$$

T is the CPU time and σ the type-A relative standard uncertainty of the Monte Carlo calculated quantity.

2.3 Detector models

In this study, the SemiFlex 3D ionization chamber (PTW 31021) and the diode detector (PTW T60016) from PTW (Freiburg, Germany) have been investigated. They were modelled in detail according to manufacturer data using the egs++ class library [27]. Cross-sections of the detector models are shown in Fig. 2. The ionization chamber has a sensitive air volume of 0.07 cm^3. The electrode is made of aluminium with a radius 0.04 cm. The Monte Carlo model of the ionization chamber consists of 47 regions. The diode detector has a sensitive volume of silicon with a volume of $3.4\times10^{-4}cm^3$. The Monte Carlo model of the diode detector consists of 30 regions. Table 2 presents the detector regions with the corresponding region numbers of the most important detector components.

2.4 Configuration for Fano cavity test

All Monte Carlo simulations were performed under Fano conditions to test the consistency of charged particle transport in presence of an external magnetic field. To realize Fano conditions with an external magnetic field, the particles source egs_fano_source from the EGSnrc C++ class library has been used. This radiation source emits particles proportional to the mass density at the current source position with uniformly distributed direction in 4π [27]. The detectors were placed in a water phantom large enough to enable charged particle equilibrium in the modeled detectors. With respect to the range of electrons, a phantom of size $(12\times10\times10)$ cm^3 was chosen for electrons with initial energies of 0.1 MeV and 1 MeV. For the 6 MeV electrons a larger phantom sized $(20\times20\times20)$ cm^3 had to be chosen. In addition, all materials of the investigated detector geometries were replaced by water with density of the original material. The density correction and I value were set to those of water for all materials so that the mass stopping power of all materials were identical. All calculations were performed in an external magnetic field of 1.5 T which was perpendicular to the symmetry axis of the detectors (see Fig. 2). With this simulation setup, the Fano conditions as described by Bouchard [16] could be satisfied even in the presence of

Table 1
Summary of the main properties and parameters for the Monte Carlo simulations with EGSnrc in this work.

Item	Description	References
Code	EGSnrc 2020 master brunch	Kawrakow *et al.* [26]
	egs++ library	Kawrakow *et al.* [27]
	egs_chamber	Wulff *et al.* [28]
	emf_macros.mortran	Bielajew *et al.* [10]
Timing	See Table 3	
Source description	egs++ egs_fano_source surrounding the detector to achieve charged particle equilibrium within the detector geometry; initial particle energies: monoenergetic electrons with energies 0.1 MeV, 1 MeV and 6 MeV	Kawrakow *et al.* [27]
Cross-sections	XCOM photon cross section with multiconfiguration DiracFock renormalization factor for the photoelectric effect (mcdf-xcom)	
Transport parameters	Boundary crossing algorithm: Exact, transport and particle production threshold energy of 512 keV and 1 keV for electron and photon, respectively; EM ESTEPE = 0.25–0.005	
Variance reduction techniques	Russian Roulette range rejection technique with a survival probability of 1/128	
Statistical method	History-by-history	
Post-processing	None	

Please cite this article as: Alissa, M., Zink, K., & Czarnecki, D., Investigation of Monte Carlo simulations of the electron transport in external magnetic fields using Fano cavity test, Z Med Phys, https://doi.org/10.1016/j.zemedi.2022.07.002

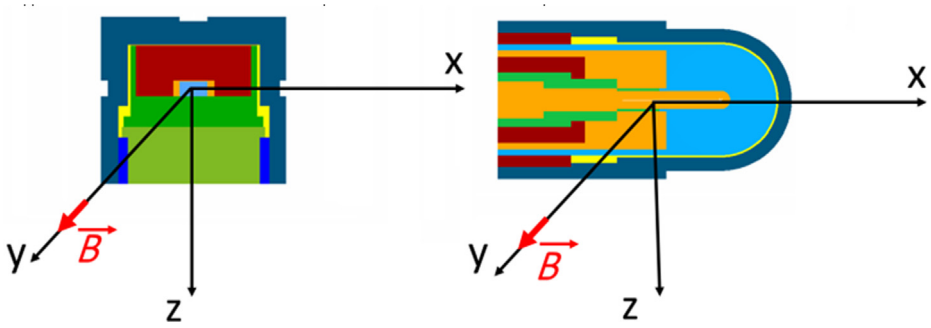

Figure 2. Cross sections of the Monte Carlo based model of the investigated ionization chamber PTW 31021 and the Si diode T60016. Different colours represent different materials. The red arrow represents the orientation of the external magnetic field $\vec{B}$.

Table 2
Detector components and corresponding region numbers and materials.

Detector	Detector component	Materials	Region number
PTW 31021	Sensitive volume	Air	2 and 6
	Central electrode	Aluminium	1 and 5
	Wall	Graphite, PMMA	3, 4, 7 and 8
	Stem	Various materials	9 to 47
T60016	Sensitive volume	Silicon	1

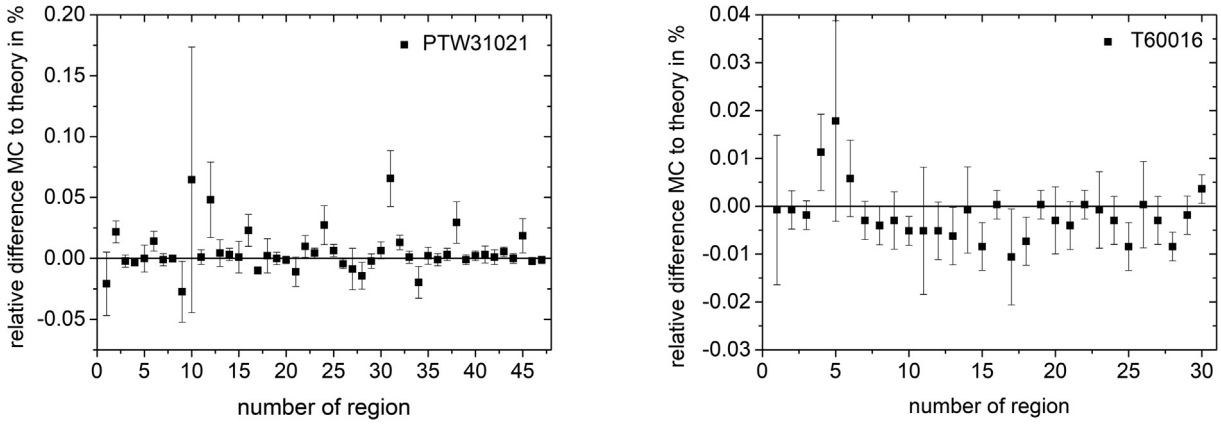

Figure 3. Relative difference of absorbed dose in all geometrical regions of the investigated ionization chamber PTW 31021 (a) and Si diode detector PTW 60016 (b) from the theoretical value under Fano conditions. Monoenergetic 1 MeV electrons were chosen as radiation source. The Monte Carlo simulations were performed with ESTEPE = 0.25 and without an external magnetic field. The type-A relative standard uncertainty of the Monte Carlo data is represented by uncertainty bars.

the applied external magnetic field. Under these conditions, the Monte Carlo calculated absorbed Dose $D_{MC,i}$ in a region i is independent of the magnetic field strength and can be calculated according to the following equation:

$$D_{MC,i} = n_i \frac{E_0}{m_i} \tag{8}$$

where m_i is the mass of region i and n_i is the number of particles emitted from the Fano source in region i. E_0 is the initial particle energy.

3 Results

3.1 Charged particle transport without external magnetic fields

Fig. 3 shows the relative difference between the Monte Carlo calculated and expected dose in each region of the ionization chamber and the diode detector without an external magnetic field under Fano conditions. The transport param-

Please cite this article as: Alissa, M., Zink, K., & Czarnecki, D., Investigation of Monte Carlo simulations of the electron transport in external magnetic fields using Fano cavity test, Z Med Phys, https://doi.org/10.1016/j.zemedi.2022.07.002

eter ESTEPE is set to the default value of 0.25. The Monte Carlo calculated absorbed dose in all regions of both detailed detector models show small deviations from theoretical values within 0.06%. The presented Fano test was performed using 1 MeV monoenergetic electrons as particle source.

3.2 Charged particle transport in external magnetic fields

3.2.1 Diode detector

When the charged particle transport is calculated in the presence of an external magnetic field (B = 1.5 T), the deviation from the theoretical dose value increases up to 0.11% within the active volume (region 1) for the Si diode detector (see Fig. 4) when a value for EM ESTEPE = 0.25 was used. Other regions of the diode detector showed comparable or even larger deviations from the theoretical value. The deviations could be significantly reduced when the EM ESTEPE value was decreased to 0.025 or 0.005. For both values the deviations between the theoretical and the Monte Carlo based dose value were well below 0.1% for all regions.

Fig. 5 shows the relative dose deviation in the sensitive volume of the diode as a function of the EM ESTEPE value for electrons with an initial energy of 1 MeV. As can be seen, the deviations are within 0.1%. However, there is a clear relation between the dose values in the sensitive volume and the applied EM ESTEPE values.

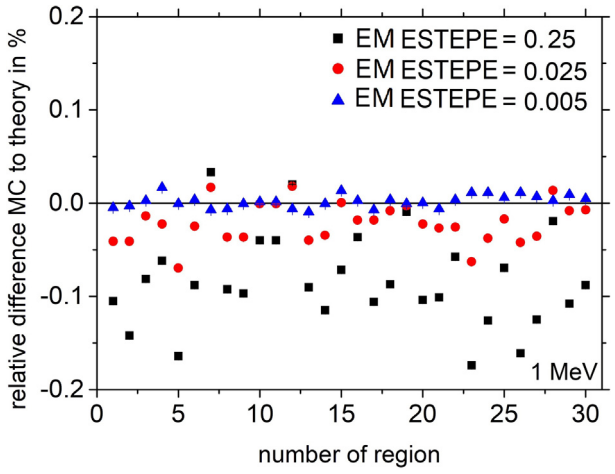

Figure 4. Relative difference of absorbed dose in all regions of the Si diode PTW 60016 from the theoretical value under Fano conditions. Monoenergetic 1 MeV electrons were chosen as radiation source. The Monte Carlo simulations were performed with different EM ESTEPE values in presence of an external magnetic field B = 1.5 T perpendicular to the symmetry axis of the detector. The type-A relative standard uncertainty of the Monte Carlo data is within the symbol size.

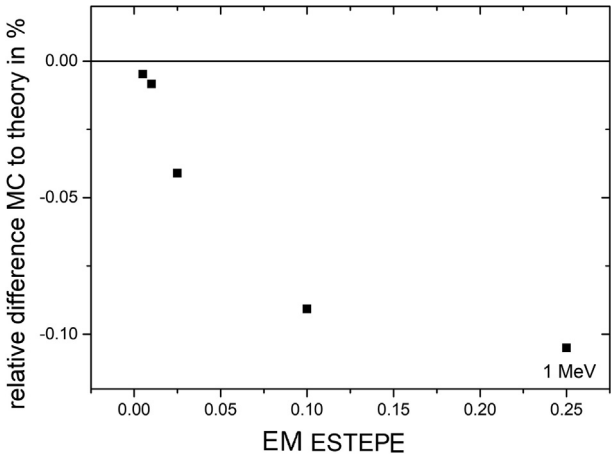

Figure 5. Relative difference of absorbed dose in the sensitve volume of the Si diode detector PTW 60016 from the theoretical value under Fano conditions as a function of the radiation transport parameter EM ESTEPE. Monoenergetic 1 MeV electrons were chosen as radiation source in presence of an external magnetic field B = 1.5 T perpendicular to the symmetric axis of the detector. The type-A relative standard uncertainty of the Monte Carlo data is within the symbol size.

3.2.2 Ionization chamber

Fig. 6 shows the relative dose deviation between the expected and Monte Carlo calculated values in all geometrical regions of the ionization chamber PTW 31021 for various EM ESTEPE values. All results presented in Fig. 6 were calculated with 1 MeV monoenergetic electrons as particle source in an external magnetic field B = 1.5 T perpendicular to the symmetry axis of the ionization chamber (see Fig. 2). The largest deviation of the Monte Carlo based dose from the expected value is observed in the air-filled regions (2, 6, 10, 12, 18, 24, 31, 38 and 45) of the ion chamber. Among these regions, part of the sensitive volume of the ionization chamber (regions 6) showed the largest deviation of about 8%. It is the largest air-filled volume. Smaller air volumes in the chamber stem also show deviations of more than 1%. To achieve a deviation below 0.1% in all regions, the EM ESTEPE value had to be reduced to 0.01. By reducing the EM ESTEPE value to 0.005, the deviations could be further reduced. Regarding only the active, air-filled volume of the ion chamber (region 2 and 6) the importance of an appropriate EM ESTEPE factor especially in low density materials become clear (see Fig. 7). Decreasing EM ESTEPE from 0.25 to 0.01, the difference between Monte Carlo based and analytical dose value decreased from around 7% to 0.1% and below, i.e. the CH steps in low density materials has to be very small to have an adequate approximation of the curved trajectories of the electrons. The comparison of Figs. 5 and 7 shows, that the relationship of the relative dif-

Please cite this article as: Alissa, M., Zink, K., & Czarnecki, D., Investigation of Monte Carlo simulations of the electron transport in external magnetic fields using Fano cavity test, Z Med Phys, https://doi.org/10.1016/j.zemedi.2022.07.002

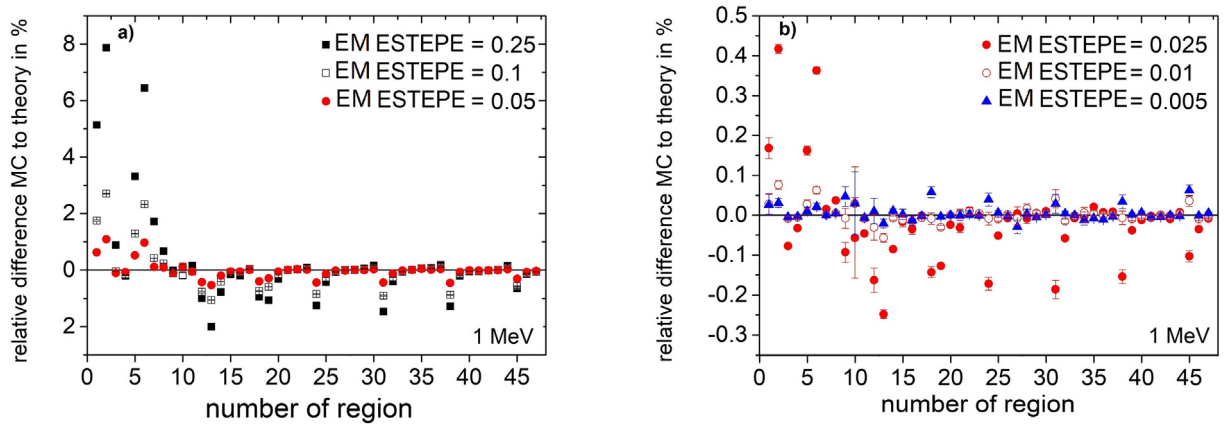

Figure 6. Relative difference of absorbed dose in all geometrical regions of the ionization chamber PTW 31021 from the theoretical value under Fano conditions. Monoenergetic 1 MeV electrons were chosen as radiation source. The Monte Carlo simulations were performed in presence of an external magnetic field B = 1.5 T oriented perpendicular to the symmetry axis of the detector. The type-A relative standard uncertainties of the Monte Carlo data are represented by uncertainty bars or they are given by the symbol size.

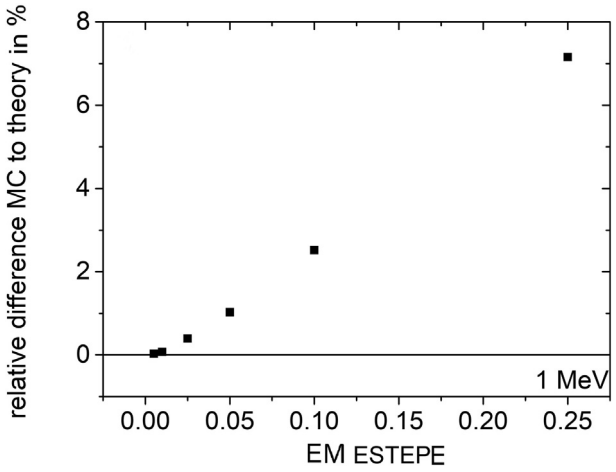

Figure 7. Mean value of the relative difference of absorbed dose from the theoretical value under Fano conditions as a function of EM ESTEPE for the two air-filled regions 2 and 6 of the ion chamber. Monoenergetic 1 MeV electrons were chosen as radiation source. The Monte Carlo simulations were performed with varying EM ESTEPE values in presence of an external magnetic field B = 1.5 T oriented perpendicular to the symmetry axis of the detector. The type-A standard uncertainties of the Monte Carlo data are given by the symbol size.

ference of Monte Carlo based and analytical dose value as a function of the EM ESTEPE value is different. Whereas for the Si-diode the difference is always negative, i.e. the Monte Carlo based dose value is smaller than the expected one, it is positive for the ion chamber. This behavior is not clear at the moment, but it is assumed that the difference is related to the different densities of the active volumes of the two detectors (air and silicon).

3.3 Fano test for various initial electron energies

Fig. 8 shows the results of the Fano cavity test for all geometrical regions of the ionization chamber for three different initial electron energies 0.1 MeV, 1 MeV and 6 MeV. As can be seen in Fig. 8 b, the deviation between the Monte Carlo calculated dose and the theoretical dose in the sensitive volume is smaller for electrons with an initial energy of 6 MeV and increases for electrons with lower initial energy. If the mean dose deviation over the two regions of the sensitive volume of the ion chamber is considered, one can see that even for the very small EM ESTEPE value of 0.01 the deviations are above 0.1% for the smallest electron energy of 0.1 MeV, i.e. in that case the Fano test has failed. Fig. 9 shows that the EM ESTEPE parameter had to be reduced to 0.005 to reduce the deviation between the Monte Carlo calculated and theoretical dose values in all regions of the ionization chamber below 0.1% for electrons with an initial energy of 0.1 MeV.

3.4 Efficiency of Monte Carlo simulations

Table 3 presents the calculation time T, the uncertainty σ and the efficiency ϵ according to Eq. 7 in dependency of the EM ESTEPE value for charged particle transport through the investigated detectors with and without an external magnetic field under Fano test conditions with monoenergetic electrons as radiation source. The magnetic field is oriented perpendicular to the symmetry axis of both detectors (see Fig. 2).

4 Discussion

The present study summarizes the results of Monte Carlo based Fano tests for two detector models in the presence of

Please cite this article as: Alissa, M., Zink, K., & Czarnecki, D., Investigation of Monte Carlo simulations of the electron transport in external magnetic fields using Fano cavity test, Z Med Phys, https://doi.org/10.1016/j.zemedi.2022.07.002

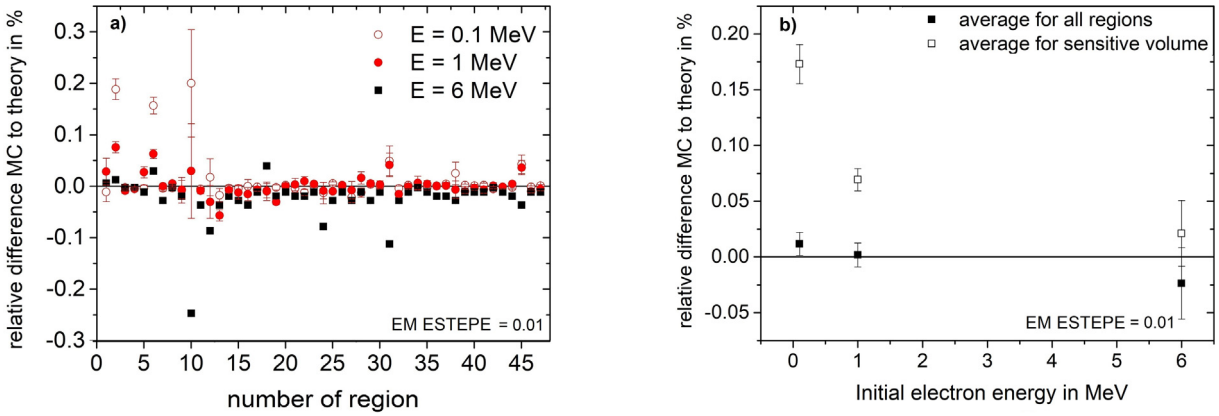

Figure 8. Relative difference of absorbed dose in all geometrical regions of the ionization chamber PTW 31021 from the theoretical value under Fano conditions in presence of an external magnetic field B = 1.5 T. In figure a) the EM ESTEPE value was set to 0.01 and the Fano test was performed with three different initial electron energies for the particle source. In figure b) the relative difference for the sensitive volume and the average of all regions is shown as a function of the initial electron energy of the radiation source for EM ESTEPE = 0.01. The type-A standard uncertainties of the data presented in panel a) and b) are given by uncertainty bars or are within the symbol size. The type-A standard uncertainties in panel b) are the combined uncertainties over the given regions.

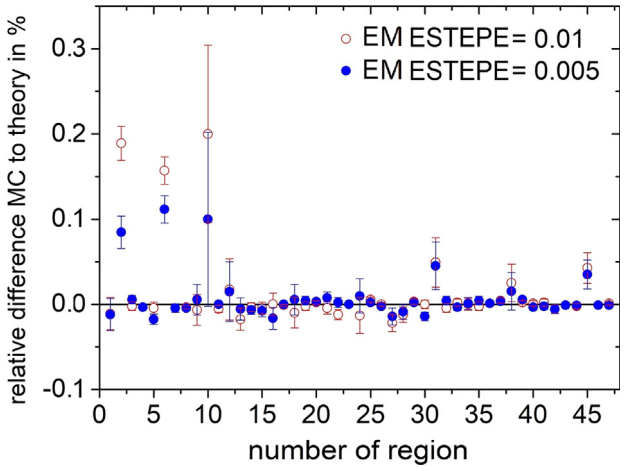

Figure 9. Relative difference of absorbed dose for all geometrical regions of the ionization chamber PTW 31021 from the theoretical value under Fano conditions for electrons with an initial electron energy of 0.1 MeV in presence of an external magnetic field B = 1.5 T. The relative dose difference is calculated for two different EM ESTEPE values. The type-A relative standard uncertainties of the Monte Carlo data are represented by uncertainty bars, or are within the symbol size.

external magnetic fields. The charged particle transport in electro-magnetic fields is a challenge for every Class-II-Monte Carlo algorithm, because the particle trajectories are curved due to the Lorentz force, therefore the condensed history method in these codes may fail due to the choice of too large CH steps. Using the Fano test [15] under the conditions of external magnetic fields [14,16] it can be checked, if the charged particle transport algorithm in a given geometry works properly. The Fano test is the only known method allowing the validation of charged particle energy deposition in heterogeneous media against an analytic expression, this way testing the charged particle step algorithm in the given geometry and also the bounding crossing algorithm.

The Fano tests in the present study were performed with the EGSnrc Monte Carlo code system [26] using the 'simple' EMF macros for the calculation of the charged particle trajectories in the presence of magnetic fields based on the work from Bielajew [12]. Within these macros the step size s can be influenced with the parameter EM ESTEPE and s is always proportional to the Larmor radius r_G (see Eq. 6). That means, the step length is automatically adapted to varying particle energies and B-fields. But it is not clear, if one EM ESTEPE value can be used for all particle energies and magnetic field strength's. The default value of EM ESTEPE is 0.020.

We performed Fano test for two detectors which are in widely clinical use, an air-filled ion chamber (PTW 31021) and a silicon diode (PTW 60016). In contrast to most other publications [4,19–21] we did not only include the active volumes but all regions of the detectors in the Fano test. Moreover, we used very detailed models of both detectors made of up to fifty regions and did not simplify the detector models [11,13]. The test was performed with different electron energies, covering a broad range of clinically used energies.

First of all, the results show, that not only the macros from Malkow and Rogers [13] within the EGSnrc code package are able to describe the charged particle transport in the presence of electro-magnetic fields adequately but also the older EMF macros from Bielajew [12]. By reducing the

Please cite this article as: Alissa, M., Zink, K., & Czarnecki, D., Investigation of Monte Carlo simulations of the electron transport in external magnetic fields using Fano cavity test, Z Med Phys, https://doi.org/10.1016/j.zemedi.2022.07.002

Table 3
Simulation efficiency for different parameters EM ESTEPE. The simulations were performed with an primary electron energy of 1 MeV for the Fano source.

	PTW 31021				PTW T60016			
B	EM ESTEPE	*T* in h	σ in %	ϵ	EM ESTEPE	*T* in h	σ in %	ϵ
1.5 T	0.25	2565	0.011	3.22	0.25	3320	0.004	18.83
	0.1	3169	0.011	2.61	0.1	3397	0.004	18.40
	0.05	3195	0.011	2.59				
	0.025	3291	0.011	2.51	0.025	3677	0.004	17.00
	0.01	4405	0.011	1.88	0.01	4210	0.004	14.85
	0.005	5350	0.011	1.54	0.005	5649	0.004	11.06
0 T	0.25	2656	0.009	4.65	0.25	2656	0.004	23.53

step size parameter EM ESTEPE in our simulations, we could reach a deviation of the Monte Carlo based and the analytical dose values in both detectors and all detector regions below 0.1%. For deviations less than this value the test is considered passed.

By comparing the results for the diode and the ion chamber, it was found that the diode can succeed the Fano test for much larger EM ESTEPE values compared to the ionization chamber (see Fig. 5 and 7). Moreover, the test was generally more successful in regions with higher densities, so a larger EM ESTEPE parameter can be applied for all solid state detectors, strongly reducing calculation times. This is clear, as the CH step length always depends on the mass density, i.e. the larger the density the smaller the step length for a given parameter EM ESTEPE.

In agreement with the results of Lee *et al.* [11], the study has shown that the deviation from theoretical values of the calculated dose with the EGSnrc magnetic field macro (emf_macros.mortran) depends on the energy of the electrons. Although the step length s is automatically adjusted via the Larmor radius r_G with particle energy, this change is not enough to pass the Fano test. For electron energies of 0.1 MeV the parameter EM ESTEPE had to be chosen as small as 0.005. Using high energy electrons as radiation source in the Fano cavity test leads to a good agreement with the theoretical dose values, even for a relative high EM ESTEPE value of 0.1. However, it should be noted that under real conditions of a bremsstrahlung's photon field, the low energy electrons cause most of the dose in a patient or in a detector. The results of this study have highlighted the importance of the choice of the energy of the initial electrons in a Fano test in order for it to retain its validity in a realistic radiation field.

An important factor for all Monte Carlo codes is the calculation efficiency ϵ. Restricting the step length of the CH steps will always reduce ϵ, i.e. the CPU time for the calculation increases for the same type-A uncertainty. We did not perform a direct comparison of the efficiency of both electro-magnetic field macros (EMF and EEMF) which are available for the EGSnrc code. But, for the diode the efficiency was reduced only by about 25% comparing the simulations with and without a B-field (see Table 3) and an EM ESTEPE value of 0.025, resulting in deviations below 0.1% in all regions. Regarding the calculation efficiency in an ion chamber, Malkov and Rogers [13] state, that the calculation time increases by about 50% using their EEMF macros and a simplified model of a NE2571 chamber. Our results for the PTW 31021 chamber show an increase of the calculation time of about a factor of 2.5 if the EMF macro is applied and a EM ESTEPE value of 0.01 is chosen. This value was necessary to pass the Fano test for the ion chamber (see Fig. 6 and Table 3). That means, the newer EEMF macros from Malkov and Rogers seem to be much more efficient than the older EMF macros, but one has to keep in mind, that in the present study a much more detailed chamber model was used, and the calculation was performed until in every region the 0.1% level was reached. If it is indeed necessary to perform the Fano test not only for the active region but also for all adjacent regions is not quite clear. Looking at the results of the Fano test for all regions of a detector model, it can be seen that the deviations from the theoretical value are different in magnitude for different region. Consequently, one cannot conclude from the result of the Fano test of a single region to the remaining regions. However, the sensitive volume of the detector models of this study had the largest deviation from the expected value. When a decrease of the deviations in the sensitive volume could be achieved, this was accompanied by a decrease of the deviations in the other regions.

According to our study we recommend to use EM ESTEPE = 0.01 for the ionization chambers to pass the Fano test and for diodes the step size restriction EM ESTEPE can be chosen as 0.1. Additionally, it was found that the result of the Fano test depends on the primary electron energy of the Fano source. Therefore, it is recommended to choose an

Please cite this article as: Alissa, M., Zink, K., & Czarnecki, D., Investigation of Monte Carlo simulations of the electron transport in external magnetic fields using Fano cavity test, Z Med Phys, https://doi.org/10.1016/j.zemedi.2022.07.002

energy for the Fano radiation source according to the subsequent simulation task. This ensures that the Monte Carlo-based model has been evaluated for the radiation spectrum of interest. Otherwise, errors could occur that were not visible in the Fano cavity test.

5 Conclusion

With the increasing use of MR-linacs in modern radiotherapy, Monte Carlo based studies of the radiation transport in the presence of an external magnetic field are becoming increasingly important. Fano cavity tests especially for gas-filled detectors are highly recommended notably if these detectors are simulated in external magnetic fields. The present study has shown, that the older EMF macro, which is part of the EGSnrc code system is able to describe adequately the charged particle transport in external magnetic fields if the step size parameter `EM ESTEPE` is adequately chosen. For an external magnetic field $\overrightarrow{B}$ = 1.5 T, step size parameters `EM ESTEPE` = 0.1 for the diode and `EM ESTEPE` = 0.01 for the ion chamber yielded good Fano test results, i.e. deviations below 0.1% between Monte Carlo based and analytical dose values. As the Fano test results and the adequate step size depends on the primary electron energy, the Fano test should always be performed for several energies covering the whole range of clinical used energies.

Declaration of Competing Interest

The authors declare that they have no known competing financial interests or personal relationships that could have appeared to influence the work reported in this paper.

References

[1] Dempsey J, Dionne B, Fitzsimmons J, Haghigat A, Li J, Low D, et al. We-e-vala-06: a real-time MRI guided external beam radiotherapy delivery system. Med Phys 2006;33(6Part20), 2254–2254.

[2] Raaymakers BW, Lagendijk JJW, Overweg J, Kok JGM, Raaijmakers AJE, Kerkhof EM, et al. Integrating a 1.5 t MRI scanner with a 6 MV accelerator: proof of concept. Phys Med Biol 2009;54(12):N229.

[3] Fallone BG, Murray B, Rathee S, Stanescu T, Steciw S, Vidakovic S, et al. First MR images obtained during megavoltage photon irradiation from a prototype integrated linac-MR system. Med Phys 2009;36(6Part1):2084–2088.

[4] Smit K, Van Asselen B, Kok JGM, Aalbers AHL, Lagendijk JJW, Raaymakers BW. Towards reference dosimetry for the MR-linac: magnetic field correction of the ionization chamber reading. Phys Med Biol 2013;58(17):5945.

[5] O'Brien DJ, Roberts DA, Ibbott GS, Sawakuchi GO. Reference dosimetry in magnetic fields: formalism and ionization chamber correction factors. Med Phys 2016;43(8Part1):4915–4927.

[6] Meijsing I, Raaymakers BW, Raaijmakers AJE, Kok JGM, Hogeweg L, Liu B, et al. Dosimetry for the MRI accelerator: the impact of a magnetic field on the response of a farmer ne2571 ionization chamber. Phys Med Biol 2009;54(10):2993.

[7] Reynolds M, Fallone BG, Rathee S. Dose response of selected ion chambers in applied homogeneous transverse and longitudinal magnetic fields. Med Pys 2013;40(4):042102.

[8] Malkov VN, Rogers DWO. Monte carlo study of ionization chamber magnetic field correction factors as a function of angle and beam quality. Med Phys 2018;45(2):908–925.

[9] Kawrakow I. Accurate condensed history Monte Carlo simulation of electron transport. i. EGSnrc, the new EGS4 version. Med Phys 2000;27(3):485–498.

[10] Bielajew AF. Electron Transport in $\overrightarrow{E}$ and $\overrightarrow{B}$ Fields. Boston, MA: Springer US; 1988. p. 421–434. https://doi.org/10.1007/978-1-4613-1059-4_19, ISBN 978-1-4613-1059-4.

[11] Lee J, Lee J, Ryu D, Lee H, Ye S-J. Fano cavity test for electron Monte Carlo transport algorithms in magnetic fields: comparison between EGSnrc, penelope, mcnp6 and geant4. Phys Med Biol 2018;63(19):195013.

[12] Bielajew AF. The effect of strong longitudinal magnetic fields on dose deposition from electron and photon beams. Med Phys 1993;20(4):1171–1179. https://doi.org/10.1118/1.597149, URL https://aapm.onlinelibrary.wiley.com/doi/abs/10.1118/1.597149.

[13] Malkov VN, Rogers DWO. Charged particle transport in magnetic fields in EGSnrc. Med Phys 2016;43(7):4447–4458.

[14] De Pooter JA, De Prez LA, Bouchard H. Application of an adapted fano cavity test for Monte Carlo simulations in the presence of B-fields. Phys Med Biol 2015;60(24):9313.

[15] Fano U. Note on the Bragg-Gray cavity principle for measuring energy dissipation. Radiat Res 1954;1(3):237–240.

[16] Bouchard H, de Pooter J, Bielajew A, Duane S. Reference dosimetry in the presence of magnetic fields: conditions to validate Monte Carlo simulations. Phys Med Biol 2015;60(17):6639.

[17] Sechopoulos I, Rogers DWO, Bazalova-Carter M, Bolch WE, Heath EC, McNitt-Gray MF, et al. Records: improved reporting of Monte Carlo radiation transport studies: report of the aapm research committee task group 268. Med Phys 2018;45(1):e1–e5.

[18] Ito K, Kadoya N, Katsuta Y, Tanaka S, Dobashi S, Takeda K, et al. Evaluation of the electron transport algorithm in magnetic field in egs5 monte carlo code. Phys Med 2022;93:46–51.

[19] Spindeldreier CK, Schrenk O, Bakenecker A, Kawrakow I, Burigo L, Karger CP, et al. Radiation dosimetry in magnetic fields with farmer-type ionization chambers: determination of magnetic field correction factors for different magnetic field strengths and field orientations. Phys Med Biol 2017;62(16):6708.

[20] Pojtinger S, Kapsch R-P, Dohm OS, Thorwarth D. A finite element method for the determination of the relative response of ionization chambers in mr-linacs: simulation and experimental validation up to 1.5 t. Phys Med Biol 2019;64(13):135011.

[21] Delfs B, Blum I, Tekin T, Schönfeld A-B, Kranzer R, Poppinga D, et al. The role of the construction and sensitive volume of compact ionization chambers on the magnetic field-dependent dose response. Med Phys 2021.

[22] Bielajew AF. Fundamentals of the Monte Carlo method for neutral and charged particle transport, vol. 1. The University of Michigan; 2001.

[23] Berger MJ. Monte Carlo calculation of the penetration and diffusion of fast charged particles. Methods Comput Phys 1963;135.

[24] Rogers DWO. Fifty years of Monte Carlo simulations for medical physics. Phys Med Biol 2006;51(13):R287.

Please cite this article as: Alissa, M., Zink, K., & Czarnecki, D., Investigation of Monte Carlo simulations of the electron transport in external magnetic fields using Fano cavity test, Z Med Phys, https://doi.org/10.1016/j.zemedi.2022.07.002

[25] Bouchard H, Bielajew A. Lorentz force correction to the boltzmann radiation transport equation and its implications for Monte Carlo algorithms. Phys Med Biol 2015;60(13):4963.

[26] Kawrakow I, Rogers DWO, Mainegra-Hing E, Tessier F, Townson RW, Walters BRB. EGSnrc toolkit for Monte Carlo simulation of ionizing radiation transport, 2000. https://doi.org/10.4224/40001303 [release v2021]

[27] Kawrakow I, Mainegra-Hing E, Tessier F, Walter BRB. The EGSnrc C++ class library. NRC Report PIRS-898 (rev A), Ottawa, Canada, 2009.

[28] Wulff J, Zink K, Kawrakow I. Efficiency improvements for ion chamber calculations in high energy photon beams. Med Phys 2008;35(4):1328–1336. https://doi.org/10.1118/1.2874554, URL https://aapm.onlinelibrary.wiley.com/doi/abs/10.1118/1.2874554.

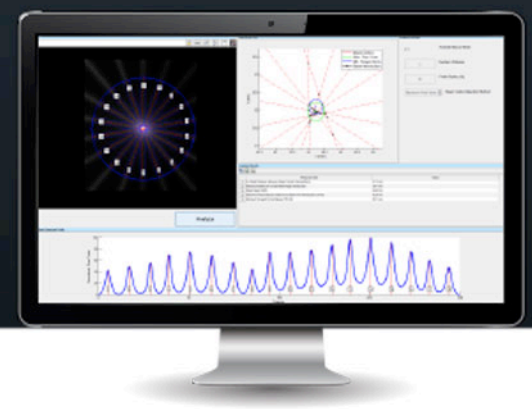

COMPREHENSIVE MACHINE QA SOLUTIONS

FROM RADIOLOGICAL IMAGING TECHNOLOGY, INC.

RIT software provides extensive machine QA capabilities, including comprehensive packages that can be used to perform a full suite of measurements in accordance with TG-142, TG-148, and/or TG-135. RIT's automated routines allow you to perform daily, monthly, and annual QA with efficiency, precision, and confidence knowing your delivery performance is optimized.

TG-142: LINEAR ACCELERATORS QA

RIT is the single-vendor software solution that performs and trends every test recommended in TG-142 and MPPG 8.a.

Perform comprehensive quality assurance of Varian, Elekta, and all linear accelerators with confidence and ease, using your EPID and RIT software. RIT *Complete*, RIT *Classic*, and RITG142 feature RIT's popular 3D Winston-Lutz Isocenter Optimization routine that will help your SRS/SBRT delivery with its sub-millimeter, fully-automated accuracy. RIT offers automated tests for Star Shot Analysis, Radiation vs. Light Field, MLC accuracy, and other beam measurements.

TG-148: HELICAL TOMOTHERAPY® QA

RIT offers a comprehensive test suite for helical TomoTherapy® and Radixact® machines, in accordance with TG-148.

Designed with the TG-148 report in mind, the RITG148+ and RIT *Complete* software packages analyze the standardized tests for helical TomoTherapy machine QA. These include Static & Rotational Output Consistency, Jaw Centering and Alignment, Overhead Laser Positioning, Interrupted Treatment, and all others recommended for daily, monthly, and annual QA. The software will also analyze image quality using the TomoTherapy Cheese phantom.

TG-135: CYBERKNIFE® ROBOTIC RADIOSURGERY QA

RIT provides a comprehensive test suite for CyberKnife® and all robotic radiosurgery, in accordance with TG-135.

The RITG135 and RIT *Complete* software packages contain five fully-automated QA tests for CyberKnife® machines: End-to-End Test, AQA Test, Iris Test, Laser Coincidence, and MLC (Garden Fence) Test for the M6 Collimator. Combining a user-friendly interface with automated film detection algorithms, the software eliminates the need for manual manipulation or alignment of images, and drastically reduces the time required to perform these tests.

RIT®

VISIT **RADIMAGE.COM** TO DEMO RIT'S ADVANCED RANGE OF MACHINE QA, MLC QA, PATIENT QA, AND IMAGING QA ROUTINES.

+1(719)590-1077, OPT. 4

SALES@RADIMAGE.COM

Visit us at the AAPM 2023 Annual Meeting in Houston, TX from July 23-26.
Exhibition Hall – Booth 621

Received: 22 September 2022 | Revised: 22 February 2023 | Accepted: 23 February 2023

DOI: 10.1002/mp.16345

RESEARCH ARTICLE

MEDICAL PHYSICS

Experimental and Monte Carlo-based determination of magnetic field correction factors $k_{B,Q}$ in high-energy photon fields for two ionization chambers

Mohamad Alissa[1,2] | **Klemens Zink**[1,2,3] | **Ralf-Peter Kapsch**[4] | **Andreas A. Schoenfeld**[5] | **Stephan Frick**[4] | **Damian Czarnecki**[1]

[1]Institute for Medical Physics and Radiation Protection, University of Applied Sciences Giessen, Giessen, Germany

[2]Department of Radiotherapy and Radiation Oncology, University Medical Center Giessen and Marburg, Marburg, Germany

[3]Marburg Ionbeam Therapy Center (MIT), Marburg, Germany

[4]German National Metrology Institute (PTB), Braunschweig, Germany

[5]Sun Nuclear, A Mirion Medical Company, Melbourne, Florida, USA

Correspondence
Mohamad Alissa, Institute for Medical Physics and Radiation Protection, University of Applied Sciences Giessen, Giessen, Germany.
Email: mohamad.alissa@lse.thm.de

Abstract

Background: The integration of magnetic resonance tomography into clinical linear accelerators provides high-contrast, real-time imaging during treatment and facilitates online-adaptive workflows in radiation therapy treatments. The associated magnetic field also bends the trajectories of charged particles via the Lorentz force, which may alter the dose distribution in a patient or a phantom and affects the dose response of dosimetry detectors.

Purpose: To perform an experimental and Monte Carlo-based determination of correction factors $k_{B,Q}$, which correct the response of ion chambers in the presence of external magnetic fields in high-energy photon fields.

Methods: The response variation of two different types of ion chambers (Sun Nuclear SNC125c and SNC600c) in strong external magnetic fields was investigated experimentally and by Monte Carlo simulations. The experimental data were acquired at the German National Metrology Institute, PTB, using a clinical linear accelerator with a nominal photon energy of 6 MV and an external electromagnet capable of generating magnetic flux densities of up to 1.5 T in opposite directions. The Monte Carlo simulation geometries corresponded to the experimental setup and additionally to the reference conditions of IAEA TRS-398. For the latter, the Monte Carlo simulations were performed with two different photon spectra: the 6 MV spectrum of the linear accelerator used for the experimental data acquisition and a 7 MV spectrum of a commercial MRI-linear accelerator. In each simulation geometry, three different orientations of the external magnetic field, the beam direction and the chamber orientation were investigated.

Results: Good agreement was achieved between Monte Carlo simulations and measurements with the SNC125c and SNC600c ionization chambers, with a mean deviation of 0.3% and 0.6%, respectively. The magnitude of the correction factor $k_{B,Q}$ strongly depends on the chamber volume and on the orientation of the chamber axis relative to the external magnetic field and the beam directions. It is greater for the SNC600c chamber with a volume of 0.6 cm^3 than for the SNC125c chamber with a volume of 0.1 cm^3. When the magnetic field direction and the chamber axis coincide, and they are perpendicular to the beam direction, the ion chambers exhibit a calculated overresponse of less than 0.7(6)% (SNC600c) and 0.3(4)% (SNC125c) at 1.5 T and less than 0.3(0)% (SNC600c) and 0.1(3)% (SNC125c) for 0.35 T for nominal beam energies of 6 MV and 7 MV. This chamber orientation should be preferred, as $k_{B,Q}$ may increase significantly

in other chamber orientations. Due to the special geometry of the guard ring, no dead-volume effects have been observed in any orientation studied. The results show an intra-type variation of 0.17% and 0.07% standard uncertainty (k=1) for the SNC125c and SNC600c, respectively.

Conclusion: Magnetic field correction factors $k_{B,Q}$ for two different ion chambers and for typical clinical photon beam qualities were presented and compared with the few data existing in the literature. The correction factors may be applied in clinical reference dosimetry for existing MRI-linear accelerators.

KEYWORDS
Dosimetry, magnetic fields, magnetic field correction factors, Monte Carlo, MR-linac

1 | INTRODUCTION

The integration of magnetic resonance tomography into clinical linear accelerators (linacs) provides high-contrast, real-time imaging during treatment which may help to reduce dose to healthy tissue, and facilitates online-adaptive workflows in radiation therapy treatments. However, the strong magnetic field of the MRI impacts the trajectories of the charged particles set in motion by the high-energy photons. Due to the Lorentz force, the trajectories become spiral and the dose distribution, as well as the dose response of applied radiation detectors, may change.[1–3] The effect of magnetic fields on the response of ionization chambers has been investigated thoroughly in experimental and Monte Carlo studies on several chamber designs.[4–11] Its magnitude depends on chamber characteristics, such as the (effective) sensitive volume and material composition, but also on the magnetic field strength, the energy spectrum of the incident beam and the chamber orientation with respect to the magnetic field and beam directions. In most cases, large Farmer-type ion chambers were investigated under reference conditions. Meijsing et al.[3] studied the response variation of the NE2571 ion chamber experimentally and with Monte Carlo simulations for different orientations and strengths of magnetic fields. They concluded that the response variation of the chamber is related to the number and length of electron trajectories entering the sensitive volume of a chamber. Spindeldreier et al.[5] investigated the impact of the active volume on the magnetic field correction factor $k_{B,Q}$ (as defined in section 2.1) by testing a series of PTW-30013 Farmer chambers with different chamber radii. They found a maximum increase in chamber response of 8.8% for the magnetic field strength of 1.1 T applied perpendicular to the incoming beam and the chamber axis. De Prez et al.[9] measured k_Q as well as $k_{B,Q}$ values for two Farmer-type chambers (PTW-30013 and IBA-FC65-G) on a pre-clinical 7 MV MRI-linac at 0 T and 1.5 T with a water calorimeter.

Recently, several studies discussed the effect of electrically shielded regions in the chamber cavity near the chamber stem. Some guard ring geometries span an electric field from the guard ring to the outer electrode (chamber wall). Consequently, electrons released in this part of the chamber cavity will not be collected by the central electrode and will not contribute to the dosimeter reading M_Q. Malkov and Rogers et al.[10,11] investigated this so-called dead volume by approximating its geometry as a slice with thickness d located next to the guard ring. They calculated the chamber's response dependence on d for a wide range of ion chambers in external magnetic fields and found a good agreement between their Monte Carlo simulations and experimental data, if the thickness d of the dead volume was between 0.5 and 1 mm. Delfs et al.[8] developed a more sophisticated model of the dead volume based on proton microbeam tomography of the effective sensitive volume, i.e. cavity volume minus dead volume, and finite element calculations of the chamber's electric field. By amending the Monte Carlo models of the respective chambers accordingly, the agreement between measurements and simulations was better than 1%. By neglecting the dead volume effect, however, differences of up to 6% were observed. Aside from investigating small thimble chambers under reference conditions, Delfs et al.[8] performed measurements revealing that the SNC125c ionization chamber (Sun Nuclear, A Mirion Medical Company, Melbourne, FL) is not affected by dead volume.

The aim of the present study is the determination of the magnetic correction factor $k_{B,Q}$ for two commercially available thimble ionization chambers SNC125c and SNC600c (Sun Nuclear, A Mirion Medical Company, Melbourne, FL), which are in wide clinical use. To perform a complete characterization of these chambers, the response variation of the two ionization chambers for different magnetic fields strengths and magnetic field directions was studied experimentally and by Monte Carlo simulations. The measurements were performed at the German National Metrology Institute (PTB, Braunschweig, Germany). The Monte Carlo models of the ion chambers were created in a previous, joint study with the Canadian National Metrology Institute (NRC, Ottawa, Canada) on the determination of the beam quality correction factors k_Q.[12] Therein, the chamber models were cross-validated by independent Monte Carlo simulations and experimental data.

The magnetic field correction factor $k_{B,Q}$ was calculated for the x-ray spectrum of the Elekta Unity MR-linac (Elekta AB, Stockholm, Sweden), with a nominal energy of 7 MV bremsstrahlung, and also for the known 6 MV spectrum of the PTB linac to back up the Monte Carlo results with experimental data. The latter spectrum may serve as approximation of the 6 MV spectrum of ViewRay MR-linacs. Thus, the correction factors shown here can be used directly for clinical MR-linacs.

2 | MATERIALS AND METHODS

2.1 | Magnetic field correction factor $k_{B,Q}$

In the presence of strong magnetic fields $\vec{B}$ the well-known equation for the determination of dose-to-water D_w in clinical photon dosimetry,[13–15] i.e.

$$D_w = M_Q \cdot N_{D,w,Q_0} \cdot k_{Q,Q_0} \tag{1}$$

has to be expanded by a new correction factor $k_{B,Q}$[9]:

$$D_w^B = M_Q^B \cdot N_{D,w,Q_0} \cdot k_{Q,Q_0} \cdot k_{B,Q} \tag{2}$$

Herein M_Q^B and M_Q are the corrected dosimeter readings at beam quality Q with and without a magnetic field $\vec{B}$, N_{D,w,Q_0} is the absorbed dose-to-water calibration coefficient at reference beam quality Q_0. Furthermore, k_{Q,Q_0} is the beam quality correction factor taking into account the different response of the ion chamber in the beam quality Q with respect to the reference beam quality Q_0. $k_{B,Q}$ is the correction factor correcting the different ion chamber response due to the presence of the external magnetic field. From equations (1) and (2) it follows, that for a given beam quality Q, $k_{B,Q}$ is given as[4]

$$k_{B,Q} = \frac{D_{w,Q}^B}{D_{w,Q}} \cdot \frac{M_Q}{M_Q^B} = \frac{D_{w,Q}^B}{D_{w,Q}} \cdot \frac{\overline{D}_{det,Q}}{\overline{D}_{det,Q}^B} \tag{3}$$

To calculate $k_{B,Q}$ with Monte Carlo simulations, the measured charges M_Q and M_Q^B in equation (3) were replaced by the scored dose per incident fluence on the phantom $\overline{D}_{det,Q}$ and $\overline{D}_{det,Q}^B$ in the air filled cavity of the ion chamber model without and with an external magnetic field $\vec{B}$.

2.2 | Experimental setup

The measurements were performed at the German National Metrology Institute (PTB). The facility has coupled an electromagnet (Type ER 073W, Bruker BioSpin GmbH) with an Elekta Precise linac operating at 6 MV nominal photon energy. The electromagnet can generate magnetic flux densities of up to 1.5 T in opposite directions between its pole shoes, where a small water phantom sized 20 × 20 × 5.9 cm^3 or 28 × 20 × 5.9 cm^3 was installed (see Figure 1). Two different types of ion chambers were investigated: the farmer-type chamber SNC600c (Sun Nuclear, A Mirion Medical Company, Melbourne, FL) and the small thimble chamber SNC125c (also Sun Nuclear). The SNC600c has a sensitive volume of 0.6 cm^3, and the chamber wall is made of resin impregnated graphite. The SNC125c has a sensitive volume of 0.1 cm^3 and the wall is made of high purity graphite. More information about the chambers is given in Figure 3 and Table 4. The chambers were placed in the water phantom at a depth of 10 g/cm^2. The field size at this water depth was 4x10 cm^2. Due to the special geometry of the electromagnet, the source-surface distance (SSD) and the source-chamber distance (SCD) differ slightly from the reference conditions given in the TRS-398 code-of-practice (CoP) (see Table 2).

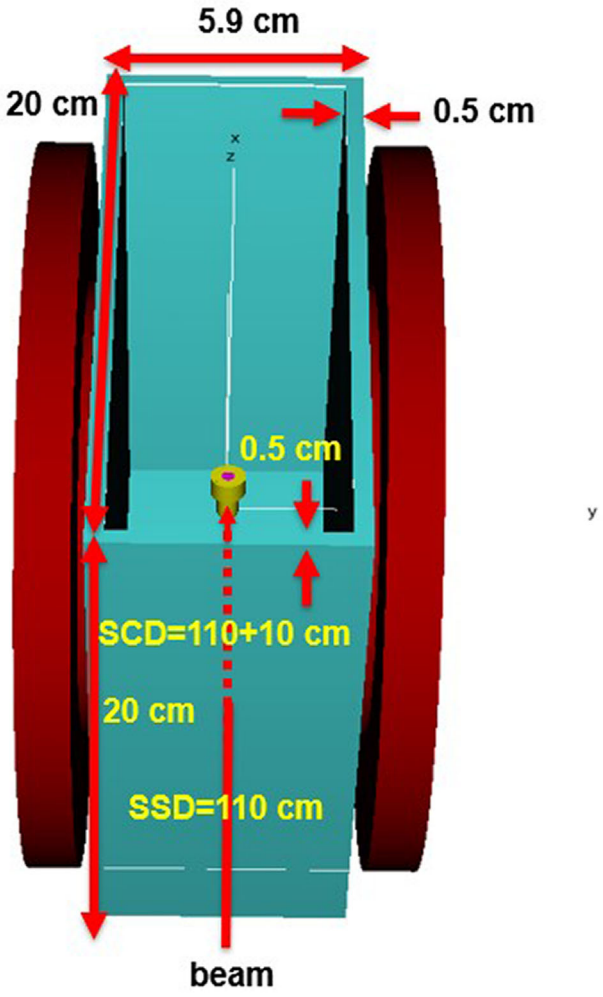

FIGURE 1 The Monte Carlo model of the experimental setup at PTB, which was used for the Monte Carlo calculations of the chamber response given in Figure 4. A longer water phantom was used for the measurements of the SNC600c chamber in orientation c (see Figure 2), which measured 28 cm instead of 20 cm in beam direction.

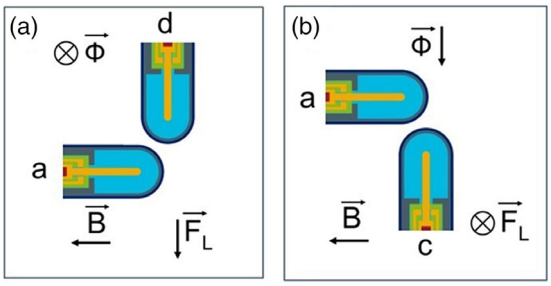

FIGURE 2 Orientations of the ion chambers relative to the magnetic field $\vec{B}$ and the photon beam direction $\vec{\phi}$. The orientation (a) is not experimentally possible due to geometry constraints of the pole faces . The direction of the Lorentz force $\vec{F}_L$ is given for B_x and (negatively charged) electrons as described by de Pooter et al.[16].

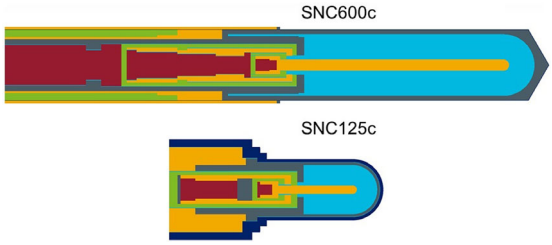

FIGURE 3 Cross sections of the Monte Carlo models of the investigated ion chambers. Both chamber drawings have a different scaling. Different colors represent different materials. The chamber models were validated in.[12].

TABLE 1 Twelve ionization chambers from different production batches used in this work.

Ionization chamber	Production date	Batch number	$N_{D,w,Q0}$ in 10^7 Gy/C
SNC125c	April 2020	256353	27.65
	April 2020	256353	27.75
	April 2021	266541	28.49
	April 2022	270233	28.21
	April 2022	270429	28.47
	June 2022	271015	28.36
SNC600c	January 2021	265733	5.163
	January 2021	265733	5.158
	January 2021	265733	5.160
	May 2022	270587	5.165
	August 2022	271546	5.091
	September 2022	271903	5.178

TABLE 2 The geometrical reference conditions according to IAEA TRS-398 code of practice and the geometrical measurement conditions as used in the experimental setup at PTB.

SET-UP	TRS-398	PTB
Source to surface distance (SSD)	90 cm	110 cm
Source to chamber distance (SCD)	100 cm	120 cm
Measurement depths	10 g/cm^2	10 g/cm^2
Field size at (SSD)	10 × 10 cm^2	4 × 10 cm^2

The experimental setup puts the magnetic field direction always perpendicular to the incident photon beam. For this reason, in the Monte Carlo set up, the beam axis was oriented along the z-axis and the magnetic field along the x-axis (see Figure 1). It should be noted that the magnetic field has only a component in the x-direction. In the following the x component of the magnetic field will be used to describe the magnetic field, where a negative sign indicates an opposing direction of the magnetic field vector. This setup results in two possible ion chamber orientations relative to the beam and to the magnetic field. A third orientation with the ion chamber axis being parallel to the magnetic field could be realized in the Monte Carlo model, but not in the experimental setup. The three orientations are given in Figure 2a and are defined as (a), (c) and (d) according to de Pooter et al.[16] In orientation (d), the average Lorentz force is parallel to the chamber axis, i.e. the secondary electrons will drift towards the tip of the chamber or towards the stem. In that case, it may be expected that the response of the chamber as a function of the magnetic field strength is non-symmetric about $B = 0$ T. In orientations (a) and (c), the Lorentz force drives the electrons towards the lateral chamber wall, and consequentially, the chamber response as a function of $\vec{B}$ should be symmetrical about $B = 0$ T. The difference between orientations (a) and (c) is that in orientation (a) the beam is perpendicular to the chamber axis, while in orientation (c) the beam and the chamber axis are parallel to each other. All measurements were performed in a water phantom of 20x20x5.9 cm^3 (Figure 1), except those with the SNC600c in orientation (c). Because of the rigid chamber stem of the SNC600c, it was placed in a longer water phantom with a length of 28 cm instead of 20 cm in beam direction. The downstream elongation of the phantom had no impact on the results, as was examined in preliminary measurements and Monte Carlo simulations. Six ionization chambers of the type SNC600c and six ionization chambers of the type SNC125c, as listed in Table 1, were investigated in this study. To quantify the reproducibility of the chamber positioning in the experimental setup, measurements with one SNC125c chamber were repeated three times on three different days.

2.3 | Monte Carlo simulations

All Monte Carlo calculations were performed with the EGSnrc code system (version 2020).[17] The simulation parameters are summarized in Table 3. In this study, the less efficient emf_macros.mortran was used for particle simulation in the external magnetic field. It should be noted that an improved macro eemf_macros.mortran is already available in the current EGSnrc installation. However, it could already be shown in a previous study by means of Fano-test that with the older macro a

TABLE 3 Summary of simulation properties and parameters used for the Monte Carlo simulations.

Item	Description	References
Code	EGSnrc code system,	Kawrakow et al.[17]
	egs++ library,	Kawrakow et al.[22]
	egs_chamber	Wulff et al.[23]
	emf macros.mortran	Bielajew[24]
Validation	Fano cavity test	Results in Appendix
Timing	Absorbed dose to water D_w in the sensitive volume of the chamber for photon spectra with B field took 150 and 280 single CPU hours (2.1 GHz), for the SNC600c and SNC125c ionization chambers, respectively.	
Source description	Collimated isotropic point sources with 7 MV (TPR20,10 = 0.691) and 6 MV photon spectrum (TPR20,10 = 0.677)	Ahmad et al.[21]
Cross-sections	XCOM photon cross section with multiconfiguration DiracFock renormalization factor for the photoelectric effect (mcdf-xcom)	
Transport parameters	Boundary crossing algorithm: Exact; transport and particle production threshold energy of 512 keV for electrons and 1 keV for photons.	
Variance reduction techniques	Intermediate phase space storage (IPSS); Photon cross-section enhancement (XCSE) volume with an XCSE factor of 128 and Russian Roulette range rejection technique with a survival probability of 1/128.	Wulff et al.[23]
Scored quantities	Absorbed dose to water and dose to air	
Statistical uncertainties	$\leq$ 0.1% for all calculated quantities	
Statistical method	History-by-history	
Postprocessing	None	

TABLE 4 Summary of the materials and geometric data of the ionization chambers.

Ionization chamber	Material	Wall Thickness	Central electrode Material	Radius	Sensitive volume Material	Radius	Length
SNC125c	Graphite	0.25 mm	Al	0.4 mm	Air	2.375 mm	7.05 mm
	PMMA	0.30 mm					
	Paint	0.05 mm					
SNC600c	Graphite	0.43 mm	Al	0.55 mm	Air	3.05 mm	22.7 mm
	Paint	0.05 mm					

comparable accuracy of the radiation transport can be achieved, albeit with higher computing time.[18] The ICRU Report 90[19] recommendations were followed with regards to the ionization energies I and the density correction δ. Radiation sources were simulated as collimated isotropic point sources with a 6 MV or a 7 MV photon spectrum. The 6 MV spectrum was extracted from a complete BEAM simulation of the Elekta Precise linac at PTB Braunschweig and may also be used to represent the ViewRay machine,[20] the 7 MV spectrum was taken from Ahmad[21] and represents the spectrum of the commercially available Elekta Unity MR-linac.

The two ion chamber types SNC600c and SNC125c were modelled with the C++ class library egspp[22] based on technical drawings provided by the manufacturer. The cross sections of the chamber models are displayed in Figure 3, further chamber details are summarized in Table 4. One distinct feature of both chambers is the geometry of the guard electrode: it is flat over the entire base area of the air-filled volume. Therefore, both chambers should show no dead-volume effects. In the present study, two series of Monte Carlo simulations were performed: (a) *PTB setup*: this geometry corresponds to the experimental setup at PTB. It includes the pole shoes and the PMMA water phantom (see Figure 1 and Table 2). For this geometry, the variation of the dose ratio $\overline{D}^{B}_{det,Q}/\overline{D}_{det,Q}$ as a function of the external magnetic field B was calculated using the 6 MV spectrum of the PTB linac, which was already used in previous studies[20] ; (b) *TRS-398 setup*: this setup corresponds to the TRS-398 reference conditions[13] (see Table 2) with water phantom dimension of 30x30x30 cm^3. Preliminary simulations of the dose ratio $\overline{D}^{B}_{det,Q}/\overline{D}_{det,Q}$ in

both setups showed that the effects of the different field and phantom sizes, as well as the slightly different setup distances on the calculated dose ratios were negligible (< 0.1%). All dose quantities for the determination of the magnetic field correction factor $k_{B,Q}$, given in eq. (3), were calculated in the TRS-398 setup. To calculate the dose to water $D^{B}_{w,Q}$ and $D_{w,Q}$, a small water disc with radius 0.1 mm and height 0.1 mm was positioned symmetrically around the point of measurement at depth $z_0 = 10$ cm. The dose to the ion chamber $\overline{D}_{det,Q}$ and $\overline{D}^{B}_{det,Q}$ was calculated within the active volume of each chamber, where the chambers' reference points were at z_0. The correction factors $k_{B,Q}$ were calculated for both photon spectra according to eq. (3).

2.3.1 | Dead volume effects

Similar to the studies from Malkov and Rogers,[10,11] the hypothetical dead volume was modeled as a slice of thickness d just above the guard ring of the cylindrical chambers SNC125c and SNC600c. For the thickness d values of 0.1, 0.2 and 0.3 mm for the small SNC125c chamber and 0.3, 0.5 and 0.7 mm for the large SNC600c chamber were applied, i.e. the dose was scored in the active volume given in Figure 3 minus the slice of thickness d. The simple dead volume model from Malkov and Rogers seems to be adequate for the SNC chambers, since the guard ring is flat and fills the entire diameter of the chamber. Delfs et al.[8] already investigated the SNC125c chamber and found that this form of guard ring does not produce a dead-volume. As the large SNC600c chamber has a very similar geometry, it was assumed that the simple model for the dead volume geometry is sufficient for the purpose of this study.

3 | RESULTS AND DISCUSSIONS

3.1 | Chamber response as a function of $\vec{B}$

Figure 4 presents the ratio $\overline{D}^{B}_{det,Q}/\overline{D}_{det,Q}$ of the investigated chambers as a function of the magnetic field strength B for the three chamber orientations shown in Figure 2 and for the 6 MV photon spectrum. Therein, the left column shows the results for the SNC125c and the right column shows those for the SNC600c. Each row corresponds to one of the three chamber orientations with respect to the magnetic field $\vec{B}$ and the beam directions. The Monte Carlo results shown in this figure were calculated in the *PTB setup*, but as mentioned above, the different setups had no significant impact on the calculated dose ratios. Repeated measurements with the same ionization chambers showed that the measurement setup uncertainty was within 0.15%. The results of measurements with 6 different ionization chambers per chamber model show an intra-type variation of 0.17% and 0.07% standard uncertainty (k=1) for the SNC125c and SNC600c, respectively. The results are consistent with those published by Woodings et al.,[23] who investigated the $k_{B,Q}$ values and intra-type variations of Farmer type ionization chambers PTW30013 and FC65-G in external magnetic fields.

The asymmetry of the data plot around $B = 0$ T for chamber orientation (d) is strongly pronounced for the smaller SNC125c chamber (Figure 4a) and has a maximum value of about 2% at $B_x = 0.8$ T. Note that in orientation (d) $\vec{F}_L$ is parallel to the chamber axis. This orientation shows good agreement between the Monte Carlo simulations and measurement data. All in all, the agreement of all measured and Monte Carlo based values for all B-field strengths is within 0.5% for this chamber model in this orientation. The deviation in the dose ratios seen for the chambers may be due to geometrical or material tolerances in the production process.

For the large chamber SNC600c in orientation (d), the asymmetry between positive and negative B-field values is well below 0.5%. The asymmetry is slightly more pronounced in the measurement data than in the Monte Carlo data leading to deviations of about 1% between measurement and simulation for negative B-fields. The reasons for this deviation are not quite clear, but one assumption is that there are still small differences in the geometry or material composition of the Monte Carlo model and the real ion chambers. The agreement of the experimental results between all chambers is excellent, i.e. within 0.16%, meaning that the specimen scatter for the SNC600c ion chambers is very small. In orientation (c) with magnetic field perpendicular to the chamber axis and the beam parallel to its axis, the ratio $\overline{D}^{B}_{det,Q}/\overline{D}_{det,Q}$ is symmetrical around $B = 0$ T, since the Lorentz force drives the electrons towards the lateral chamber wall and the geometry is symmetrical with respect to the magnetic field direction. The variation of the dose ratio is largest in this chamber orientation and reaches up to 8.5% for the SNC600c. Equivalent to Figure 4b, the experimental data for the different chambers are in nearly perfect agreement. For larger B-values there is an increasing deviation between Monte Carlo based and experimental data; the deviation is in the range of 1%. For the small chamber SNC125c and orientation (c), the variation of the dose ratio with the magnetic field strength is only in the range of 4%. Regarding the experimental data, Figure 4c clearly shows a deviation of the dose ratios for increasing B-values between the chambers.

This is in accordance with the results given in Figure 4a.

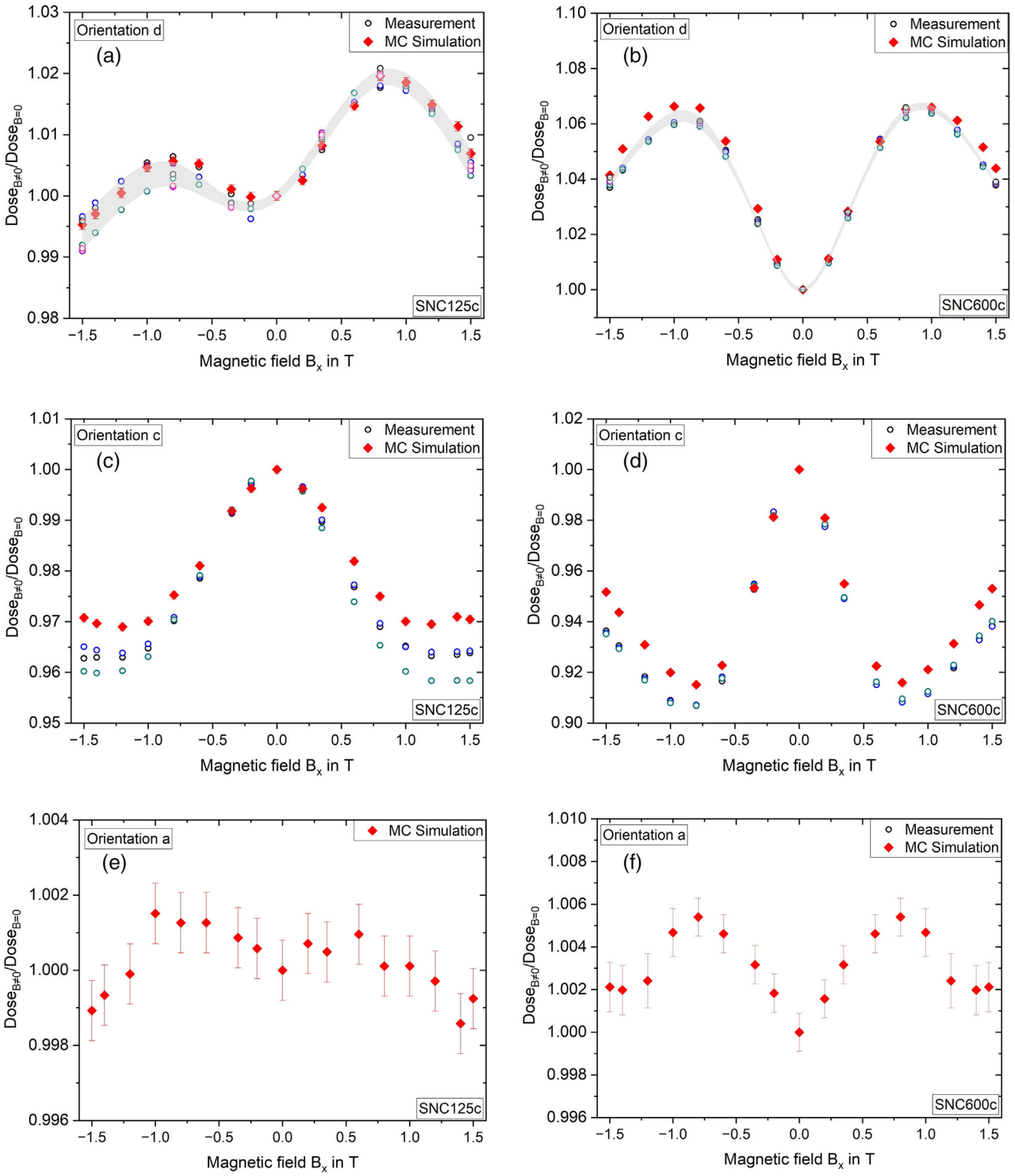

FIGURE 4 Comparison of experimental and Monte Carlo based results of the ratio $\overline{D}^{B}_{det,Q}/\overline{D}_{det,Q}$ as a function of the magnetic field B for the ion chambers SNC125c (left column) and SNC600c (right column) for 6 MV photons. Measured values for the chambers are represented by open circles. Each measurement series with an individual ionization chamber is represented by a different symbol color. Panels (a) and (b) each show the 1σ-standard deviation of six different ionization chambers as gray area, indicating the intra-type variation for the SNC125c and SNC600c respectively. The uncertainty bars in case of the Monte Carlo data represent the type-A-uncertainties, in case of the experimental data the standard deviation of the mean value of ten electrometer readings (1σ). Note the different scales of the y-axes.

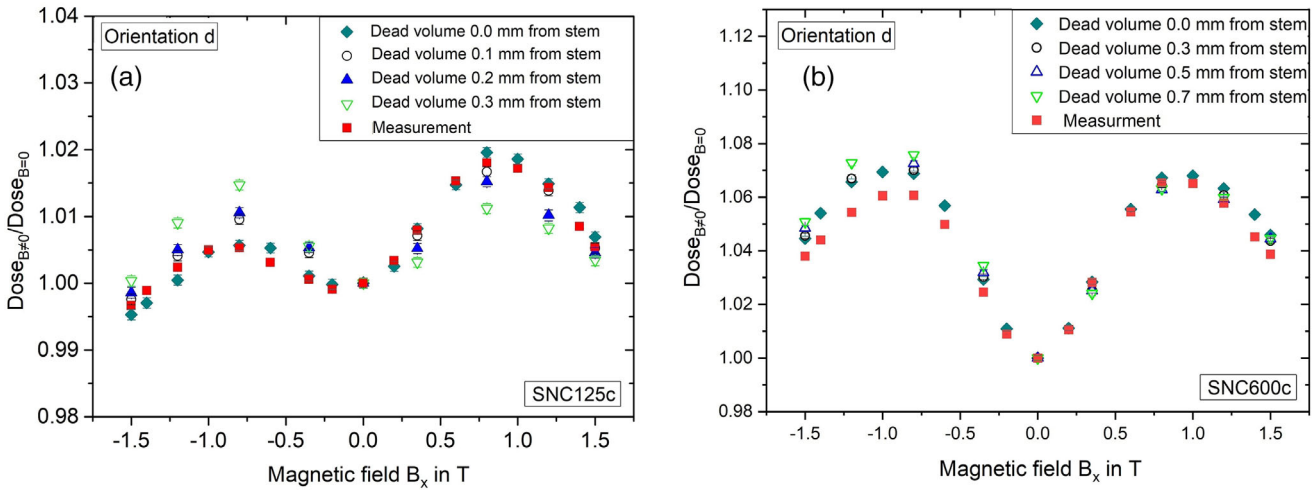

FIGURE 5 Dose ratio $\overline{D}^{B}_{det,Q}/\overline{D}_{det,Q}$ as a function of the magnetic field strength for the SNC125c and SNC600c chamber with differently sized dead volumes for the 6 MV spectrum. The dead volumes were modelled as thin slices of given thickness next to the guard ring. Note that the slice thicknesses chosen for the SNC600c were larger than those used for the SNC125c, due to its larger chamber cavity.

With increasing absolute *B*-values there are also increasing deviations between the Monte Carlo and the experimental data. These deviations are in the range of 1% for *B*-values of 1.5 T in opposite directions. This indicates that there are differences in the geometry of the Monte Carlo model and the real ion chamber. However, one has to keep in mind that chamber orientations (c) and (d), where the magnetic field is perpendicular to the chamber axis, should not be used in clinical routine, since the magnetic field effects are maximized and otherwise insignificant chamber-to-chamber variation can become apparent. Instead, orientation (a) (Figure 4e & f) should be used, where $\overline{D}^{B}_{det,Q}/\overline{D}_{det,Q}$ is near unity. The deviation from unity is less than 0.6% for the SNC600c and less than 0.2% for the SNC125c at all magnetic field strengths. Therefore, this orientation appears as the optimal direction for clinical dosimetry. For both chambers, the Monte Carlo data show a small asymmetry around $B = 0$ T. Due to the small dimensions of the water phantom between the pole shoes of the electromagnet, unfortunately, no measurement data could be acquired in this orientation.

3.1.1 | Effect of a dead volume

Figure 5 shows the potential effect of dead volume on the dose ratios $\overline{D}^{B}_{det,Q}/\overline{D}_{det,Q}$ for both chambers. The best agreement between measurement and Monte Carlo simulation results in a zero dead volume for both chambers. This is in agreement with the findings of Delfs,[8] who examined the effective sensitive volume of the SNC125c chamber with proton microbeam scans and concluded that it has no dead volume. According to our measurements and Monte Carlo simulations, this is also true for the SNC600c chamber. This result is expected, since the geometry of the SNC600c's guard is very similar to that of the SNC125c. In orientation (a) the effect of dead volume does not play a role since the Lorenz force will not deflect electrons toward or against the stem.

3.2 | Magnetic field correction factor $k_{B,Q}$

The magnetic field correction factor $k_{B,Q}$ was calculated according to equation (3) using the TRS-398 setup described in section 2.3, i.e. a 30x30x30 cm^3 water phantom, a field size of 10x10 cm^2 and the setup distances summarized in Table 2. The dose ratios $\overline{D}^{B}_{det,Q}/\overline{D}_{det,Q}$ shown in Figure 4 were also recalculated in this geometry, but the ratios do not differ by more than 0.1% from those calculated in the PTB setup. The factors $k_{B,Q}$ of both ion chambers, all chamber orientations and both photon spectra are presented in Figure 6 as a function of the magnetic field *B* and compared to available data from literature.[8]

The magnitude of $k_{B,Q}$ strongly depends on the chamber volume, i.e. is greater for the SNC600c chamber than for the SNC125c chamber. It also depends on the orientation of the chamber relative to magnetic field and beam directions. For orientation (c) both chambers show an under-response for magnetic fields $B \neq 0$, i.e. $k_{B,Q} > 1$. For the SNC600c chamber the under-response is up to 9% for a magnetic field $B_x \approx 0.8$ T. For the smaller SNC125c chamber it is about 3% for $B_x \approx 1.0$ T. As the Lorentz force in this orientation drives the electrons towards the chamber wall (see Figure 2), the resulting correction factor $k_{B,Q}$ is symmetrical about $B = 0$ T. The impact of the different photon spectra used here (6 MV

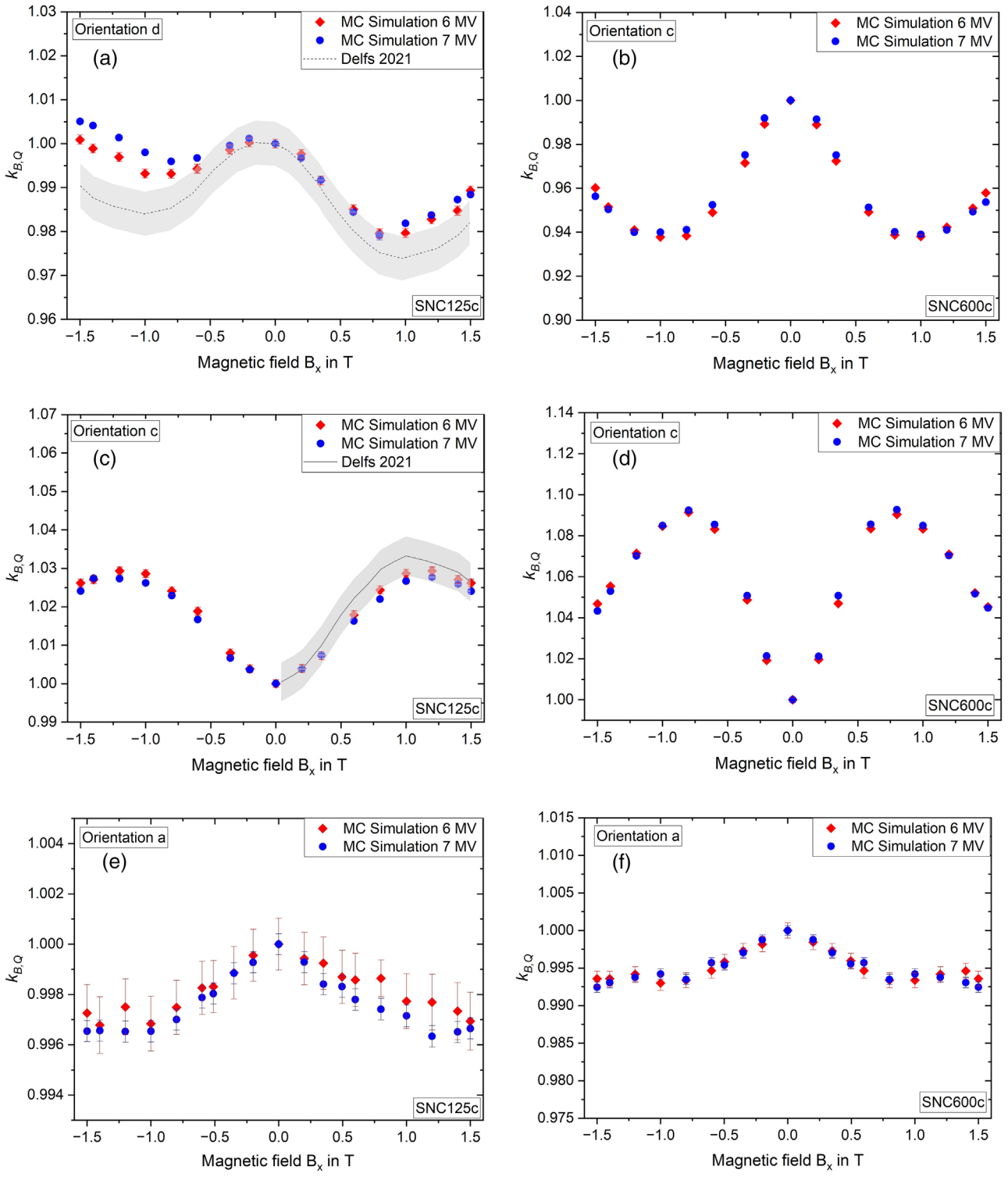

FIGURE 6 Magnetic field correction factors $k_{B,Q}$ of the ion chambers SNC125c and SNC600c as a function of the magnetic field strength B for different chamber orientations with respect to the magnetic field and beam directions (see Figure 2). Two different photon spectra were applied: the 6 MV spectrum of the PTB-linac[20] and the 7 MV spectrum of the Elekta Unity MR-linac.[21] The type-A standard uncertainty is given by the uncertainty bars or by the symbol width. The data from Delfs et al.[8] were calculated with a 6 MV linac spectrum in a geometry that closely resembles the PTB setup of the present study. The uncertainty of Delf's values is given by the shaded area. Note the different scales of the y-axes.

TABLE 5 Magnetic field correction factors for existing MRI-linear accelerators for ionization chambers SNC125c and SNC600c for orientation (a). The differences between $k_{B,Q}$ values for opposing magnetic field directions are within the statistical uncertainty.

Ionization chamber	*B* field	Source 6 MV $k_{B,Q}$	Source 7 MV $k_{B,Q}$
SNC125c	$B_x = \pm 0.35$ T	0.999(0)	0.998(7)
	$B_x = \pm 0.5$ T	0.998(6)	0.998(2)
	$B_x = \pm 1.5$ T	0.997(1)	0.996(5)
SNC600c	$B_x = \pm 0.35$ T	0.997(0)	0.997(0)
	$B_x = \pm 0.5$ T	0.995(4)	0.995(2)
	$B_x = \pm 1.5$ T	0.993(1)	0.992(4)

and 7 MV) is below 0.2% for both chambers and all *B*-values. The Monte Carlo based $k_{B,Q}$ data from Delfs et al.[8] agree within one standard uncertainty with the results of this study, as can be seen in Figure 6c, while for orientation (d) the agreement is within 1%-1.5% (see Figure 6a).

An asymmetry of $k_{B,Q}$ around $B = 0$ T is clearly visible when the SNC125c chamber is positioned in orientation (d). The variation of the correction factor for *B*-values between ±1.5 T is in the range of 2%. An influence of the photon energy is visible only for negative *B* fields and amounts to no more than 0.5% for B_x =-1.5 T. Delfs et al. also produced $k_{B,Q}$ data for a 6 MV spectrum, which agree with the results of this study to within 1% for all magnetic field strengths.

The correction factor $k_{B,Q}$ and its variation with the external *B*–field is smallest in chamber orientation (a), which is the preferred orientation for clinical use. For the SNC125c chamber, the largest deviation from unity is 0.4% at magnetic field strengths near $B_x = 1.5$ T. Even for the larger SNC600c chamber, the deviation from unity is less than 1.2% over the whole range of investigated $\vec{B}$-values. In both cases, the deviation from unity increases with increasing magnetic field strength. While the $k_{B,Q}$ values corresponding to the SNC125c are nearly the same for both energy spectra, they differ in the range of 0.5% for the larger SNC600c chamber. Table 5 summarizes the magnetic field correction factors $k_{B,Q}$ for commercially available MRI-linacs.

4 | CONCLUSION

The objective of the present study was the dosimetric investigation of the SNC125c and SNC600c ionization chambers in external magnetic fields. Together with the data from a previous study, in which the beam quality correction factors k_Q was determined for high-energy photon fields, the dosimetric behavior of these chambers is comprehensively characterized and the correction factors are available to the users for application in clinical routine with minimized dosimetric uncertainties.

The good agreement of experimental data and Monte Carlo simulations validated the applicability of the EGSnrc code system for radiation transport simulations in external magnetic fields. The results clearly showed that the magnetic field correction factor $k_{B,Q}$ strongly depends on the chamber volume and the chamber orientation with respect to the beam and magnetic field directions. The smallest deviation of $k_{B,Q}$ from unity occurs in case when the magnetic field is directed parallel to the chamber axis.[3,5,11,24–26] In that case, the correction factor is below 1.2% for the 0.6 cm^3 SNC600c and below 0.4% for the small SNC125c chamber, even for a $\vec{B}$-field strength of 1.5 T, which is the maximum magnetic field strength of commercially available MRI-linacs.

Furthermore, a change in the dose response was confirmed when a dead volume was introduced to the ionization chamber model, the magnitude of which depends on the size and shape of the dead volume. As the effect of the magnetic field is significantly reduced in orientation (a), the effect of the dead volume may likewise be reduced in that orientation. Still, the simulation of the magnetic field correction factor $k_{B,Q}$ is challenging if an ionization chamber is affected, as prior research has demonstrated. The comparison of the simulated data with measurement data indicated that the investigated ionization chambers do not have a dead volume within the ionization chamber's air cavity. As a result, ionization chambers without a dead volume, like the SNC125c and SNC600c, may be modeled particularly well in Monte Carlo simulations.

ACKNOWLEDGMENTS

The authors have nothing to report.
Open access funding enabled and organized by Projekt DEAL.

CONFLICTS OF INTEREST STATEMENT

The authors declare no conflicts of interest.

REFERENCES

1. Raaijmakers AJ, Raaymakers BW, Lagendijk JJ. Integrating a MRI scanner with a 6 MV radiotherapy accelerator: dose increase at tissue–air interfaces in a lateral magnetic field due to returning electrons. *Phys Med Biol*. 2005;50(7):1363.
2. Raaijmakers AJ, Raaymakers BW, Lagendijk JJ. Magnetic-field-induced dose effects in MR-guided radiotherapy systems: dependence on the magnetic field strength. *Phys Med Biol*. 2008;53(4):909.
3. Meijsing I, Raaymakers B, Raaijmakers A, et al. Dosimetry for the MRI accelerator: the impact of a magnetic field on the response of a Farmer NE2571 ionization chamber. *Phys Med Biol*. 2009;54(10):2993.
4. O'Brien DJ, Roberts DA, Ibbott GS, Sawakuchi GO. Reference dosimetry in magnetic fields: formalism and ionization chamber correction factors. *Med Phys*. 2016;43(8Part1):4915-4927.

5. Spindeldreier C, Schrenk O, Bakenecker A, et al. Radiation dosimetry in magnetic fields with Farmer-type ionization chambers: determination of magnetic field correction factors for different magnetic field strengths and field orientations. *Phys Med Biol*. 2017;62(16):6708.
6. Pojtinger S, Dohm OS, Kapsch RP, Thorwarth D. Ionization chamber correction factors for MR-linacs. *Phys Med Biol*. 2018;63(11):11NT03.
7. Reynolds M, Fallone B, Rathee S. Dose response of selected ion chambers in applied homogeneous transverse and longitudinal magnetic fields. *Med Phys*. 2013;40(4):042102.
8. Delfs B, Blum I, Tekin T, et al. The role of the construction and sensitive volume of compact ionization chambers on the magnetic field-dependent dose response. *Med Phys*. 2021;48(8):4572-4585.
9. Prez Ld, Woodings S, Pooter Jd, et al. Direct measurement of ion chamber correction factors, k_Q and k_B, in a 7 MV MRI-linac. *Phys Med Biol*. 2019;64(10):105025.
10. Malkov VN, Rogers D. Sensitive volume effects on Monte Carlo calculated ion chamber response in magnetic fields. *Med Phys*. 2017;44(9):4854-4858.
11. Malkov VN, Rogers D. Monte Carlo study of ionization chamber magnetic field correction factors as a function of angle and beam quality. *Med Phys*. 2018;45(2):908-925.
12. Alissa M, Zink K, Tessier F, Schoenfeld AA, Czarnecki D. Monte carlo calculated beam quality correction factors for two cylindrical ionization chambers in photon beams. *Phys Med*. 2022;94:17-23.
13. Absorbed Dose Determination in External Beam Radiotherapy, no. TRS-398 in Technical Reports Series. International Atomic Energy Agency - IAEA, Vienna, 2001.
14. Almond PR, Biggs PJ, Coursey BM, et al. AAPM's TG-51 protocol for clinical reference dosimetry of high-energy photon and electron beams. *Med Phys*. 1999;26(9):1847-1870.
15. DIN 6800-2, Procedures of dosimetry with probe-type detectors for photon and electron radiation - Part 2: Ionization chamber dosimetry of high energy photon and electron radiation, DIN - Normenausschuss Radiologie (NAR), 2020.
16. de Pooter J, Billas I, de Prez L, et al. Reference dosimetry in mri-linacs: evaluation of available protocols and data to establish a code of practice. *Phys Med Biol*. 2021;66(5):05TR02.
17. Kawrakow I, Mainegra-Hing E, Rogers DWO, Tessier F, Walters BRB. The EGSnrc Code System: Monte Carlo Simulation of Electron and Photon Transport, 2021. https://doi.org/10.4224/40001303
18. Alissa M, Zink K, Czarnecki D. Investigation of monte carlo simulations of the electron transport in external magnetic fields using fano cavity test, Zeitschrift fuer Medizinische Physik, (2022). https://doi.org/10.1016/j.zemedi.2022.07.002
19. Seltzer SM, Fernandez-Varea JM, Andreo P, et al. Report 90: Key data for ionizing-radiation dosimetry: Measurement standards and applications. *J ICRU*. 2014;14(1):1742-3422.
20. Tikkanen J, Zink K, Pimpinella M, et al. Calculated beam quality correction factors for ionization chambers in MV photon beams. *Phys Med Biol*. 2020;65(7):075003.
21. Ahmad SB, Sarfehnia A, Paudel MR, et al. Evaluation of a commercial MRI Linac based Monte Carlo dose calculation algorithm with GEANT 4. *Med Phys*. 2016;43(2):894-907.
22. Kawrakow I, Mainegra-Hing E, Tessier F, Walter BRB. The EGSnrc C++ class library, 2009.
23. Woodings SJ, van Asselen B, van Soest TL, et al. Technical note: Consistency of ptw30013 and fc65-g ion chamber magnetic field correction factors. *Medical Physics*. 46(8):3739-3745. https://aapm.onlinelibrary.wiley.com/doi/pdf/10.1002/mp.13623
24. Reynolds M, Rathee S, Fallone BG. Ion chamber angular dependence in a magnetic field. *Med Phys*. 2017;44(8):4322-4328.
25. Asselen Bv, Woodings SJ, Hackett SL, et al. A formalism for reference dosimetry in photon beams in the presence of a magnetic field. *Phys Med Biol*. 2018;63(12):125008.
26. Pojtinger S, Dohm OS, Thorwarth D. Optimal orientation for ionization chambers in MRGRT reference dosimetry. *Curr. Dir. Biomed. Eng*. 2017;3(2):273-275.
27. Sechopoulos I, Rogers DWO, Bazalova-Carter M, et al. Records: improved reporting of Monte Carlo radiation transport studies: report of the AAPM research committee task group 268. *Med Phys*. 2018;45(1):e1-e5.
28. Bouchard H, Pooter Jd, Bielajew A, Duane S. Reference dosimetry in the presence of magnetic fields: conditions to validate Monte Carlo simulations. *Phys Med Biol*. 2015;60(17):6639.
29. Bielajew AF. Electron Transport in E and B Fields, Springer US. 1988:421-434. https://doi.org/10.1007/978-1-4613-1059-4_19

How to cite this article: Alissa M, Zink K, Kapsch R-P, Schoenfeld AA, Frick S, Czarnecki D. Experimental and Monte Carlo-based determination of magnetic field correction factors $k_{B,Q}$ in high-energy photon fields for two ionization chambers. *Med Phys*. 2023;1-12. https://doi.org/10.1002/mp.16345

APPENDIX A: FANO CAVITY TEST

The report AAPM TG-268[27] from the American Association of Physicists in Medicine strongly recommends a Fano test for all Monte Carlo studies of detectors with gaseous cavities. In Monte Carlo simulations, the trajectories of charged particles are approximated by condensed history steps, and it is possible that simulation results incorporating magnetic field effects are inaccurate, especially if particles cross boundaries between materials with high and low densities.

In this work, the charged particle transport was tested under Fano conditions as described by Bouchard et al.[28] and Alissa et al.[18] in presence of a magnetic field for all regions *i* of the two ionization chamber models. To realize the Fano conditions with an external magnetic field, a radiation source was used that distributes electrons in the whole geometry proportional to the density of the material at the current position. In that way, the number of particles n_i emitted in region *i* depends on the volume and density of the region *i*, and thus on the mass m_i of region *i*. Hence, the total number of particles *N* emitted by the source and the irradiated mass can be described by the following equation.

$$\frac{n_i}{N} = \frac{m_i}{\sum m_i} \tag{A.1}$$

where $\sum m_i$ is the sum over all masses irradiated by the source. The size of the volume of the Fano source was chosen to be large enough to create secondary particle equilibrium in the regions of interest. The electrons are emitted isotropic in all directions and all bremsstrahlung photons were discharged. Furthermore, all materials were replaced by water. In that case, the following

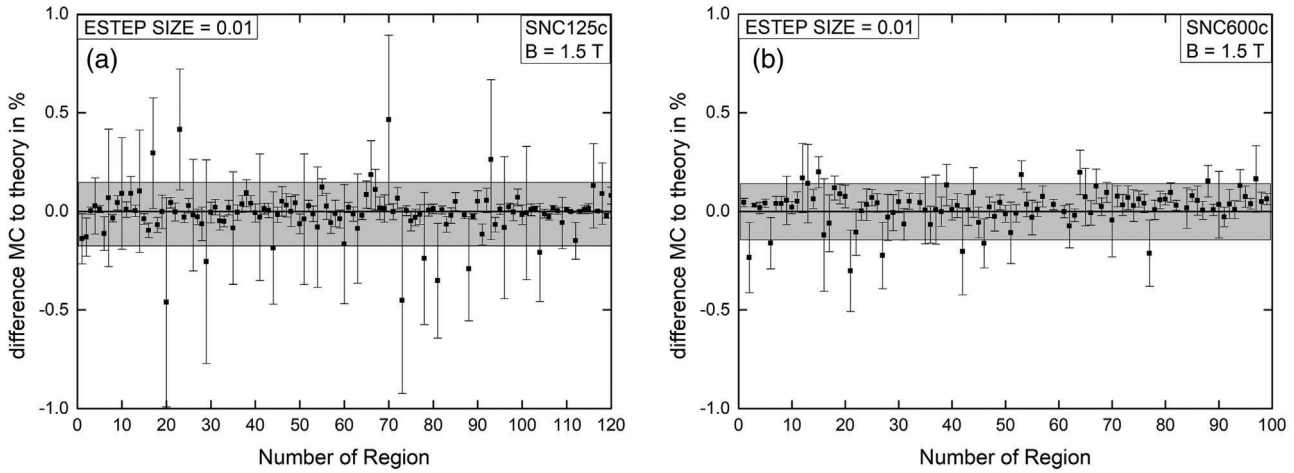

FIGURE A.1 Results of the Fano cavity test for the SNC600c and SNC125c ion chambers in presence of a magnetic field of 1.5 T. The y-axis of both panels show the relative deviation of the Monte Carlo based dose from the expected dose value for each geometrical region of the chambers. The type-A standard uncertainty is represented by the uncertainty bars.

equations holds:

$$D_{\mathrm{MC},i} = n_i \frac{E_0}{m_i} \tag{A.2}$$

where $D_{MC,i}$ is the Monte Carlo-based dose value within the i-th region without normalization to the particle source, E_0 is the energy of the primary electrons of the Fano source, and n_i/m_i is constant for all regions. The Fano particle source included in the EGSnrc c++ class library[22] was used and had a volume of 7x5x5 cm^3. The energy of the primary electrons was $E_0 = 1$ MeV and the ESTEPE-parameter within the emf_macro.mortran[29] was set to 0.01. In addition, all materials of the investigated chambers were replaced by water with the density of the original material. The I-value and the density effect corrections were set to the corresponding values of water with density $\rho = 1$ g/cm^3. Monte Carlo results are acceptable, when the relative difference between the theoretically expected value E_0/m_i and the Monte Carlo based dose value $D_{MC,i}$ for every region i within the chamber is less than 0.1%.

The results for the both ion chambers are shown in Figure (A.1). Regarding the small SNC125c chamber, regions 2 and 4 correspond to the active chamber volume and starting from region 10 the volumes belong to the chamber stem. In the SNC600c model, the regions 2 and 6 correspond to the sensitive volume, and the chamber stem regions start with region number 8. Taking into account the uncertainty of the Monte Carlo results, the difference in percent between calculated and expected dose value for all regions of the ionization chambers SNC600c and SNC125c is within 0.1%, i.e. both chambers passed the Fano test for all regions.

Physica Medica 117 (2024) 103179

Contents lists available at ScienceDirect

Physica Medica

journal homepage: www.elsevier.com/locate/ejmp

Original paper

Monte Carlo calculated beam quality correction factors for high energy electron beams

Mohamad Alissa [a], Klemens Zink [a,b], Arnd Röser [c], Veronika Flatten [d], Andreas A. Schoenfeld [d], Damian Czarnecki [a,*]

[a] Institute of Medical Physics and Radiation Protection, University of Applied Sciences Giessen (THM), Wiesenstraße 14, Giessen, 35390, Germany
[b] Department of Radiotherapy and Radiation Oncology, University Medical Center Giessen and Marburg, Baldingerstraße, Marburg, 35043, Germany
[c] Helios Universitätsklinikum Wuppertal, Heusnerstraße 40, Wuppertal, 42283, Germany
[d] Sun Nuclear, A Mirion Medical Company, 3275 Suntree Blvd, Melbourne, 32940, FL, USA

ARTICLE INFO

Keywords:
Dosimetry
Beam quality correction factor
Ionization chamber
Monte Carlo simulation
High energy electron beams

ABSTRACT

Purpose: As the dosimetry protocol TRS 398 is being revised and the ICRU report 90 provides new recommendations for density correction as well as the mean ionization energies of water and graphite, updated beam quality correction factors k_Q are calculated for reference dosimetry in electron beams and for independent validation of previously determined values.

Methods: Monte Carlo simulations have been performed using EGSnrc to calculate the absorbed dose to water and the dose to the active volumes of ionization chambers SNC600c, SNC125c and SNC350p (all Sun Nuclear, A Mirion Medical Company, Melbourne, FL). Realistic clinical electron beam spectra were used to cover the entire energy range of therapeutic electron accelerators. The Monte Carlo simulations were validated by measurements on a clinical linear accelerator.

With regards to the cylindrical chambers, the simulations were performed according to the setup recommendations of TRS 398 and AAPM TG 51, i.e. with and without consideration of a reference point shift by $r_{cav}/2$.

Results: k_Q values as a function of the respective beam quality specifier R_{50} were fitted by recommended equations for electron beam dosimetry in the range of 5 MeV to 18 MeV. The fitting curves to the calculated values showed a root mean square deviation between 0.0016 and 0.0024.

Conclusion: Electron beam quality correction factors k_Q were calculated by Monte Carlo simulations for the cylindrical ionization chambers SNC600c and SNC125c as well as the plane parallel ionization chamber SNC350p to provide updated data for the TRS 398 and TG 51 dosimetry protocols.

1. Introduction

Plane parallel and thimble ionization chambers are used for measurements of the absorbed dose to water in high energy electron beams. The corresponding formalisms are described in national and international dosimetry protocols [1–3]. When dose measurements are performed in radiation fields deviating from the reference beam quality (Co-60), the measurement signal must be corrected using the beam quality correction factor k_Q.

The international IAEA TRS 398 Code of Practice is being revised, and new correction factors for several ionization chambers will be included in the protocol's update. To achieve a high quality selection of published k_Q values, the TRS task group motivates multiple independently determined data sets per chamber model. Our research groups have been contributing to the update of the TRS 398 protocol by providing k_Q values in multiple publications [4–8].

In this study, we extended our investigation to calculate the beam quality correction factors k_Q for reference dosimetry in high-energy electron beams by using Monte Carlo simulations.

2. Materials and methods

2.1. Beam quality correction factor for electron beams

R_{50} functions as beam quality specifier in high energy electron beams and is the depth at which the electron depth dose curve decreases to 50% of its maximum value. It is used in accordance with the

* Corresponding author.
E-mail address: damian.czarnecki@lse.thm.de (D. Czarnecki).

https://doi.org/10.1016/j.ejmp.2023.103179
Received 19 January 2023; Received in revised form 5 October 2023; Accepted 16 November 2023
Available online 1 December 2023

dosimetry protocols TRS 398 [3] and the task group report 51 of the AAPM [2]. The reference depth z_{ref} was determined according to TRS 398 using Eq. (1). The calculation of z_{ref} is identical to the calculation of d_{ref} in TG 51 [2].

$$z_{ref} = 0.6\,R_{50} - 0.1\ \mathrm{g\ cm^{-2}} \tag{1}$$

The beam quality correction factor k_Q is defined as shown in the following equation.

$$k_Q = \left(\frac{D_w}{M_{det}}\right)_Q \Big/ \left(\frac{D_w}{M_{det}}\right)_{Co\text{-}60} \tag{2}$$

where D_w is the absorbed dose to water and M_{det} is the detector response of the investigated ionization chamber at the beam qualities Q of the clinical electron beam and Co-60. In order to calculate k_Q values from Monte Carlo simulations, it must be assumed that the detector response M_{det} is proportional to the dose in the sensitive volume D_{det} of the detector. This results in the following equation to calculate the k_Q values from Monte Carlo simulations.

$$k_Q = \left(\frac{D_w}{D_{det}}\right)_Q \Big/ \left(\frac{D_w}{D_{det}}\right)_{Co\text{-}60} \tag{3}$$

The correction factor k_Q as a function of the beam quality R_{50} has been described in the literature by the following two equations.

$$k_Q = a + b\,(R_{50})^c \tag{4}$$

$$k_Q = a' + b' \exp\left(-R_{50}/c'\right) \tag{5}$$

In the work of Rogers [9], Eq. (4) was used for plane-parallel chambers and Eq. (5) for cylindrical ionization chambers. The TG 51 dosimetry protocol adopted the suggestion [2]. However, further work [10,11] has shown that function (5) fits k_Q data for plane-parallel ionization chambers and function (4) fits k_Q data for cylindrical chambers slightly better. Although the differences are small, these recommendations were included in the TRS 398 [3] as well as the DIN 6800-2 dosimetry protocols [1]. In this work, data for both ionization chamber types were fitted to Eq. (4) as well as (5).

2.2. Calibration with an intermediate beam quality

To facilitate a cross calibration in an arbitrary electron beam quality Q_{cross}, TG 51 and TRS 398 introduce an intermediate beam quality Q_{int}, which is suggested to be R_{50} = 7.5 g/cm^2 in both protocols. The corresponding beam quality correction factor $k_{Q,Q_{int}}$ was calculated according to Eq. (6).

$$k_{Q,Q_{int}} = \left(\frac{D_w}{D_{det}}\right)_Q \Big/ \left(\frac{D_w}{D_{det}}\right)_{Q_{int}} \tag{6}$$

Thereby, the beam quality correction factor $k_{Q,Q_{cross}}$ can be calculated according to Eq. (7).

$$k_{Q,Q_{cross}} = \frac{k_{Q,Q_{int}}}{k_{Q_{cross},Q_{int}}} \tag{7}$$

In analogy to the correction factor k_Q, the correction factor $k_{Q,Q_{int}}$ was fitted to the following equation.

$$k_{Q,Q_{int}} = \frac{a + b\,(R_{50})^c}{a + b\,(7.5)^c} = \frac{1 + b/a\,(R_{50})^c}{1 + b/a\,(7.5)^c} \tag{8}$$

Thereby, it was ensured that the function at R_{50} = 7.5 cm corresponds to unity. Moreover, the equation can be expressed as follows,

$$k_{Q,Q_{int}} = \frac{1 + \alpha\,(R_{50})^c}{1 + \alpha\,(7.5)^c} \tag{9}$$

where $\alpha = b/a$.

Table 1
Summary of main properties and parameters of the Monte Carlo simulations.

Item	Description	References
Code	EGSnrc 2020 master branch	Kawrakow et al. [12]
	egs++ library, EGSnrc 2020 master branch	Kawrakow et al. [13]
	egs_chamber, EGSnrc 2020 master branch	Wulff et al. [14]
Validation	Fano cavity test	
Timing	absorbed dose to water D_w in the sensitive volume of chamber for photon spectra and full linac head simulations took 2800 and 11000 h, respectively, for each energy and ionization chamber	
Source description	Collimated isotropic high energy electron spectra	Ding and Rogers [15]
Cross-sections	XCOM photon cross section with multiconfiguration Dirac–Fock renormalization factor for the photoelectric effect (mcdf-xcom)	
Transport parameters	Boundary crossing algorithm: Exact, transport and particle production threshold energy of 512 keV and 1 keV for electron and photon, respectively	
Variance reduction techniques	Russian Roulette range rejection technique with a survival probability of 1/128.	Wulff et al. [14]
Scored quantities	Absorbed dose to water and dose to air	
Statistical uncertainties	$\leq 0.1\%$ for all calculated quantities	
Statistical method	History-by-history	
Postprocessing	None	

2.3. Monte Carlo set-up

The Monte Carlo calculations were performed using the EGSnrc code system. The simulation parameters can be found in Table 1.

2.3.1. Ionization chamber models

This investigation made use of the Monte Carlo model of the ionization chamber SNC600c and SNC125c (Sun Nuclear, A Mirion Medical Company, Melbourne, FL) that THM (Technische Hochschule Mittelhessen University of Applied Sciences, Giessen, Germany) developed in the original work published by Alissa et al. [8]. Furthermore, a detailed model of the plane parallel ionization chamber SNC350p (Sun Nuclear Corporation, Melbourne, FL) was developed with the EGSnrc C++ class library [13] according to technical drawings provided by the manufacturer. Fig. 1 shows a cross section of the detailed model of the SNC350p with a sensitive volume height and diameter of 2 mm and 15.6 mm, respectively. A cross section view of the SNC600c model and corresponding Fano test results are presented in Alissa et al. [8]. The SNC350p model has likewise been Fano tested with similar results.

2.3.2. Ionization chamber positioning

The ionization chambers were placed in a water phantom of size $30 \times 30 \times 30$ cm^3. The reference point of the plane parallel chamber, which is on the inner surface of the entrance window, at the center of the window, was positioned at the reference depth z_{ref} (in g cm^{-2}) taking into account the density of the entrance window. The dosimetry protocols TRS 398 and TG 51 use different positioning requirements for thimble ionization chambers in electron dosimetry. While TG 51 positions the reference point of the chamber, which is on the chamber axis at the center of the cavity volume, at z_{ref}, TRS 398 recommends a downstream shift of the reference point by $r_{cav}/2$, where r_{cav} is the radius of the air cavity of the ionization chamber. Both methods have been addressed in this study.

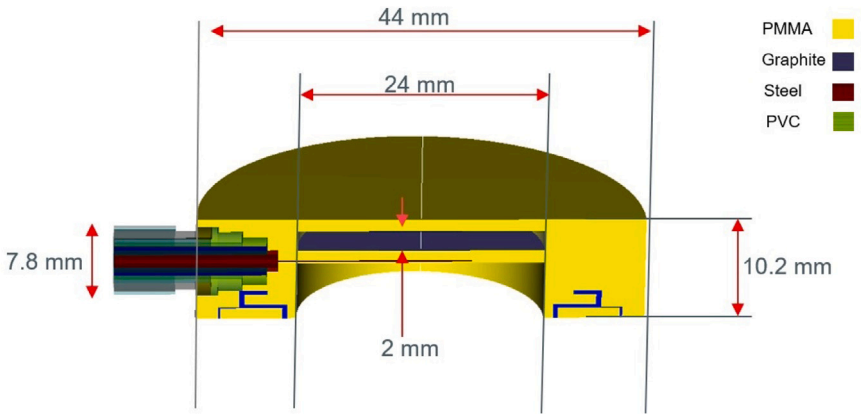

Fig. 1. Cross-section view of the Monte Carlo model of the plane parallel ionization chamber SNC350p. The image is not to scale. Different materials are represented by different colors. (For interpretation of the references to color in this figure legend, the reader is referred to the web version of this article.)

The Co-60 γ-spectrum used in this work was originated from the publication by Han et al. [16]. In the Co-60 radiation field, the dose D_w was calculated in 5 cm water depth and the ionization chambers were position at 5 cm water depth and 100 cm source to surface distance.

2.3.3. Radiation field

A divergent collimated electron source with a field size of 10 × 10 cm^2 at the phantom surface and a source to surface distance of 100 cm was used to simulate the radiation field according to reference conditions of TRS 398 and TG 51. Realistic clinical electron beam spectra have been taken from the work of Ding and Rogers [15]. They calculated electron beam spectra using Monte Carlo simulations of various clinical linear accelerator head models. These spectra cover the entire energy range of therapeutic electron beam applications.

2.4. Experimental validation

Cross-validation measurements were performed in a water phantom with a TrueBeam (Varian) linear accelerator for all five available electron energies (6 MeV, 9 MeV, 12 MeV, 15 MeV and 18 MeV). A metrological control using thermoluminescent detectors traceable to a secondary dose standard was performed and evaluated prior to the measurements to maximize beam quality control and accuracy of R_{50}. To obtain an experimental value for k_Q for all three chambers, a reference measurement was performed with a calibrated PTW Roos chamber (PTW, Freiburg, Germany). All three chambers of interest and the reference chamber were positioned according to TRS 398 and TG 51 guidelines so that the measurement setups match the Monte Carlo simulation setups. All measurements were repeated with a second chamber of the same chamber type. For each chamber, three to five data points were acquired, where a data point corresponds to the measured signal when irradiated with 100 MU, which approximately is an absorbed dose of 1 Gy at z_{ref}.

The $k_{Q,exp}$ was determined by taking the mean of all data points for each chamber type and calculating:

$$k_{Q,\mathrm{exp}} = \frac{M_{\mathrm{ref}} \cdot N_{D,\mathrm{w,ref}} \cdot k_{Q,\mathrm{ref}} \cdot \Pi_i k_{i,\mathrm{ref}}}{M_{\mathrm{exp}} \cdot N_{D,\mathrm{w,exp}} \cdot \Pi_i k_{i,\mathrm{exp}}} \tag{10}$$

where all reference values correspond to the reference chamber measurement and all experimental values correspond to the respective chamber of interest. M is the measured signal, assuming the setup according to TRS 398 or TG 51, $N_{D,w}$ the calibration factor and $\Pi_i k_i$ is the product of all correction factors k_i that correct the detector signal due to deviations from the reference conditions during calibration. $k_{Q,ref}$ was obtained from the updated TRS 398 protocol draft.

Table 2
Calculated electron beam quality specifier R_{50} and reference depth z_{ref}.

Linac	Energy in MeV	R_{50} in cm	z_{ref} in cm
Philips SL75–20	5	2.091	1.155
	10	4.123	2.373
	14	6.014	3.508
	17	6.952	4.071
	20	8.075	4.745
Siemens KD2	6	2.308	1.285
	11	4.202	2.421
	21	8.301	4.880
Varian Clinac 2100D	6	2.635	1.481
	9	3.968	2.281
	12	5.171	3.000
	18	7.711	4.526

3. Results

Table 2 shows the electron beam spectra investigated in this study, as well as the calculated electron beam quality specifiers R_{50} and reference depths z_{ref} calculated from Eq. (1).

3.1. Beam quality correction factors k_Q with Co-60 as reference beam quality

Fig. 2 presents Monte Carlo calculated and measured k_Q values for the plane parallel ionization chamber SNC350p as a function of the electron beam quality specifier R_{50}. The k_Q values in this work are compared with those from the NRC Report IRS-1860r [17].

The Monte Carlo calculated and measured k_Q values for the Farmer-type ionization chamber SNC600c are shown in Fig. 3 as a function of the electron beam quality specifier R_{50}, with and without a shift of $r_{cav}/2$ according to the dosimetry protocols TRS 389 and TG 51 of the AAPM, respectively. The results presented in Fig. 3 are compared to k_Q values from measurements and published values from the NRC Report IRS-2065 [18].

The uncertainty of the measured data in Figs. 2–4 is estimated at 3% and is largely due to the uncertainty of the calibration factors of the reference and investigated ionization chamber. Eqs. (4) and (5) were fitted to the k_Q data for the investigated ionization chambers. The fit parameters with the corresponding χ^2 values of the fits to Eqs. (4) and (5) are presented in Tables 3 and 4, respectively.

3.2. Calibration with an intermediate beam quality Q_{int}

To calculate the beam quality correction factor $k_{Q,Q_{int}}$ with the intermediate beam quality Q_{int} at R_{50} = 7.5 g/cm^2, the ratio between the dose D_{det} and the dose to water D_w was interpolated from the

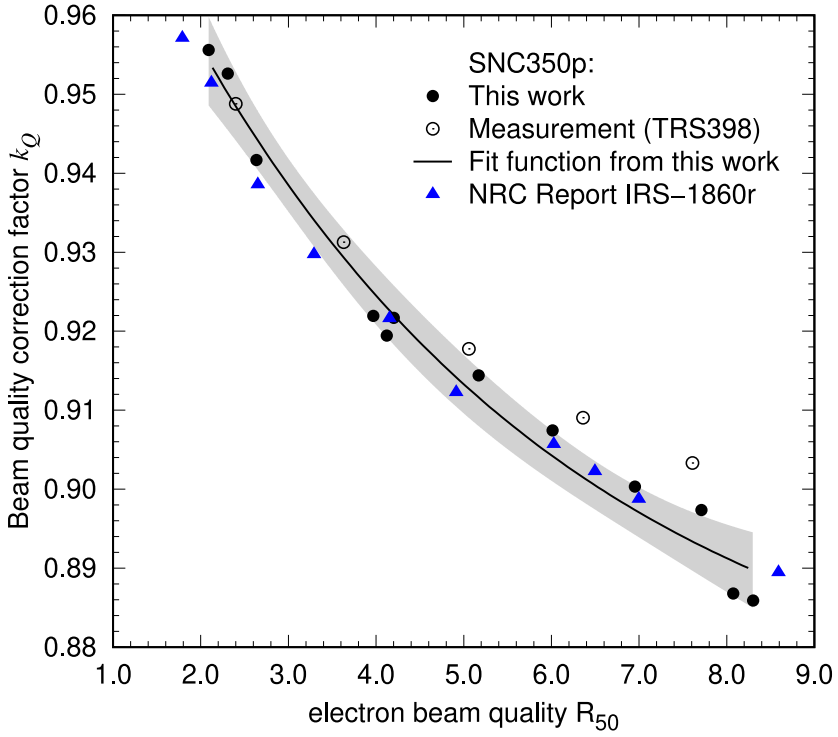

Fig. 2. Monte Carlo calculated and measured electron beam correction factor k_Q for the plane parallel ionization chamber SNC350p as a function of the electron beam quality specifier R_{50} in comparison to data from NRC report IRS-1860r [17]. The solid line and the shaded area are the fit function (see Eq. (4)) and the 95% confidence bound of the data calculated in this work. The statistical uncertainty markers of the Monte Carlo calculated values are within the symbol size (i.e., 1 σ < 0.1%). The uncertainty of the measured data is estimated at 3%, largely due to the uncertainties of the calibration factors (not presented for reasons of clarity).

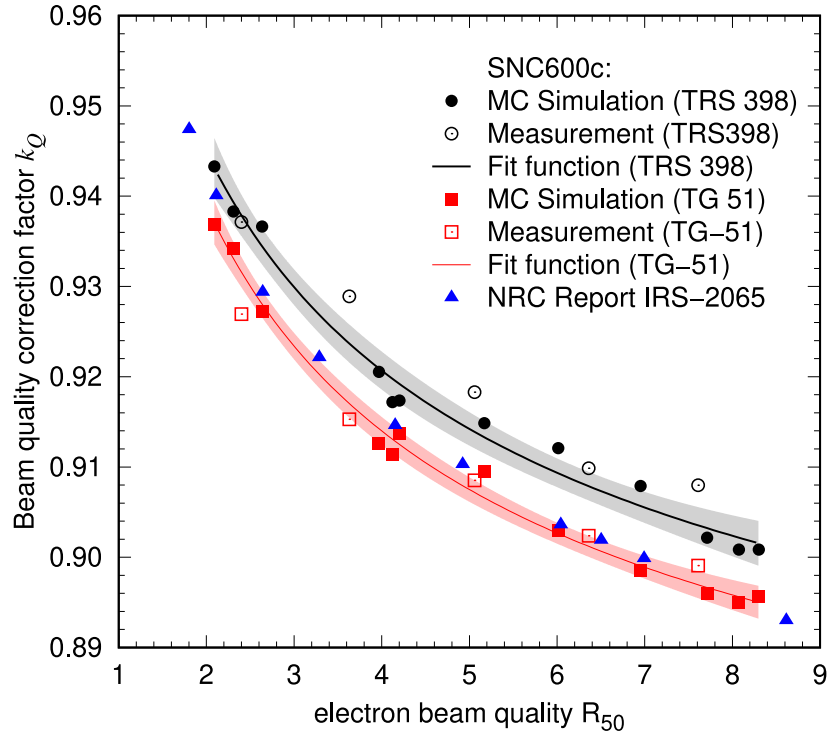

Fig. 3. Monte Carlo calculated and measured electron beam correction factor k_Q for the Farmer-type ionization chamber SNC600c as a function of the electron beam quality specifier R_{50}. The k_Q values in this work were calculated according TRS 398, i.e. with a shift of $r_{cav}/2$ of the ionization chambers, and according to TG 51 to validate the data of NRC Report IRS-2065. The solid lines and the shaded areas are the fit functions (see Eq. (4)) and the 95% confidence bounds for the data calculated in this work. The statistical uncertainty of the Monte Carlo calculated values are within the symbol size (i.e., 1 σ < 0.1%). The uncertainty of the measured data is estimated at 3%, largely due to the uncertainties of the calibration factors (not presented for reasons of clarity).

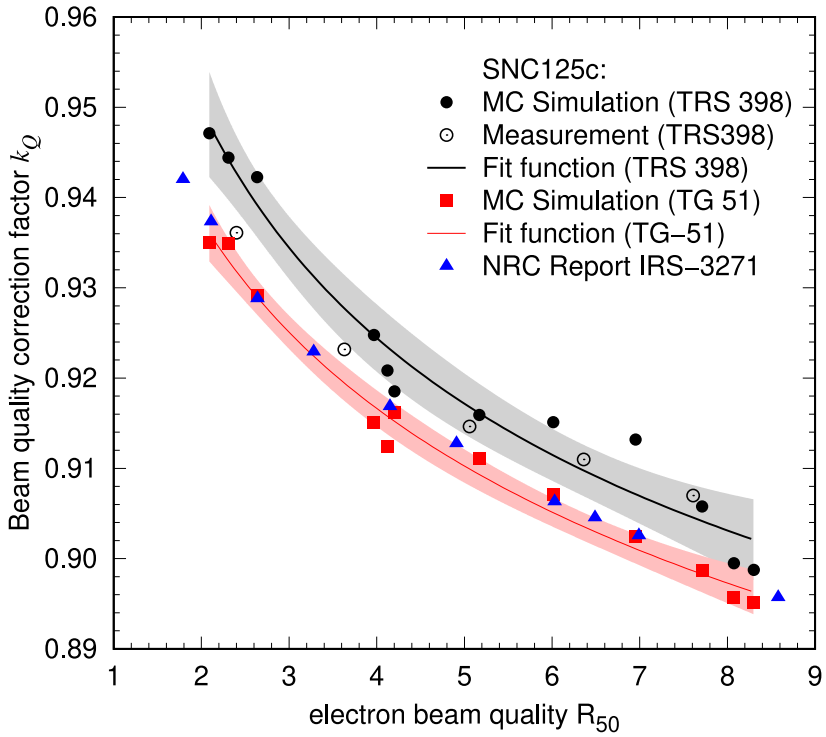

Fig. 4. Monte Carlo calculated and measured electron beam correction factor k_Q for the cylindrical ionization chamber SNC125c as a function of the electron beam quality specifier R_{50}. The k_Q values in this work were calculated according TRS 398, i.e. with a shift of $r_{cav}/2$ of the ionization chambers, and according to TG 51. The solid lines and the shaded areas are the fit functions (see Eq. (4)) and the 95% confidence bounds for the data calculated in this work. The statistical uncertainty of the Monte Carlo calculated values are within the symbol size (i.e., 1 σ < 0.1%). The uncertainty of the measured data is estimated at 3%, largely due to the uncertainties of the calibration factors (not presented for reasons of clarity).

Table 3
Fitting parameter for the function $k_Q = a + b(R_{50})^c$.

Ionization	TRS 398			
chamber	a	b	c	χ^2
SNC350p	−1.387	2.378	−0.02060	9.9e−05
SNC600c	0.8458	0.1312	−0.4043	3.4e−05
SNC125c	0.7922	0.1880	−0.2535	1.1e−04
	TG 51			
	a	b	c	χ^2
SNC350p		same value as above		
SNC600c	0.8471	0.1260	−0.4568	1.9e−05
SNC125c	0.6337	0.3260	−0.1022	3.2e−05

Table 4
Fitting parameter for the function $k_Q = a' + b' \exp(-R_{50}/c')$.

Ionization	TRS 398			
chamber	a'	b'	c'	χ^2
SNC350p	0.8677	0.1370	4.544	1.2e−04
SNC600c	0.8956	0.09227	3.0932	4.1e−05
SNC125c	0.8933	0.09849	3.501	1.2e−04
	TG 51			
	a'	b'	c'	χ^2
SNC350p		same value as above		
SNC600c	0.8895	0.0945	2.988	2.4e−05
SNC125c	0.8856	0.08326	4.0830	3.9e−05

date of the investigate spectra using function (4). Table 5 shows the interpolated ratio D_w/D_{ch} for the intermediate beam quality Q_{int} with the confidence interval of 95%.

Beam quality correction factors $k_{Q,Q_{int}}$ were calculated from the data presented in Figs. 2–4 and Table 5 using R_{50} = 7.5 g/cm^2 as intermediate beam quality Q_{int}. The $k_{Q,Q_{int}}$ values for the investigated

Table 5
Interpolated D_w/D_{det} values for the intermediate beam quality Q_{int} (R_{50} = 7.5 g/cm^2).

Ionization chamber	TRS 389	TG 51
SNC350p	1.019(4)	
SNC600c	1.009(2)	1.002(2)
SNC125c	1.008(4)	1.001(2)

Table 6
Fitting parameter for the function $k_{Q,Q_{int}} = \frac{1+\alpha(R_{50})^c}{1+\alpha(7.5)^c}$.

Ionization	TRS 398		
chamber	α	c	χ^2
SNC350p	0.3905	−0.2174	1.8E−04
SNC600c	0.1551	−0.4043	4.2E−05
SNC125c	0.2373	−0.2535	1.4E−09
	TG 51		
	α	c	χ^2
SNC350p		same value as above	
SNC600c	0.1488	−0.4568	2.3E−05
SNC125c	0.5229	−0.1009	4.0E−05

ionization chambers are shown in Fig. 5. For the cylindrical ionization chamber SNC600c and SNC125c determined with and without a shift of $r_{cav}/2$ according to the dosimetry protocols TRS 398 [3] (left panel of Fig. 5) and TG 51 [2] (right panel of Fig. 5), respectively.

The $k_{Q,Q_{int}}$ values in Fig. 5 are fitted to Eq. (9). The fit parameters from the fit functions in Fig. 5 and the corresponding χ^2 are summarized in Table 6.

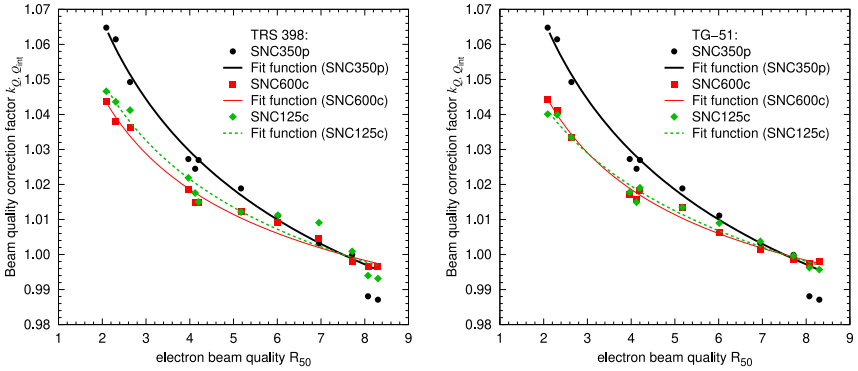

Fig. 5. Monte Carlo calculated electron beam quality correction factor $k_{Q,Q_{int}}$ for the plane parallel ionization chamber SNC350p and the cylindrical ionization chambers SNC600c and SNC125c as a function of the electron beam quality specifier R_{50} as derived from the data presented in Figs. 2–4. The $k_{Q,Q_{int}}$ values in this work were calculated according TRS 398, i.e. with a shift of $r_{cav}/2$ of the ionization chamber (left panel), and according to TG 51, i.e. without any shift (right panel). Solid lines represent corresponding fit functions (see Table 6). The statistical uncertainty of the Monte Carlo calculated values is within the symbol size (i.e. 1 σ < 0.1%).

4. Discussion

The calculated R_{50} and z_{ref} values are in good agreement with the values published by Ding and Rogers [15]. Moreover, this study provides calculated k_Q and $k_{Q,Q_{int}}$ data for reference dosimetry in high energy electron beams according to the TRS 398 and TG 51 dosimetry protocols. To achieve high quality k_Q data, TRS 398 motivates to intercompare independent data sets from different research groups. The measurements obtained in this work confirm the Monte Carlo calculated k_Q values. It should be noted that no Monte Carlo simulations were performed with a Varian TrueBeam spectrum, as was done in the experimental setup. However, as demonstrated in this work by Monte Carlo simulations, the k_Q values as a function of R_{50} follow the same functional relationship for different linac spectra. Moreover, the determined data for the SNC350p are in good agreement with the data published in the NRC report IRS-1860r. Under the reference conditions of the AAPM TG 51 Report, NRC Report IRS-2065 and IRS-3271 provide k_Q values for the SNC600c and SNC125c, respectively, which have been validated in this work. Additionally, this study provides k_Q data for the reference conditions of TRS 398 and $k_{Q,Q_{int}}$ data for a reference beam quality of R_{50} = 7.5 g/cm^2.

Both NRC Reports used the recommendations of ICRU Report 37, which have recently been updated in ICRU Report 90 with respect to the density correction and the mean ionization energies of water and graphite. This study followed the updated recommendations of ICRU 90. The good agreement of the data sets in Figs. 2 and 3 confirms that the impact of the updated recommendations is insignificant for k_Q in electron reference dosimetry, as has been shown in previous studies [7].

5. Conclusion

Electron beam quality correction factors k_Q, as well as $k_{Q,Q_{int}}$ values for the reference beam quality of R_{50} = 7.5 g/cm^2, were calculated by Monte Carlo simulations for the Farmer-type ionization chamber SNC600c and the plane parallel ionization chamber SNC350p, as well as for the thimble ionization chamber SNC125c to provide additional data for the TRS 398 and TG 51 dosimetry protocols. Previous data produced under consideration of ICRU 37 were updated and validated under consideration of ICRU 90. The small uncertainties in the calculated values, the good agreement with already published data and the experimental validation show high confidence.

Declaration of competing interest

The authors declare that they have no known competing financial interests or personal relationships that could have appeared to influence the work reported in this paper.

References

[1] DIN 6800-2. Procedures of dosimetry with probe-type detectors for photon and electron radiation - Part 2: Ionization chamber dosimetry of high energy photon and electron radiation. DIN - Normenausschuss Radiologie (NAR); 2008.
[2] Almond PR, Biggs PJ, Coursey BM, Hanson WF, Huq MS, Nath R, et al. AAPM's TG-51 protocol for clinical reference dosimetry of high-energy photon and electron beams. Med Phys 1999;26(9):1847–70. http://dx.doi.org/10.1118/1.598691, URL https://aapm.onlinelibrary.wiley.com/doi/abs/10.1118/1.598691.
[3] Andreo P, Burns DT, Hohlfeld K, Huq MS, Kanai T, Laitano F, et al. Absorbed dose determination in external beam radiotherapy: An international code of practice for dosimetry based on standards of absorbed dose to water. Technical reports series No. 398, International Atomic Energy Agency; 2006.
[4] Zink K, Wulff J. Beam quality corrections for parallel-plate ion chambers in electron reference dosimetry. Phys Med Biol 2012;57(7):1831. http://dx.doi.org/10.1088/0031-9155/57/7/1831.
[5] Andreo P, Burns DT, Kapsch RP, McEwen M, Vatnitsky S, Andersen CE, et al. Determination of consensus k_Q values for megavoltage photon beams for the update of IAEA TRS-398. Phys Med Biol 2020;65(9):095011. http://dx.doi.org/10.1088/1361-6560/ab807b.
[6] Czarnecki D, Zink K, Pimpinella M, Borbinha J, Teles P, Pinto M. Monte Carlo calculation of quality correction factors based on air kerma and absorbed dose to water in medium energy X-ray beams. Phys Med Biol 2020;65(24):245042. http://dx.doi.org/10.1088/1361-6560/abc5c9.
[7] Czarnecki D, Poppe B, Zink K. Impact of new ICRU Report 90 recommendations on calculated correction factors for reference dosimetry. Phys Med Biol 2018;63(15):155015. http://dx.doi.org/10.1088/1361-6560/aad148.
[8] Alissa M, Zink K, Tessier F, Schoenfeld AA, Czarnecki D. Monte Carlo calculated beam quality correction factors for two cylindrical ionization chambers in photon beams. Phys Med 2022;94:17–23. http://dx.doi.org/10.1016/j.ejmp.2021.12.012.
[9] Rogers DWO. A new approach to electron-beam reference dosimetry. Med Phys 1998;25(3):310–20. http://dx.doi.org/10.1118/1.598211, URL https://aapm.onlinelibrary.wiley.com/doi/abs/10.1118/1.598211.
[10] Muir BR, Rogers DWO. Monte Carlo calculations for reference dosimetry of electron beams with the PTW Roos and NE2571 ion chambers. Med Phys 2013;40(12):121722. http://dx.doi.org/10.1118/1.4829577, URL https://aapm.onlinelibrary.wiley.com/doi/abs/10.1118/1.4829577.
[11] Muir BR, Rogers DWO. Monte Carlo calculations of electron beam quality conversion factors for several ion chamber types. Med Phys 2014;41(11):111701. http://dx.doi.org/10.1118/1.4893915, URL https://aapm.onlinelibrary.wiley.com/doi/abs/10.1118/1.4893915.
[12] Kawrakow I, Mainegra-Hing E, Rogers DWO, Tessier F, Walters BRB. The EGSnrc code system: Monte Carlo simulation of electron and photon transport. Report PIRS-701, National Research Council of Canada; 2010.
[13] Kawrakow I, Mainegra-Hing E, Tessier F, Walter BRB. The EGSnrc C++ class library. NRC Report PIRS-898 (rev A), Ottawa, Canada, 2009.
[14] Wulff J, Zink K, Kawrakow I. Efficiency improvements for ion chamber calculations in high energy photon beams. Med Phys 2008;35(4):1328–36. http://dx.doi.org/10.1118/1.2874554.
[15] Ding G, Rogers D. Energy spectra, angular spread, and dose distributions of electron beams from various accelerators used in radiotherapy. Report PIRS-0439, National Research Council of Canada; 1995.
[16] Han K, Ballon D, Chui C, Mohan R. Monte Carlo simulation of a cobalt-60 beam. Med Phys 1987;14(3):414–9. http://dx.doi.org/10.1118/1.596120, URL https://aapm.onlinelibrary.wiley.com/doi/abs/10.1118/1.596120.

[17] McEwen M, Tessier F. Characterization of a SNC350p parallel-plate ionization chamber for electron beam reference dosimetry. Report IRS-1860r, Ottawa, Canada, National Research Council of Canada; 2014.

[18] Tessier F. Monte Carlo calculation of the k_Q quality conversion factor for the SNC600c ionization chamber for electron beam reference dosimety. Report IRS-2065, Ottawa, Canada, National Research Council of Canada; 2015.

Verzeichnis der akademischen Lehrerenden

Meine akademischen Lehrenden waren in Universität Damaskus:

- Prof. Dr. Mohammad Qaqa
- Prof. Dr. Fawzi Awad
- Prof. Dr. Mohammad Saeed Mahasneh
- Prof. Dr. King Al-Shoufi
- Prof. Dr. Youssef Abu Ali
- Prof. Dr. Ahmed Al-Yahya
- Prof. Dr. Bassam Maasrani
- Prof. Dr. Mohammad Abdelhafiz
- Prof. Dr. Suhaim Tarabishi
- Prof. Dr. Hassan Khurayta
- Prof. Dr. Saeed Al-Masri
- Prof. Dr. Riyadh Shweikani

Meine akademischen Lehrenden waren in Gießen

- Prof. Dr. Klemens Zink

Danksagung

Ich möchte mich herzlich bei Professor Klemens Zink bedanken, dessen außergewöhnliche Unterstützung und inspirierende Anleitung unentbehrlich für mich waren. Er hat mir geholfen, neue wissenschaftliche Horizonte zu eröffnen und mein kritisches Denken wesentlich zu stärken. Ebenso bin ich Professorin Rita Engenhart-Cabillic für ihre hingebungsvolle Unterstützung und ihren wissenschaftlichen Beitrag zu verdanken, die maßgeblich zum Erfolg meiner Arbeit beigetragen haben. Ein besonderer Dank geht auch an meinen Kollegen Dr. Damian Czarnecki für die fruchtbare Zusammenarbeit und Freundschaft, die einen bedeutenden Einfluss auf meine Entwicklung hatten. Ich möchte auch meinen Kollegen an der Institut für Medizinische Physik und Strahlenschutz (IMPS) für ihre wertvolle Unterstützung und Zusammenarbeit danken, die meine akademische Laufbahn bereichert haben. Des Weiteren danke ich Dr. Andreas Schönfeld für seine wertvollen Beiträge zu meiner Arbeit. Zuletzt widme ich diese Arbeit meiner Familie, deren unerschütterliche Unterstützung und Motivation immer eine wichtige Stütze für mich waren. Sie sind die Quelle meiner Inspiration und bleiben immer in meinem Herzen.